Glyphosate Transport and Inorganic Nitrogen Turnover in Floodplain Soils Induced by Heavy Rainfall After Summer Drought

Dissertation

der Mathematisch-Naturwissenschaftlichen Fakultät

der Eberhard Karls Universität Tübingen

zur Erlangung des Grades eines

Doktors der Naturwissenschaften

(Dr. rer. nat.)

vorgelegt von

Johanna Schlögl

aus Freiburg im Breisgau

Tübingen

2024

Gedruckt mit Genehmigung der Mathematisch-Naturwissenschaftlichen Fakultät der Eberhard Karls Universität Tübingen.

Tag der mündlichen Qualifikation:	15.07.2024
Dekan:	Prof. Dr. Thilo Stehle
1. Berichterstatter:	Prof. Dr. Stefan B. Haderlein
2. Berichterstatter:	Jun. Prof. Dr. Eva Marie Muehe

Für meine Eltern, Friederike und Heinz, die mir all dies hier überhaupt erst ermöglicht haben.

Für meine Großeltern, Renate und Albrecht, die mir in so vielen Belangen Vorbilder sind.

Acknowledgements

The phase in my life of working on my PhD project and finally finishing this thesis was a good one and a challenging one at the same time. It would not have been what is was without many people's support. Here, I want to say Thank You and I hope, I won't forget anyone.

First and foremost, I thank Stefan Haderlein for offering a PhD position in his group to me and for his supervision throughout the project even when I had already left Tübingen. Thank you for fruitful discussions and new perspectives on my research as well as guidance and support.

I also thank Andreas Kappler, my second supervisor, who was always ready to discuss my project and to give valuable input. Thank you for being part of my examination committee.

I want to thank the German Research Foundation (DFG) for funding this work within the Collaborative Research Centre 1253 "CAMPOS – Catchments as Reactors".

I am very grateful to Marie Muehe for taking the time to evaluate my thesis and to join the examination committee.

I want to thank Christiane Zarfl for taking the time to chair my exam and for the interest in my work.

I want to thank everyone who proofread parts of this thesis and gave valuable feedback.

A special thank you goes to Christian Griebler, Lena Cramaro, and Clemens Karwautz in Vienna for the collaboration during the project and especially when incorporating the microbiology data into our publication. Clemens, thank you for the data evaluation and interpretation and to all of you for always being willing to discuss and answer my questions.

I thank Wolfgang Wanek and Christine Stumpp for the collaboration and their contributions to the publications.

I am very grateful to many people in the former ZAG and later GUZ lab: Monika Hertel for general lab supervision and an open ear for any issue, to Sara Wild, Franziska Schädler, Ellen Röhm and Bernice Nisch for analyses of ions, inorganic nitrogen species and TOC. I owe a lot of gratitude to my Hiwis Charlotte, Lydia, Michelle, and Yuge, for their assistance and enormous help with the processing of numerous field samples. There are more people whom I thank for supporting my lab work: Hartmut Schulz, Prachi Joshi and my Bachelor and Master students Michelle Engelhardt, Andrea Loria, and Frieder Straub.

I was lucky to do a lot of field work and I am very thankful to all collaborators and supporters, especially, but not only, to the "irrigation experiment" field work crew: Lena Cramaro, Benedikt Wimmer, Hannes Wirsching, Christian Poll, Christian Griebler, Marc Jantz, Thomas

Siller, Stefan Klingler, and Simon Martin. I also thank H. K., who allowed us to realize the field experiment at a corner of his land.

I had a lot of great colleagues, especially within the CAMPOS team. Thank you all for the interdisciplinary scientific exchange on our projects during our retreats and meetings as well as for the evenings in the Tübingen pubs after work.

I also thank the colleagues from my work group Environmental Mineralogy and Chemistry for the nice and supportive working atmosphere. A very special thank you goes to Edisson Subdiaga who took over the role as my mentor in the ZAG labs, who introduced me to many of the lab methods I used during my PhD work and who became a friend through all this.

I want to thank the very cooperative ZAG/GUZ administration team, especially Elisabetha Kraft and Monika Schäffling, who were a great support.

I want to thank everyone, who motivated me to finish my dissertation during the past two years. I also thank my current employer for allowing me to reduce my working hours during the past months, which helped a lot to finish this thesis.

I thank Tom Schiedek, who boosted my choice to study geoscience from the very beginning.

I want to thank my friends in Tübingen and elsewhere. Thank you for your support whenever it was necessary and for the distraction, that was very much needed from time to time. Thank you Johanna, Moritz and Oskar, Lars, Michi, Edisson, Michelle, Stefan K., Natalia, Kay, Jana, Katrin, and Verena for making Tübingen and its surroundings a place that felt and always will feel like home to me.

Ein großer Dank gilt meiner Familie, im Besonderen meinen Großeltern, meiner Patentante und meinem Bruder. Danke für eure Unterstützung und all die schöne Zeit mit euch.

An Lars, meinen Partner und größten Unterstützer: Danke für all die schönen, abwechslungsreichen Momente mit dir. Danke für deine Unterstützung, besonders in den letzten Monaten: für die Aufmunterung, wenn meine Motivation am Boden war, und dafür, dass du an den Tagen, an denen ich nur diese vorliegende Arbeit im Kopf hatte, dafür gesorgt hast, dass ich nicht hungrig ins Bett gegangen bin. DANKE für deine Liebe, deine Geduld und deine Akzeptanz dafür, dass ich in den letzten zwei Jahren einiges meiner (unserer!) Freizeit in das Fertigstellen dieser Dissertation investiert habe.

Der größte Dank geht an meine Eltern. Danke für eure Stärke und Zuversicht ganz zu Beginn und für eure seitdem immerwährende Unterstützung. Euer Vertrauen in meine Entscheidung, Geowissenschaften zu studieren, hat mich all die Jahre getragen und hat schlussendlich diese Dissertation überhaupt erst ermöglicht.

Abstract

Soil system functioning is essential for both humans and the environment. Soils are involved in all biogeochemical cycles, e. g., the carbon or the nitrogen cycle, thereby fulfilling their key function of cycling and retaining nutrients that are used by natural ecosystems as well as for agriculture. The application of fertilizer and pesticides during agricultural use puts soil functions under a constant stress. While soils can help in attenuating micropollutants or nitrate and thereby prevent them from leaching into the groundwater, soil functions can be impaired by the application of pesticides or fertilizer. Another stressor for soils is climate change, which enhances the frequency and intensity of droughts and rainfall events.
The goal of this thesis was to investigate the effects of a heavy rainfall event after a summer drought on soil redox potentials, inorganic nitrogen turnover, vertical transport of water, nitrate, and glyphosate and the soil microbial community in a fine-textured floodplain soil. It was hypothesized that (i) shrinkage cracks forming during the drought period can act as preferential flow paths thereby allowing dissolved and particle-bound compounds to leach into the subsoil during a heavy rainfall event, (ii) upon rewetting of the dry soil a pulse of inorganic nitrogen is observed ("Birch effect"), which, after a few days, transitions to the "usual" redox-driven nitrogen turnover processes, and (iii) the rewetting of the dry soil impacts the soil microbial community, especially its active fraction.

In preparation for the field study, the methodology for the quantification of nitrate and ammonium concentrations in soil samples was reviewed by testing the stability of samples during storage and extraction under different conditions (storage temperature, extraction time and extraction solution, oxygen availability). In summary, it is recommended, to freeze field soil samples immediately after sampling, to store them frozen and to extract them with 2 M KCl to avoid any impairment of ammonium and nitrate concentrations.

At a floodplain in the catchment of the Ammer river close to Tübingen, SW Germany, a field experiment was conducted to test the above listed hypotheses by simulating a heavy rainfall event on a dry soil. The floodplain soil was a fine-textured Gleysol, that exhibited pronounced shrinkage cracks after a summer drought period. On a harvested summer barley acre, the field experiment setup with nine equally-sized plots was installed. Three plots each were treated similar: (i) Plots received the simulated heavy rainfall event (deuterium-labeled water) and a light daily irrigation for 10 consecutive days. (ii) Plots were sprayed with glyphosate one day before the simulation of the heavy rainfall event as described in (i). (iii) Dry plots received no treatment and served as control plots. 50-cm soil cores were retrieved from all plots two hours after the simulated heavy rainfall event (i. e., day 0), on days 6/8 and 14. Analyses of the pore water content, the δ^2H-signature of the pore water, glyphosate, ammonium and nitrate concentrations, the microbial community on DNA and RNA level, and extracellular enzyme

activities were conducted. Additionally, in situ soil redox conditions were monitored in different soil depths.

The role of shrinkage cracks as preferential flow paths was evaluated by the δ^2H-signature of the pore water, the isotope mass balance and the water mass balance, which consistently showed that already on day 0 irrigation water had reached depths down to 50 cm below ground level, i. e., the maximum depth investigated. Also glyphosate was found alongside with elevated isotopic signatures over entire core profiles. As glyphosate is strongly sorbing to mineral particles, this finding is surprising and indicates that a particle-bound transport of glyphosate through preferential flow paths must have occurred. Nitrate as very soluble compound is also prone to transport along preferential flow paths. Although a loss of nitrate in the topsoil was observed upon the heavy rainfall event, no nitrate accumulation was observed in the subsoil. As, however, other processes of nitrate loss could be excluded, it was assumed that the nitrate leached even further down than 50 cm below ground level and was therefore not recovered.

The assessment of nitrogen turnover processes occurring upon the soil rewetting by the simulated heavy rainfall event revealed: (i) Upon the initial rewetting of the soil during the simulated heavy rainfall event, a pulse of inorganic nitrogen in the form of ammonium appeared in the top ten centimeters of the soil (Birch effect). Except from that, ammonium behaved very conservatively, which can be explained by the high fraction of sorbed ammonium having a limited bioavailability compared to exchangeable ammonium. (ii) In situ redox potentials dropped from oxidizing to reducing within hours to days in response to the simulated heavy rainfall event and stayed low especially in the subsoil and controlled the inorganic nitrogen turnover processes in later stages of the field experiment (days 6 and 14). (iii) Nitrate contents responded to changes of in situ redox potentials, with a denitrification-related decrease at reducing conditions and a nitrification-driven increase at oxidizing conditions.

The effect of the simulated heavy rainfall event on the soil microbial community composition on both DNA and RNA (active fraction) level was negligible. However, lower diversity indices of the active fraction were measured on rewetted plots compared to dry plots, which indicated a certain selection for taxa better adapted to dry-wet-cycles.

The presented thesis demonstrates that the methodology of the described field experiment was suitable to study several interacting processes during the rewetting of a dry soil during a (simulated) heavy rainfall event. The insights promote the understanding of these interacting processes and the protection of soil and groundwater resources during drought periods and heavy rainfall events and lay a profound basis for further studies.

Zusammenfassung

Böden, die ihre Ökosystemfunktionen zuverlässig erfüllen, sind wichtig für Mensch und Umwelt. Böden sind an allen biogeochemischen Kreisläufen beteiligt, z. B. am Kohlenstoff- oder Stickstoff-Kreislauf, wobei sie dort wichtige Aufgaben übernehmen, um Nährstoffe im Kreislauf zu führen und zu halten, damit diese sowohl den natürlichen Ökosystemen als auch für die Lebensmittelproduktion in der Landwirtschaft zur Verfügung stehen. Landwirtschaftliche Nutzung setzt Böden aber auch unter Stress, etwa durch die Anwendung von Dünger oder Pestiziden. Anthropogen eingetragene Stoffe wie organische Mikroschadstoffe oder Nitrat können zwar in Böden zurückgehalten und abgebaut werden, beeinträchtigen durch ihr Vorhandensein aber auch die Funktionsweise von Böden. Ein weiterer Stressor für Böden ist der Klimawandel und die mit ihm häufiger werdenden extremen Wetterereignisse wie Dürreperioden und Starkregen.
Das Ziel der hier präsentierten Arbeit war es, die Auswirkungen eines Starkregenereignisses nach einer sommerlichen Dürreperiode auf die Redoxbedingungen, den Umsatz von anorganischem Stickstoff, den vertikalen Transport von Regenwasser, Nitrat und Glyphosat sowie die mikrobielle Gemeinschaft in einem feinkörnigen Auenboden zu untersuchen. Folgende Hypothesen wurden aufgestellt: (I) Schrumpfungsrisse, die während einer Dürreperiode in feinkörnigen Böden entstehen, können als präferentielle Fließwege dienen und so den Transport von gelösten und partikelgebundenen Stoffen mit dem Starkregen in den Unterboden ermöglichen. (II) Während der Wiederbefeuchtung des trockenen Bodens kommt es zu einem Puls von mineralisiertem Stickstoff (der sogenannte „Birch-Effekt“), der aber nach wenigen Tagen in die „üblichen“ redoxgetriebenen Stickstoff-Umsatz-Prozesse übergeht. (III) Die Wiederbefeuchtung beeinflusst die Zusammensetzung der mikrobiologischen Gemeinschaft im Boden.

Zur Vorbereitung der Feldstudie wurde zunächst die Methodik zur Bestimmung der Nitrat- und Ammoniumkonzentration im Boden daraufhin geprüft, welche Bedingungen während der Probenlagerung und der Extraktion (Lagerungstemperatur, Extraktionsdauer und Extraktionslösungen, Sauerstoffverfügbarkeit) die Stabilität der Nitrat- und Ammonium-Konzentrationen gewährleisten können. Zusammenfassend wird empfohlen, Bodenproben bei der Feldarbeit direkt nach der Entnahme einzufrieren, sie gefroren zu lagern und mit 2 M KCl zu extrahieren, um jedwede Verfälschung der Ammonium- und Nitrat-Konzentrationen zu vermeiden.

In einer Aue im Einzugsgebiet der Ammer in Südwestdeutschland, 7 km westlich von Tübingen, wurde in einem Feldexperiment ein Starkregenereignis auf einem ausgetrockneten Boden simuliert, um die oben genannten Hypothesen zu prüfen. Der Auenboden war ein feinkörniger Gley, der nach einer sommerlichen Dürreperiode ausgeprägte Schrumpfungsrisse aufwies. Auf einem abgeernteten Getreidefeld wurden für das Experiment

neun gleich große Parzellen abgegrenzt. Jeweils drei Parzellen wurden gleich behandelt: (I) Auf diesen Parzellen wurde mit Deuterium-dotiertem Wasser ein Starkregenereignis simuliert. In den zehn darauffolgenden Tagen wurden die Parzellen mit nicht-deuteriertem Wasser leicht weiter beregnet. (II) Die Parzellen wurden einen Tag vor dem simulierten Starkregenereignis (wie unter (I) beschrieben) zusätzlich mit Glyphosat behandelt. (III) Die Parzellen, die als trockene Kontroll-Parzellen dienten, erhielten keine Behandlung. 50 cm lange Bodenkerne wurden zwei Stunden nach dem simulierten Starkregen (Tag 0) sowie an den Tagen 6/8 und 14 des Experiments von allen Parzellen entnommen. An den Kernen wurden Analysen des Porenwassergehalts, der δ^2H-Signatur des Porenwassers, der Glyphosat-, Ammonium- und Nitratkonzentration, der mikrobiellen Gemeinschaft auf DNA- und RNA-Ebene sowie der extrazellulären Enzymaktivitäten vorgenommen. Des Weiteren wurde mittels permanent installierten Redoxsonden in verschiedenen Tiefen das in situ Redoxpotential gemessen.

Um die Rolle von Trockenrissen als präferentielle Fließwege zu beurteilen, wurden die δ^2H-Signatur des Porenwassers, der Porenwassergehalt und die Glyphosatkonzentrationen entlang der einzelnen Bodenkerne ausgewertet. Die Daten zeigten übereinstimmend, dass bereits zwei Stunden nach dem simulierten Starkregen Teile des Beregnungswassers und des Glyphosats die maximale untersuchte Tiefe von 50 cm erreicht hatten. Da Glyphosat stark an mineralischen Bodenbestandteilen sorbiert, sind diese Funde überraschend und legen nahe, dass partikelgebundener Transport von Glyphosat stattgefunden haben muss. Nitrat als leicht löslicher Stoff ist auch anfällig für Transport in präferentiellen Fließwegen. Obwohl ein Verlust von Nitrat im Oberboden während des Starkregens beobachtet wurde, gab es keine Nitratakkumulation im Unterboden. Da jedoch andere Prozesse, die den Rückgang von Nitrat im Oberboden erklären könnten, ausgeschlossen werden konnten, wurde angenommen, dass das Nitrat in Bodenschichten unterhalb der maximalen untersuchten Tiefe von 50 cm verlagert wurde.

Die Untersuchung der Prozesse des Stickstoffumsatzes ergab, dass während der Wiederbefeuchtung des Bodens durch das simulierte Starkregenereignis in den obersten 10 cm des Bodens eine vorübergehende Zunahme von Ammonium zu beobachten war (Birch-Effekt). Abgesehen davon verhielt sich Ammonium sehr konservativ, was auf den großen Anteil an sorbiertem Ammonium zurückgeführt werden kann, welches im Vergleich zu weniger stark gebundenem austauschbarem Ammonium nur eingeschränkt bioverfügbar ist. Die in situ gemessenen Redoxpotentiale fielen innerhalb von Stunden bis wenigen Tagen nach dem Starkregenereignis von oxidierenden zu reduzierenden Bedingungen und blieben besonders im Unterboden stabil auf reduzierendem Niveau. Die vorherrschenden Redoxpotentiale kontrollierten den Umsatz von Nitrat zu den späteren Zeitpunkten des Experiments (Tag 6 und 14). Die Nitratgehalte nahmen wie erwartet bei reduzierenden Bedingungen ab (Denitrifikation) und bei oxidierenden Bedingungen zu (Nitrifikation).

Der Effekt des Starkregenereignisses auf die Zusammensetzung der mikrobiellen Gemeinschaft des Bodens war sowohl auf DNA- als auch auf RNA-Ebene vernachlässigbar. Lediglich systematisch niedrigere alpha-Diversitätsindizes (RNA-Ebene) auf beregneten

Parzellen im Vergleich zu den trockenen Kontroll-Parzellen wiesen darauf hin, dass eine gewisse Selektion hin zu besser an Trocken-Nass-Zyklen angepassten Taxa stattfand.

Die vorliegende Arbeit zeigt, dass die Methodik des beschriebenen Feldexperiments geeignet war, um verschiedene miteinander interagierende Prozesse während der Wiederbefeuchtung eines ausgetrockneten Bodens durch ein (simuliertes) Starkregenereignis zu untersuchen. Die Erkenntnisse dieser Arbeit vertiefen das Verständnis des Zusammenwirkens dieser Prozesse und fördern somit Möglichkeiten zum Schutz von Boden- und Grundwasser-Ressourcen während der durch den voranschreitenden Klimawandel häufiger auftretenden Dürreperioden und Starkregenereignisse. Die Arbeit legt außerdem eine gründliche Basis für weitere Studien zu diesem Thema.

Table of Contents

List of Figures

List of Tables

List of Abbreviations

AMPA	(Aminomethyl)phosphonic acid
Anammox	Anoxic ammonia oxidation
ANOVA	Analysis of variance
AP	Acid phosphatase
a.s.l.	Above sea level
ASV	Amplicon Sequence Variant
BG	β-glucosidase
bgl	Below ground level
CFA	Continuous flow analysis
C_{org}	Organic carbon
DIN	Deutsches Institut für Normung (German Institute for Standardization)
DNA	Deoxyribonucleic acid
cDNA	Complementary DNA
DNRA	Dissimilatory nitrate reduction to ammonium
DWD	Deutscher Wetterdienst (German Meteorological Service)
ETo	Reference evapotranspiration
FAO	Food and Agriculture Organization of the United Nations
HRE	Heavy rainfall event
Irr_{HRE}	Irrigation water of the simulated heavy rainfall event
Irr_{tot}	Sum of all irrigation and natural precipitation water at a certain time point in the experiment
ISP	Integral suspension pressure method
lat	Latitude
long	Longitude
MUF	4-methylumbelliferyl
NAG	N-acetylglucosaminidase (“exochitinase”)
NEDD	N-1-Naphthylethylenediamine di-HCl
NMDS	Non-metric multidimensional scaling
NW	North-west
N_{org}	Organic nitrogen
PCR	Polymerase chain reaction
PVC	Polyvinyl chloride
Redox	Reduction–oxidation
RH	Relative humidity
RH_{max}	Maximum RH in a certain time period
RH_{min}	Minimum RH in a certain time period
RNA	Ribonucleic acid
rRNA	Ribosomal RNA

Rs	Global radiation
SHE	Standard hydrogen electrode
SOM	Soil organic matter
SW	South-west
TOC	Total organic carbon
T	Temperature
$\mathbf{T_{max}}$	Maximum temperature
$\mathbf{T_{mean}}$	Mean temperature
$\mathbf{T_{min}}$	Minimum temperature
TÜ	Tübingen
VSMOW	Vienna Standard Mean Ocean Water
$\mathbf{\delta^2H}$	Isotope ratio of hydrogen
$\mathbf{\delta^{15}N}$	Isotope ratio of nitrogen
$\mathbf{\delta^{18}O}$	Isotope ratio of oxygen

1 Introduction

1.1 Motivation

The functioning of the soil system is of great importance for both humans and the environment (Adhikari & Hartemink, 2016). Soils are involved in all biogeochemical cycles, e. g., the carbon or the nitrogen cycle. In most of the turnover processes microbes are involved, e. g., in the decomposition of organic matter and thus the supply of nutrients (Blume et al., 2016). These nutrients are then used by other microbes, soil fauna or plants. Soils are also important when it comes to the production of food. These agriculturally used soils are under a special pressure as they receive fertilization and high inputs of agrochemicals (Hedlund et al., 2020). An additional stressor is climate change, which promotes drought periods and heavy rainfall events (Coumou & Rahmstorf, 2012).

Under severe summer drought periods as they, e. g., have occurred in SW Germany in the years 2018, 2019, and 2020 (Umweltforschungszentrum, 2023), soils experience a decrease of water content which leads to higher concentrations of dissolved compounds in the soil solution and interrupted diffusion of nutrients when the water film in soil pores and along soil particles eventually breaks down (Manzoni et al., 2012). Thereby nutrients are immobilized. The interruption of nutrient flows in the soil water and the desiccation itself can lead to starvation or dehydration of plants and microbial cells, whereby the latter can form spores to survive drought periods (Schimel, 2018). The lower water saturation of dry soils implicates that oxygen can penetrate deeper into dry than into moist soils (Haberer et al., 2012). Especially in fine-textured soils with a high clay content, shrinkage cracks of substantial width and depth can form allowing oxygen to reach deep soil layers. Upon rewetting after a drought period, often induced by heavy rainfall events, nutrients and other easily dissolvable compounds are remobilized. If shrinkage cracks are present, they can act as preferential flow paths enabling a fast transport of compounds to the subsurface (Beven & Germann, 2013; Jarvis et al., 2016). Even particle-bound transport through preferential flow paths can occur when the macropores are wide and straight enough (Larsson & Jarvis, 2000). Rewetting as well induces a reactivation of microbial cells and microbial turnover processes are initiated. When dry soils are rewetted usually a pulse of inorganic carbon and nitrogen is observed, which stems from the mineralization of osmoregulatory substances and dead microbial cells (Birch, 1958, 1960; Unger et al., 2010). It is also known as the "Birch effect".

The presented thesis investigated the effects of a heavy rainfall event after a summer drought period on an agriculturally used floodplain soil in SW Germany. In the following introduction, the main topics of the presented thesis are addressed in detail and an overview over the objectives of the thesis and its structure is presented.

1.2 Floodplains as landscape elements of high biogeochemical activity

Floodplain soils are biogeochemically active landscape elements (Lair et al., 2009; Venterink et al., 2003). Due to recurrent inundation and dry periods or alternating groundwater levels they are exposed to fluctuating oxygen availability. Fluctuating redox conditions drive biogeochemical cycling in soils, that is sequestration, (re-)mobilization, and turnover of nutrients (Coby et al., 2011) and pollutants (Venterink et al., 2003). During dry periods in summer and fall and especially in fine-textured soils, shrinkage cracks of substantial width and depth form enabling deep penetration of oxygen (Haberer et al., 2012). Upon rewetting in winter or spring, these cracks close, resulting in limited or interrupted atmospheric oxygen supply and ultimately anoxic conditions. Climate change might enhance the frequency of these dry-wet cycles making them occur more often within a season by increasing the probability of drought as well as heavy rainfall events (Coumou & Rahmstorf, 2012).

Redox-active soil components and the measurement of in situ soil redox potentials

Besides oxygen, other inorganic and organic soil components such as iron(oxy)hydroxides, iron-containing clay minerals or soil organic matter (SOM) can act as electron donors or acceptors in soil redox reactions. While iron(oxy)hydroxides involved in redox reactions have been extensively studied, other redox-active soil components such as SOM or iron-containing clay minerals have only come into the focus of research during the past ten to fifteen years (Aeschbacher et al., 2010; Gorski et al., 2012; Lau et al., 2015; Tratnyek et al., 2011). For SOM, the nominal oxidation state of carbon expresses if oxidation or reduction is feasible under certain thermodynamic conditions (LaRowe & Van Cappellen, 2011). They are both able to accept and donate electrons over a wide range of redox potentials (Aeschbacher et al., 2012; Gorski et al., 2012). Thereby they do not leave any visible marks such as iron(oxy)hydroxides of iron sulfide minerals do. Soil organic matter and iron containing clay minerals also allow for a meaningful measurement of in situ redox potentials as they readily equilibrate with common redox electrodes (Aeschbacher et al., 2011; Sander et al., 2015).

Soil inorganic nitrogen cycling

The two quantitatively most important inorganic nitrogen compounds in soils are ammonium and nitrate. Both serve as nutrients that can be taken up by plants and soil microbes but also as electron donor and acceptor, respectively, in redox reactions. In agriculturally used soils, nitrogen input mostly comes from organic fertilizers and organic residues. The anthropogenic nitrogen input by fertilization significantly exceeds the natural input by biological fixation (Blume et al., 2016; Fowler et al., 2013). Under oxic conditions, ammonium is oxidized to nitrate (nitrification) and under anoxic conditions, nitrate is reduced to NO, N_2O and finally N_2 (denitrification) (Thamdrup, 2012). Besides, nitrate can also be reduced to ammonium in the dissimilatory nitrate reduction to ammonium (DNRA) and ammonium can be oxidized under

anoxic conditions (anoxic ammonia oxidation, Anammox) (Thamdrup, 2012). The presented thesis focuses on the investigation of the occurrence of nitrification and denitrification.
Nitrate and ammonium behave quite differently in soils. Nitrate as anion is not prone to sorption on the net negatively charged surface of most soil-forming mineral particles. Therefore, it is largely dissolved in the soil solution and thus, prone to leaching to the subsoil or even groundwater (Blume et al., 2016). On the other hand, ammonium as cation, sorbs well to the surface of soil mineral particles (exchangeable ammonium) and is even incorporated in the interlayer of clay minerals (interlayer ammonium) generating an ammonium pool recalcitrant towards further redox reactions (Buss et al., 2004; Cavalli et al., 2015).

Birch effect

Besides the "usual" redox driven nitrogen turnover in soils, special processes occur, when dry soils are rewetted either artificially, e. g., in laboratory experiments (Birch, 1958, 1960; Fierer & Schimel, 2002), or naturally by rainfall after a drought period (Cui & Caldwell, 1997; Unger et al., 2010), the so-called "Birch effect". Upon the rewetting of dry soils, a pulse of mineralized carbon (CO_2) and nitrogen (NH_4^+ and NO_3^-) is observed (Birch, 1958, 1960; Cui & Caldwell, 1997). The enhanced mineralization of carbon and nitrogen usually lasts up to several days and is recurring with every dry and wet-cycle (Fierer & Schimel, 2002). Birch (Birch, 1958, 1960) assumed that the pulse of carbon and nitrogen mineralization after soil drying and rewetting was induced by increased microbial activity regarding humus (i. e., soil organic matter) decomposition, the decomposition of desiccated dead microbial cells or a change of accessibility of organic matter during drying and rewetting for microbial decomposition. Further studies until today have hypothesized (Fierer & Schimel, 2002; Jarvis et al., 2007; Saetre & Stark, 2005) and shown, e. g., by stable carbon isotope measurements (Unger et al., 2010), that the mineralization pulse upon rewetting of dry soils originates from the mineralization of osmoregulatory substances that were excreted by the soil microorganisms to regulate the hypo-osmotic stress under drying, and the mineralization of dead microbial cells. The mineralization pulse upon rewetting results in a loss of carbon in the form of CO_2 from the soil system. Inorganic nitrogen in the form of ammonium remains in the soil and can be used as nutrient or function as electron acceptor in redox reactions. Inorganic nitrogen in the form of nitrate can be used as nutrient as well but can also be lost by leaching or denitrification.

Extraction of soil inorganic nitrogen: Methods and applicability in the presented thesis

The determination of soil inorganic nitrogen content is important in many scientific and technical fields such as the study of redox reactions or fertilizer management (Mengel, 1991). For the extraction of the inorganic nitrogen species, ammonium and nitrate, from soils, typically a 0.01 to 0.0125 M $CaCl_2$ solution or a 1 or 2 M KCl solution, respectively, is used. The lower concentrated $CaCl_2$ solution mimics the ionic strength of a typical soil solution and thus targets compounds that are easily dissolved, in the case of inorganic nitrogen compounds this

is nitrate. Ammonium, on the other hand, due to its positive charge, is more strongly sorbed to soil particles (Blume et al., 2016; Buss et al., 2004) and thus needs a stronger solution that allows cationic exchange on mineral particle surfaces to be extracted. With 1 or 2 M KCl, the sorbed ammonium can be exchanged by the potassium cation (Kuderna et al., 1993). For nitrate, the extraction efficiency of 0.0125 M $CaCl_2$ and 2 M KCl is similar (Wheatley et al., 1989). When it comes to the analysis of soil redox states or reactions with the help of nitrate and ammonium concentrations, it is also important to ensure the stability or conservation of the two compounds during sampling, sample storage, sample processing and extraction as they are highly susceptible to microbial turnover. Depending on the study site and the study goal, the in situ soil redox conditions can be oxidizing or reducing and these in situ conditions should be preserved. Drying of soils has been shown to be no appropriate method to conserve nitrate and ammonium concentrations (Houba & Novozamsky, 1998; Nelson & Bremner, 1972; Nina & Sigunga, 2012; van Erp et al., 2001). Freezing at temperatures < -18 °C showed satisfactory preservation of soil nitrate and ammonium during sample storage over several months (Houba & Novozamsky, 1998; Nelson & Bremner, 1972). However, thawing of samples before sample processing and extraction altered nitrate and ammonium concentrations (Esala, 1995; Ma et al., 2005) and should thus be avoided. The stability of nitrate and ammonium during extractions with 0.0125 M $CaCl_2$ and 2 M KCl for up to two hours was shown by Wheatley et al. (1989) for fully oxidized samples. As to the author's knowledge, no tests with reduced samples, e. g., from the reduced horizon of a Gleysol, are described in the literature so far. For these samples, however, it might be necessary to adapt certain aspects of sampling, sample handling and extraction of inorganic nitrogen compounds.

Soil microbial communities during drying and rewetting cycles

Drying and rewetting of a soil imposes stress on soil microbial community. The process of drying triggers an equilibration of the microbial cells to the drop in water potential and they form osmoregulatory substances, that keep the water within and around their cells (Schimel, 2018). Additionally, when the connection of soil pores by water (films) decreases or ceases at all during drought, the transport of resources in between and to the microbial cells is interrupted. This is also reflected in microbial activity, which decreases with decreasing water potential until it eventually ends (Manzoni et al., 2012). Drought causes microbial cells first to optimize their access to nutrients by accumulating osmoregulatory substances within and around their cells and later forces them into dormancy or death (Schimel, 2018).
Whereas during drying, microbial biomass is rather constant or even increasing, upon rewetting of a dry soil, soil biomass decreases even if activity rises (Parker & Schimel, 2011). Rewetting usually does not equally increase activity of the whole microbial community but of certain phyla (Barnard et al., 2013; Placella et al., 2012). The stress that is put on microbial communities by rewetting (Barnard et al., 2013; Schimel, 2018) can cause a preference for microbial taxa adapted to drying and rewetting cycles (Armstrong et al., 2016; Fierer et al., 2003; Veach & Zeglin, 2020). The joint occurrence of the described increase in microbial activity

and the pulse of mineralized carbon and nitrogen (Birch, 1958, 1960) upon rewetting of soils raises the question if there exists a cause-effect relationship. A causality in both directions was described in literature, either microbial activity causes the respiration pulse (Aanderud et al., 2015; Placella et al., 2012) or the release/mobilization of organic matter upon rewetting causes the peak in microbial activity (Göransson et al., 2013) and the question is not yet solved.

1.3 Preferential flow in macropores

Macropores in the form of shrinkage cracks appear in floodplain soils during drought periods and they can act as preferential flow paths upon irrigation or the onset of rainfall (Jarvis et al., 2016). The occurrence of preferential flow in macropores depends on the pore size, pore continuity and pore tortuosity (Beven, 1981; Bouma, 1981; Flury et al., 1994; Nimmo, 2021; Skopp, 1981). The higher the quantity or intensity of irrigation or precipitation is, the more likely preferential flow in macropores occurs because the peds of dry soil in between the macropores are initially not capable to take up large volumes of water in a short time (Bouma & Dekker, 1978; Hardie et al., 2011; Jarvis et al., 2016; Nimmo, 2012).

Solute transport and particle-bound transport during preferential flow

Besides the deep penetration of oxygen (Haberer et al., 2012) and water through these macropores, they also allow for rapid and irregular solute (Kelly & Pomes, 1998; Perret et al., 2000) and particle-bound (de Jonge et al., 2004; McGrath et al., 2010) transport of compounds into the subsoil. Substances that are prone to solute transport are usually easily dissolvable in water and of anionic nature so they are less susceptible to sorption on soil mineral particles. An important example is nitrate, the leaching of which to the subsoil or even groundwater bodies has adverse effects on nutrient availability in soils and the quality of groundwater resources (Sánchez Pérez et al., 2003). Compounds that sorb strongly to either mineral particles, e. g., glyphosate or phosphate (de Jonge et al., 2000; de Jonge et al., 2004; Gimsing & Borggaard, 2002; Wimmer et al., 2023), or organic matter, e. g., nonpolar organic contaminants, such as pesticides (Zehe & Flühler, 2001) are expected to be transported particle-bound, when found at higher concentrations than expected in the subsoil or in tile drains (Kjær et al., 2011; Norgaard et al., 2014).

1.4 Objectives and structure of the thesis

Rewetting of soils by a heavy rainfall event or artificial irrigation after a drought period results in processes and challenges which interact and are interdependent, which rises the following questions: (i) What is the role of shrinkage cracks upon heavy rainfall events, can they serve as preferential flow paths and, if yes, for which types of compounds? (ii) Which nitrogen turnover processes dominate at which time point after the onset of a heavy rainfall event? (iii) How does the sudden rewetting affect the soil microbial community?

To increase knowledge about the effects of heavy rainfall events after summer droughts on soils, this thesis investigated the interplay of various processes in a multidisciplinary approach, assessing the following research questions:

Study 1

- What are suitable storage and extraction conditions for the determination of the redox-sensitive inorganic nitrogen species nitrate and ammonium in clay-rich soil samples?

Study 2

- How does the water of a heavy rainfall event after a summer drought distribute in a dry fine-textured soil with a net of shrinkage cracks?
- Do shrinkage cracks serve as preferential flow paths? Is the pesticide glyphosate transported along these preferential flow paths with the heavy rainfall water?

Study 3

- Is nitrate as a well soluble compound transported along shrinkage cracks during a heavy rainfall event?
- How do in situ soil redox potentials develop upon the heavy rainfall event and a postulated closure of shrinkage cracks?
- Is the inorganic nitrogen turnover upon rewetting of a dry soil shaped by a pulse of respiration (the so-called Birch effect) or is it driven by changes of the in situ redox potentials?
- How does the soil microbial community react to a sudden rewetting after a summer drought? Can a shift in the active microbial community be observed?

The presented thesis has five chapters. **Chapter 1** is a general introduction, where the necessary background information is given and the research questions are introduced. **Chapter 2** presents a methodological study (Study 1) on the sample storage and sample handling of field soil samples designated for the extraction and analysis of nitrate and ammonium in studies that focus on redox processes in soils. For these studies, it is very important that the in situ concentrations of the two nitrogen species remain unaltered. Also the extraction process is examined to determine extraction conditions, that prevent the alteration of nitrate and ammonium concentrations. **Chapter 3** and **Chapter 4** describe and discuss the results of Study 2 and Study 3, respectively, i. e., of a field experiment during which a heavy rainfall event (24.3 mm within one hour) was simulated after a summer drought period on a dry fine-textured floodplain soil. The water of the simulated heavy rainfall event was labelled with deuterated water (D_2O) as a conservative tracer to follow and quantify the water flow in the soil. After the simulation of the heavy rainfall event an even daily irrigation

of 5.2 mm day^{-1} was applied to sustain closure of the shrinkage cracks. In situ soil redox potentials were measured with depth-resolved and permanently installed redox probes. Before the heavy rainfall event, glyphosate was applied to the dry soil. Two hours after the heavy rainfall event simulation (day 0) and at days 6, 8 and 14, 50-cm soil cores were retrieved from locations with initial shrinkage cracks and from the soil peds in between to determine glyphosate concentrations, the soil water isotope ratio (δ^2H), extractable ammonium and nitrate concentrations, total (DNA-level) and active (RNA-level) microbial community composition, and extracellular enzyme activities along the soil profile. **Chapter 3** discusses the water flow and the transport of glyphosate along preferential flow paths as induced by the simulated heavy rainfall event after a summer drought. Alongside, the dynamics of shrinkage cracks and in situ redox potentials after this heavy rainfall event are described and discussed. **Chapter 4** discusses the water flow, in situ redox potentials, solute transport and turnover processes of inorganic nitrogen as well as changes in the soil microbial community after the simulated heavy rainfall event after a summer drought. **Chapter 5** summarizes the major findings presented in Chapters 2, 3, and 4, discusses their interplay and environmental implications and **Chapter 6** gives an outlook on possible follow-up studies.

2 Inorganic nitrogen extraction revisited: stability of nitrate and ammonium during sample storage and extraction

Johanna Schlögl, Andreas Kappler, Stefan B. Haderlein

Status in the publication process: Manuscript in preparation

Author contributions:
Johanna Schlögl: Conceptualization, Methodology, Investigation*, Data curation, Formal analysis, Validation, Visualization, Writing – original draft preparation; **Andreas Kappler**: Conceptualization, Methodology, Funding acquisition, Supervision, Writing – review and editing; **Stefan B. Haderlein**: Conceptualization, Methodology, Funding acquisition, Project administration, Resources, Supervision, Writing – review and editing.

*with the help of: Michelle Engelhardt, Yuge Bai and Hartmut Schulz

2.1 Abstract

The determination of the concentration of inorganic nitrogen compounds (nitrate and ammonium) in soils is important in a variety of environmental problems, e. g., fertilizer need or studies of nitrogen turnover in redox-dynamic systems. Especially for the study of redox dynamics, it is important to preserve the actual nitrate and ammonium concentrations and not only the sum of inorganic nitrogen compounds. Despite of widely used extraction methods with 0.0125 M $CaCl_2$ and 2 M KCl as extractants, there are contradictory results about the stability of samples during the extraction process itself and during storage beforehand.
First, the presented study tested sample stability during extraction for four different extraction durations (15, 30, 60, and 180 min) for both extractants (0.0125 M $CaCl_2$ and 2 M KCl) and under both oxic and anoxic conditions. Additionally, extraction efficiencies of both extractants were compared. Second, sample stability during storage was tested for 48 h at three typical storage temperatures (20°C, 4°C, and -21°C) as well under both oxic and anoxic conditions. The experiments showed, that nitrate and ammonium concentrations were stable under all tested extraction conditions except of during extractions with 0.0125 M $CaCl_2$ at anoxic conditions for longer than 30 min. Extraction efficiencies of both extractants were similar for nitrate and were in general higher for ammonium with 2 M KCl. Only storage at -21 °C guaranteed full sample stability for both compounds. From the results, advice for sampling and sample storage as well as for the choice of the appropriate extractant are derived.

2.2 Introduction

Inorganic nitrogen compounds, i. e., nitrate (NO_3^-) and ammonium (NH_4^+), are highly bioavailable forms of nitrogen and thus important nutrients. In soils, nitrate and ammonium can be taken up, transformed or released by various processes and numerous organisms including bacteria, fungi and plants (Thamdrup, 2012). Nitrate and ammonium represent extreme redox states of the element nitrogen (+V in nitrate, -III in ammonium) and therefore play an important role in redox processes and element cycling as microbial electron acceptor and donor, respectively (Thamdrup, 2012). There are other inorganic nitrogen species such as nitrite or N_2O gas, that are important for environmental processes, but in terms of quantity, nitrate and ammonium are the most important nitrogen species in soils (Blume et al., 2016) and thus, this study focuses on those two. The biggest reservoir of nitrogen on earth is elemental N_2 gas in the atmosphere. N_2 gas can be transformed to ammonium by lightning strikes in the atmosphere or by specific N-fixing bacteria in soils (Fowler et al., 2013). In soils, ammonium can also be derived from organic nitrogen (N_{org}) in the processes of depolymerization and mineralization (Schimel & Bennett, 2004). Under oxic conditions, ammonium can be microbially oxidized to nitrate (nitrification) while under anoxic conditions, nitrate can be reduced to N_2 (denitrification) or to ammonium (dissimilatory reduction of nitrate to ammonium (DNRA)) (Thamdrup, 2012).

Inorganic nitrogen is considered a key parameter for characterizing the N-availability and N-status of soils in agriculture and thus the need for N-fertilization in the beginning of the growth period. To determine the inorganic nitrogen content of soils, simple extraction procedures are widely used. Ammonium and nitrate are extracted with either 0.0125 M $CaCl_2$ at a solid-extractant ratio of 1:4 (Kuderna et al., 1993; Mengel, 1991) or 2 M KCl at a solid-extractant ratio of 1:10 for 30 min (Carter & Gregorich, 2008; Ma et al., 2005). A solution of 0.0125 M $CaCl_2$ in inorganic nitrogen extractions is intended to mimic the common salt concentration in soil water (Houba et al., 1986) representing the ions that would be dissolved or desorbed in the soil solution in a natural soil. 2 M KCl on the other hand offers a higher extraction efficiency for ammonium compared to 0.0125 M $CaCl_2$ because also adsorbed ammonium is extracted (Kuderna et al., 1993; Wheatley et al., 1989). Extraction times of 15 to 120 min (oxic conditions) yielded stable nitrate and ammonium concentrations for both extractants in soils of different texture (Wheatley et al., 1989), whereas an extraction time of 20 hours with 2 M KCl led to a 2 to 3.5-fold increase of ammonium concentrations (Esala, 1994), which was attributed to better dispersion of soil clay particles and enhanced diffusion of ammonium from interlayers of clay minerals. Also leaching of ammonium from microbial cells was postulated as a reason (Esala, 1994).

However, not only the extraction conditions but also the sample handling and preservation is a crucial step, during which a transformation of nitrate and ammonium in a soil sample can occur before inorganic nitrogen analysis. Drying of soils at different temperatures turned out to be inappropriate as a preservation method for later inorganic nitrogen analysis (Houba & Novozamsky, 1998; Nelson & Bremner, 1972; Nina & Sigunga, 2012; van Erp et al., 2001). Tests for freezing as preservation method gave variable results. Nelson and Bremner (1972) and Houba and Novozamsky (1998) saw good preservation of nitrate and ammonium concentrations at -5 °C over 9 months and at -18 °C over 24 months, respectively. Ma et al. (2005) and Nina and Sigunga (2012) however, observed profound alterations in both compounds during preservation at -15 °C and -10 °C, respectively, presumably due to the higher storage temperatures compared to -18 °C in Houba and Novozamsky (1998). Additionally, Ma et al. (2005) thawed the samples for 4 h at room temperature before extraction but they did not investigate the effects of this storage period. Esala (1995) tested the effects of thawing before extraction and found no changes in concentrations of both inorganic nitrogen compounds for thawing periods of up to four hours. Own preliminary studies (unpublished) revealed pronounced changes in concentrations of both ammonium and nitrate during the thaw period (> 4 hours) consistent with observations in permafrost soils, where thawing initiates an N_2O flux (Keuper et al., 2012; Salmon et al., 2018; Voigt et al., 2017). Soil organic N and microbial debris mineralization and consecutive nitrification and denitrification are seen as the responsible processes (Voigt et al., 2017).

It can be argued, that slight shifts in concentrations of nitrate and ammonium do not influence the sum of inorganic nitrogen compounds significantly regarding the derived need of fertilizer. However, in studies with the goal to investigate dynamics of redox conditions in soils, the ability to determine the actual concentrations of ammonium and nitrate as redox-

sensitive species and, hence, sample stability during sampling as well as sample handling and processing are crucial. Unfortunately, the published studies do not allow to draw firm conclusions on sample stability during the commonly used inorganic nitrogen extraction procedures as there are contradictory results about the preservation methods. Furthermore, a systematic evaluation of sample preservation and extraction under anoxic conditions is lacking.

Four parameters in the sample handling and the extractions were identified to potentially lead to a change in concentration of ammonium and nitrate: the choice of the extraction solution, the extraction time, the temperature, at which the samples are stored between sampling and extraction, and the availability or absence of oxygen during storage and the extraction. The present study focused on elucidating the combined effects of these parameters (i. e., extraction solution and extraction time plus oxygen availability as well as storage temperature plus oxygen availability).

To evaluate the influence of extraction time and oxygen availability on the stability of inorganic nitrogen compounds, extractions with 2 M KCl and 0.0125 M $CaCl_2$, respectively, were performed for four different time intervals (15-180 min) under both oxic and anoxic conditions. The effects of the storage temperature and oxygen availability during storage were investigated for three different temperatures (20°C, 4°C and -21°C) over a storage time of 48 h under both oxic and anoxic conditions. From the results, recommendations for the extraction procedure and the sample handling are derived.

2.3 Materials and Methods

Chemicals

Experiments:

- KCl, p.a., Honeywell, Germany
- $CaCl_2$, anhydrous ≥ 98 %, Merck, Germany
- NH_4NO_3, p.a., Merck, Germany

All solutions were made with ultrapure water (GenPure Pro UV-TOC, Thermo Fisher Scientific, Germany).

Continuous flow analysis (CFA):

- Hydrazine
- Sulfanilamide
- N-1-Naphthylethylenediamine di-HCl (NEDD)
- Ammonium sulfate
- Potassium nitrate
- Sodium nitrite

All chemicals for the CFA were purchased from Sigma Aldrich, Germany, and are of ACS grade.

All solutions used in the anoxic experiment series were de-oxygenated by flushing them with N_2 under constant stirring for at least 1 h per liter of solution prior to transfer into the anoxic glovebox.

Soil samples

The soil samples came from a field site in the Ammer valley floodplain, approx. 7 km west of Tübingen, SW Germany (lat. 48.521266, long. 8.972687, 394 m a.s.l.). The floodplain lies in the eastern part of the catchment of the Ammer river. It stretches in a west-east direction and is enclosed by Keuper hills on its northern and southern rims. The Keuper units mainly comprise terrestrial sediments such as sand-, mud- and dolostones. The soil in the floodplain is characterized as Gleysol and is on average 2 m thick. It consists of fine-grained clay mineral-rich alluvial sediments from the surrounding Keuper hills. The soil is typically water saturated in its lower half throughout the year and shows typical gleyic properties in some locations (Martin et al., 2020). The cores taken for this study were of 50 cm length and thus only the Ah and the Go horizons were sampled. Within the first 50 cm of depth, the soil has a uniform texture of 11 ± 4 wt% of sand, 56 ± 6 wt% of silt and 32 ± 4 wt% of clay, a soil organic matter (SOM) content (quantified as total organic carbon (TOC)) of 2-2.5 wt% in the upper 15 cm and around 1 wt% between 15 and 50 cm, and a pH of 7.0-7.3 (determined on six individual samples after stirring the samples in a 1:1 (v:w) mix with deionized water for 30 min). Soil cores of 50 cm length and 3.5 cm diameter were taken with a HUMAX soil corer (GreenGround, Switzerland), and frozen on dry ice immediately after retrieval. In the lab, samples were stored frozen (-21°C) until further use. Information on which cores were used for which experiments is given below in Section "Experiments".

Experiments

Two types of experiments were conducted to examine (i) the stability of ammonium and nitrate during the extraction process with 2 M KCl or 0.0125 M $CaCl_2$, respectively, and (ii) the stability of ammonium and nitrate during sample handling and storage.
For (i), subsamples of one sample were extracted with 2 M KCl or 0.0125 M $CaCl_2$ for 15, 30, 60 and 180 minutes under both oxic and anoxic conditions and the extracted amount of ammonium and nitrate was determined. This experiment will be referred to as "extraction time and extraction efficiency experiment" in the following.
For (ii), subsamples of one sample were stored under oxic or anoxic conditions at three different storage temperatures, i. e., at 20 °C (room temperature, hereinafter called room T), at 4 °C in the cold room and at -21 °C in the freezer for time periods of several hours up to two days. In the following, this experiment will be referred to as "storage experiment".

Extraction time and extraction efficiency

All samples were stored frozen until use for the experiment. The extraction time experiment was conducted under both oxic and anoxic conditions. For both the oxic and the anoxic experiment series with 0.0125 M $CaCl_2$, a soil sample from the above described field site from 10-20 cm depth was used. For the anoxic extraction with 2 M KCl, a mixture of two field soil samples from different depths (5-10 cm and 20-30 cm) was used. For the oxic series with 2 M KCl, the extraction method was applied to another sample that came from 10-20 cm depth. The fact, that two different samples were used for the two experimental series with 2 M KCl because of limited sample availability is considered legitimate as for the goal of the study it was only necessary to look separately at the oxic and anoxic extraction series but not to compare both series among each other.

For the anoxic series, sample preparation and inorganic nitrogen extraction were conducted under a 100% N_2-atmopshere in a glovebox (MBraun, Germany). The respective soil sample was put in a glass bottle, flushed with N_2 for 5 minutes and the bottle was immediately sealed with a rubber stopper prior to the transfer into the glovebox. The soil was stored in the glovebox overnight prior to the following steps to let the sample assimilate to the anoxic conditions.
On the next day, inorganic nitrogen was extracted from this original soil sample with 2 M KCl and 0.0125 M $CaCl_2$, respectively, for 30 minutes. Afterwards, the sample was spiked with an ammonium nitrate solution. This had two reasons: First, this step should make sure that independent from the beforehand overnight storage at anoxic (or oxic) conditions of the sample both inorganic nitrogen species are present in the beginning of the experiment. Second, with a defined spike of ammonium and nitrate and a comparison with the original sample, it could later be determined, with which efficiency both inorganic nitrogen species can be extracted.
For the extraction with 2 M KCl, 25 g of soil sample were spiked with 1.25 mL of a 0.0037 M NH_4NO_3 solution to a final concentration of approx. 14.95 µg NH_4NO_3 g^{-1} soil, that is 2.616 µg N g^{-1} soil of both NH_4^+ and NO_3^-.
For the experiment with 0.0125 M $CaCl_2$, 21 g of soil were spiked with 1.25 mL of a 0.0037 M NH_4NO_3 solution, which led to a final concentration of 17.80 µg NH_4NO_3 g^{-1} soil, that is 3.115 µg N g^{-1} soil of both NH_4^+ and NO_3^-. From the same sample, ammonium and nitrate were also extracted with 2 M KCl for direct comparison of the extraction efficiency.
From the spiked samples of each experiment, 12 times 1.2 g of soil were weighed into plastic tubes and the following extraction procedure was applied. The plastic tubes were put in bottles, which were closed with butyl rubber stoppers to maintain anoxic conditions and the bottles were put on the shaker outside of the glovebox. Three samples at a time were retrieved from the shaker after 15, 30, 60 and 180 minutes, respectively, and samples underwent the sample preparation procedure described below (see Section "Extraction and determination of

inorganic nitrogen compounds"). For the oxic experiment, all steps were conducted as described above but under atmospheric conditions instead of inside an anaerobic chamber.

Sample storage

Sample preparation comprised spiking with 0.0037 M NH_4NO_3, similar to the extraction time experiment with 2 M KCl described above.
The spiked soil sample was carefully mixed and inorganic nitrogen extraction was performed right away according to the standard procedure to determine the concentrations at the beginning of the experiment (t_0). Additionally, ammonium and nitrate were extracted from the original, unspiked sample.
The rest of the spiked soil was split into three subsamples, of which one was stored in the glovebox at room T (20°C), one at 4°C and at -21°C. The latter two were put into bottles which were closed tightly with butyl rubber stoppers and only opened inside the glovebox during the extraction procedure. During sample handling the oxygen level of the glovebox constantly remained unchanged below the detection limit (1 ppm), indicating that sample storage and opening under anoxic condition was successful.
For samples stored at -21°C and 4°C, inorganic nitrogen extraction was performed 24 h and 48 h after the spike according to the scheme described below. For samples stored at room T, two additional extractions were done at 2.5 and 5 h after the spike.
A similar experiment was conducted under oxic conditions, where all steps of the experiment and extractions were conducted at ambient atmospheric conditions and sample bottles were opened at least twice a day to aerate them.

Extraction and determination of inorganic nitrogen compounds

Inorganic nitrogen extraction with 2 M KCl followed the protocol from Carter and Gregorich (2008). For the extraction with 0.0125 M $CaCl_2$ the same protocol was used. For the anoxic experiment series, inorganic nitrogen extractions were conducted in an anoxic glovebox as follows:
After sample manipulation in the glovebox (see Section "Experiments"), 1.2 g of a sample were weighed into a plastic tube and 12 mL of 2 M KCl or 0.0125 M $CaCl_2$, respectively, were added immediately. All extractions were done in triplicates. The plastic tubes were put into glass bottles, which were sealed with butyl rubber stoppers and transferred out of the glovebox. Samples in the glass bottles were then shaken for 30 minutes (standard procedure) at 230 motions per minute (mpm) on a horizontal shaker. For the "extraction time experiment", the extraction time was varied from 15-180 min (for details, see Section "Experiments"). After shaking, plastic tubes were taken out of the bottles, centrifuged for 15 min (eppendorf HERMLE Z320) and again transferred into the glovebox, where they were opened. The oxygen level inside the glovebox always remained at low levels (< 5 ppm) during opening of the plastic tubes, indicating that oxygen contamination during centrifugation oxygen was insignificant.

The supernatant was filtered through 0.2 μm syringe filters (regenerated cellulose, Sartorius, Germany) and filled into 2 mL plastic tubes. These were stored cool and in a sealed glass bottle to maintain the anoxic atmosphere until analysis. For the oxic experiment series, extractions were done similarly, but all steps were done outside the glovebox under a natural atmosphere.

Samples were analyzed for nitrate and ammonium by continuous flow analysis (CFA) within maximum three days. CFA was done with a AA3 HR AutoAnalyzer System from Seal Analytical (Germany). Dialyzer membranes (Seal Analytical, Germany) were installed in all channels to exclude interferences with suspended solids. Nitrate was analyzed following ISO 13395. Nitrate is reduced to nitrite by hydrazine, which then reacts with sulfanilamide and NEDD forming a pink complex that can be measured at 550 nm. Nitrite concentration was determined before the reduction step and then subtracted from the measured nitrate concentration. Ammonium analysis followed the ISO 11732 protocol. The analyte reacts with salicylate and dichloroisocyanuric acid to form a blue complex, that is measures at 660 nm. Standard series were prepared from potassium nitrate, sodium nitrite and ammonium sulfate. Calibration curves were done for ammonium and nitrite; nitrate standards were used to assess the recovery of the reduction step to nitrite. Standards were prepared in 2 M KCl to account for signal shifts due to the sample matrix of 2 M KCl. For the samples in the 0.0125 M $CaCl_2$ matrix, this was not necessary.

Data evaluation

Measured nitrate and ammonium concentrations (mg N L^{-1}) were corrected for baseline and blank values, they were normalized to the initial sample weight and are given in μg N g^{-1} soil. For data evaluation and display, the mean and the standard errors of the three replicate extractions were calculated and the sum of nitrate and ammonium (sum inorganic nitrogen) in μg N g^{-1} soil was calculated. Standard errors of sum inorganic nitrogen were calculated by Gaussian error propagation.

2.4 Results and Discussion

Extraction efficiency and influence of extraction time

The objectives of the extraction time experiment were to assess (i) the stability of the inorganic nitrogen compounds ammonium and nitrate during their extraction with 2 M KCl and 0.0125 M $CaCl_2$, respectively and (ii) the extraction efficiency of both extraction solutions for ammonium and nitrate.

Extraction of nitrate and ammonium from soil with 2 M KCl

The concentrations of nitrate and ammonium extracted with 2 M KCl (Figure 1A and B) for 15, 30, 60 and 180 minutes do not differ significantly ($p > 0.05$). Small differences (< 0.3 μg N g^{-1}

soil for nitrate and < 0.6 µg N g^{-1} soil for ammonium) between the concentrations originate from variations of the total inorganic nitrogen concentrations of the subsamples. The data demonstrate that extraction with 2 M KCl for 15 to 180 minutes does not cause an over- or underestimation of inorganic nitrogen compound concentrations in soils. This is in line with findings from Wheatley et al. 1989, who showed sample stability for inorganic nitrogen extractions with 2 M KCl for up to 120 min.

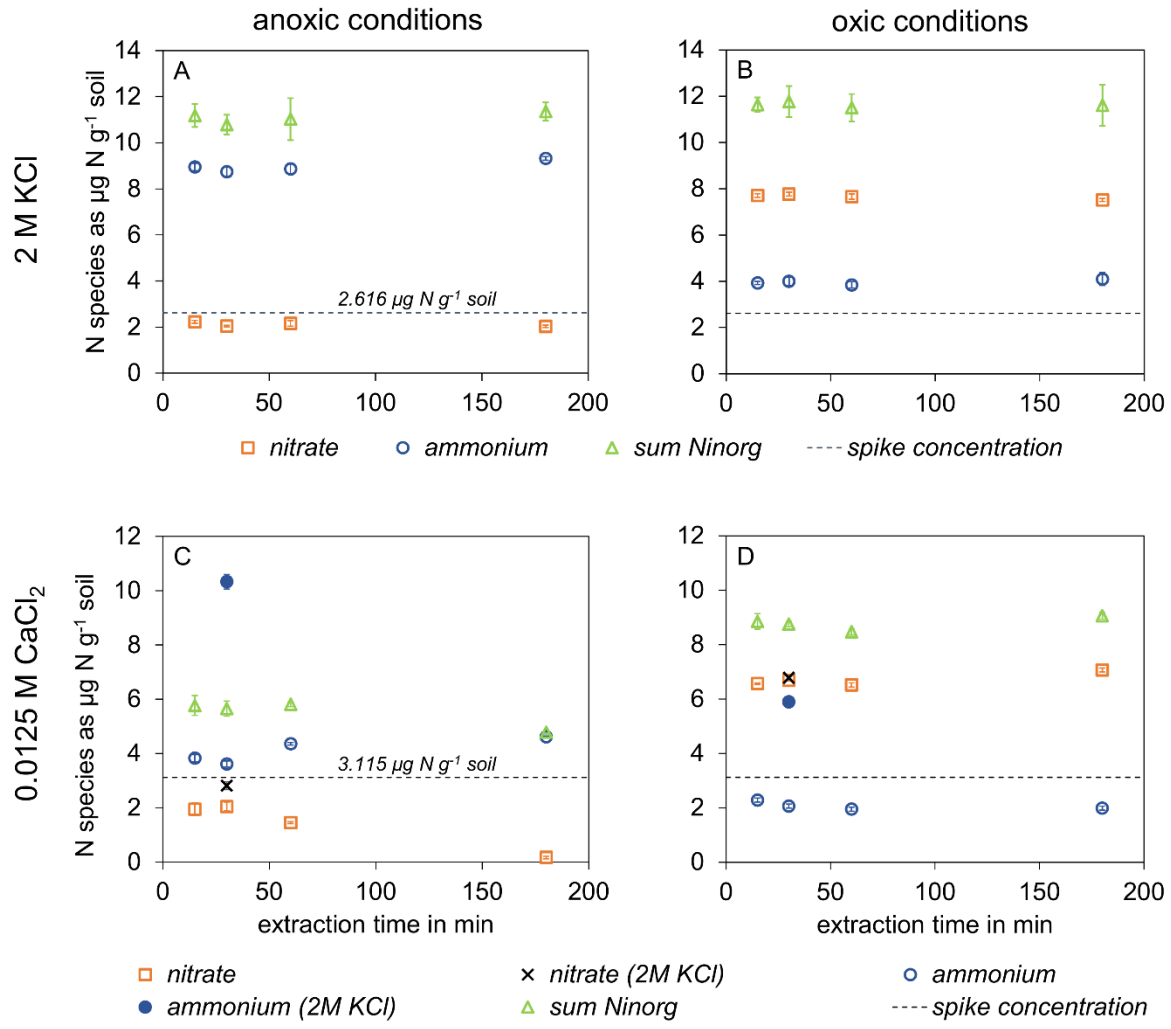

***Figure 1**: Effect of extraction solution (2 M KCl (panels **A**, **B**) vs. 0.0125 M $CaCl_2$ (panels **C**, **D**)) and extraction time (15, 30, 60, 180 min) on extracted concentrations of nitrate (orange squares), ammonium (blue circles) and the sum of both inorganic nitrogen species (sum N_{inorg}, green triangles) in µg N g^{-1} soil under anoxic and oxic extraction conditions. The black symbols in panels C and D refer to a subsample extracted with 2 M KCl (nitrate: black cross, ammonium: filled blue circle). Shown are mean values and standard errors of three replicate extractions. Note the different scales of the y-axes. Dashed lines and concentrations written above them depict the target spike concentrations.*

The decisive factor for the stability of both inorganic nitrogen compounds during the 180 min extraction likely is the high salt content of the extraction solution (2 M KCl, 14.9% salt solution). This hampers the activity of soil microbes not adapted to high salinity levels so no nitrogen turnover processes involving ammonium and nitrate take place anymore (Oren, 2001). This suggests that if small amounts of oxygen diffused into the plastic tubes of the anoxic samples

during centrifugation, this did not influence the concentrations in the extraction solution. It also means, the extraction time can be varied to a certain extent, which is an important result since extraction times of 30 to 60 minutes are often not feasible with high sample numbers. Extraction times beyond 180 minutes were not tested in this study as it focused on practical aspects during sample handling. However, one study suggests, that considerably longer extraction times can have effects on the concentration of ammonium in the extraction solution: Esala (1994) observed a 2 to 3.5-fold increase of ammonium concentrations (but not of nitrate concentrations) after 20 hours extraction with 2 M KCl, which was explained by better dispersion of soil clay particles and enhanced diffusion of ammonium from interlayers of clay minerals, which is known to be recalcitrant towards microbial turnover. Therefore, further studies on the extraction time for a quantitative extraction of ammonium are needed.

Extraction of nitrate and ammonium from soil with 0.0125 M $CaCl_2$

During the extraction with 0.0125 M $CaCl_2$ under oxic conditions (Figure 1D), concentrations of both inorganic nitrogen compounds remained stable as well, which supports and extends the findings of Wheatley et al. (1989). The slight drop in ammonium concentrations (0.3 µg N g^{-1} soil) at longer extractions times (30, 60 and 180 min) can be interpreted as random variability rather than loss as the variations are not significant ($p > 0.05$) and due to issues with the extraction efficiency of 0.0125 M $CaCl_2$ that will be discussed below.

The results for the $CaCl_2$ extractions under anoxic conditions (Figure 1C), however, show a significant decrease of nitrate ($p < 0.05$) and significant increase of ammonium ($p < 0.05$) at extraction times of 60 and 180 min. Nitrate decreased from 1.94 µg N g^{-1} soil at 15 min to 0.16 µg N g^{-1} soil at 180 min and ammonium increased from 3.83 µg N g^{-1} soil at 15 min to 4.62 µg N g^{-1} soil at 180 min. As extractant, 0.0125 M $CaCl_2$ with its much lower salinity (0.18% salinity) compared to 2 M KCl, should mimic the typical soil water salt concentration and ionic strength and is thus not suitable (and not intended) for inhibiting microbial activity. Sample stability at extraction times longer than 30 minutes thus cannot be guaranteed with 0.0125 M $CaCl_2$ under anoxic conditions and should be avoided. Under oxic conditions, however, the nitrate concentration is stable for all extraction periods. Usually nitrate is used as electron acceptor in microbial metabolism when all oxygen in the respective environment is consumed (Canfield & Thamdrup, 2009; Zhang & Furman, 2021). As during the oxic extractions, oxygen is present, the microbial community is not expected to perform denitrification and nitrate concentrations therefore are constant during the extraction period of up to 180 min. Under anoxic conditions, however, the microbes start reducing the nitrate to use it as electron acceptor for energy generation and thus nitrate concentrations decline. The parallel but not stoichiometrically congruent increase in ammonium concentration suggests a mixture of denitrification and either mineralization of organic soil N or dissimilatory nitrate reduction to ammonium (DNRA) as the responsible processes.

Nitrate concentrations below the spiked target concentration: sample instability

The extraction of nitrate with 0.0125 M $CaCl_2$ under anoxic conditions yielded nitrate concentrations below the spiked target concentration (Figure 1C). Inorganic nitrogen concentrations in the soil sample before the spike show, that there is hardly any nitrate in the samples (Table 1, data corresponds to concentrations displayed in Figure 1C) so the extracted concentration after the spike should exactly meet the spike concentration. The loss of nitrate under anoxic conditions could be due to degradation in the time between the spike and the start of the extraction, which was up to 30 minutes. The experiment was designed in a way that all extractions should start at the same time point and this time span was needed to weigh all the samples into the extraction tubes before adding the extraction solution. Additionally, as described above, nitrate loss during the extraction with 0.0125 M $CaCl_2$ under anoxic conditions is an issue. This observation is supported by the comparative extraction from the same spiked sample with 2 M KCl, which lies only slightly below the target spike concentration and yielded a 1.37 times higher nitrate concentration than the respective 0.0125 M $CaCl_2$ extraction (Figure 1C). The extractions with both extractants were started at the same time. So most likely, the main part of nitrate loss during extraction with 0.0125 M $CaCl_2$ occurred during extraction and not beforehand. This gives clear evidence, that under anoxic conditions, 2 M KCl is more suitable to conserve present nitrate than 0.0125 M $CaCl_2$. Under oxic conditions, nitrate concentrations extracted with 0.0125 M $CaCl_2$ were stable until the maximum tested extraction time (180 min). In the study by Esala (1994), even at longer extraction times (20 h) nitrate concentrations remained stable.

***Table 1**: Ammonium and nitrate concentrations before and after the spike with ammonium nitrate derived from extractions with 0.0125 M $CaCl_2$ and 2 M KCl from the same sample (extraction time 30 min). Values are mean values from replicate extractions (n = 3) and standard errors are given. Concentration differences before and after the spike were calculated to assess the extraction efficiency of both extractants.*

	Extractant 0.0125 M $CaCl_2$		**Extractant 2 M KCl**	
	oxic	**anoxic**	**oxic**	**anoxic**
	NO_3^- as μg N g^{-1} soil			
Before the spike	3.7 ± 0.09	0.04 ± 0.03	3.62 ± 0.03	0.00 ± 0.01
After the spike	6.69 ± 0.03	2.0 ± 0.2	6.78 ± 0.06	2.8 ± 0.2
Difference	2.99 ± 0.06	1.96 ± 0.17	3.16 ± 0.03	2.8 ± 0.19
	NH_4^+ as μg N g^{-1} soil			
Before the spike	0.9 ± 0.02	2.7 ± 0.1	2.9 ± 0.06	7.0 ± 0.15
After the spike	2.1 ± 0.07	3.6 ± 0.12	5.9 ± 0.12	10.3 ± 0.27
Difference	1.2 ± 0.05	0.9 ± 0.02	3.0 ± 0.06	3.3 ± 0.12

Ammonium concentrations below the spiked target concentration: extraction efficiency

Under oxic conditions (Figure 1D), ammonium extracted by 0.0125 M $CaCl_2$ is underestimated, as the concentrations (2.0 to 2.3 μg N g^{-1} soil) do not meet the spiked target concentration (3.115 μg N g^{-1} soil). From the soil sample used for the comparative extraction with 0.0125 M $CaCl_2$ and 2 M KCl, ammonium was extracted before the spike (Table 1) and afterwards (Figure 1C and D) for both oxic and anoxic conditions. The difference in ammonium concentrations between these time points corresponds to the spiked concentration of 3.115 μg N g^{-1} soil for the extractions with 2 M KCl. This suggests that there was no loss of ammonium in the time between the spike and the start of extractions under both conditions. A certain loss of ammonium during the extraction with 0.0125 M $CaCl_2$ due to the presence of oxygen (nitrification) cannot be excluded but too low ammonium concentrations can also be an issue of low extraction efficiency of 0.0125 M $CaCl_2$. This is suggested by a comparison of the ammonium concentrations extracted with 2 M KCl from the same sample (Table 1). The concentration of ammonium extracted with 0.0125 M $CaCl_2$ (2.1 μg N g^{-1} soil) is only 35.5 % of that extracted with 2 M KCl (5.9 μg N g^{-1} soil) (Figure 1D, filled blue circle). The same phenomenon can be observed under anoxic conditions (Figure 1C), where the 0.0125 M $CaCl_2$ extracted concentration (3.6 μg N g^{-1} soil) is 34.9 % of the concentration extracted by 2 M KCl (10.3 μg N g^{-1} soil). Kuderna et al. (1993) showed, that the ratio of 1 M KCl-extractable ($ammonium_{KCl}$) to 0.0125 M $CaCl_2$-extractable ammonium ($ammonium_{CaCl_2}$) is dependent on the C_{org} content of the respective samples. Pelster et al. (2018) showed that also the clay content of soils governs the fractions of ammonium in the 2 M KCl-extractable and the more readily available water-extractable pool (comparable with the 0.0125 M $CaCl_2$-extractable pool). In the presented study, the soil's high clay content of 32 wt-% is suggested as the reason for the dominance of the $ammonium_{KCl}$ pool. Due to K^+ as competing ion for ammonium for clay mineral sorption sites with a very similar ionic radius (K^+ = 1.33 Å vs. NH_4^+ = 1.43 Å, Kuderna 1992), 2 M KCl effectively extracts all dissolved *and* sorbed ammonium, whereas 0.0125 M $CaCl_2$ presumably only targets dissolved ammonium.

The above discussed 2 to 3.5-fold increase of ammonium concentrations in 20 h extractions with 2 M KCl (Esala, 1994) questions the exhaustiveness of a 2 M KCl extraction after 30 min. However, the here presented numbers (Table 1) with about 100 % recovery of the ammonium spike suggest that for the herein tested soil the 2 M KCl extraction was exhaustive. This topic should be addressed in further studies.

Storage time and conditions

After pre-tests with samples from the described field site, that were stored at room temperature, strongly deviating nitrate and ammonium concentrations were observed (unpublished). The objective of the storage time and conditions experiment was to assess the stability of nitrate and ammonium during short-term sample storage and to develop an operating procedure for sample handling during inorganic nitrogen extractions. Storage under

both oxic and anoxic conditions was each tested at three common storage temperatures (T) 20 °C, 4 °C, and -21 °C. For the handling of oxygen-sensitive samples, it is also important to know the influence of the presence or absence of oxygen on unwanted change in ammonium and nitrate concentrations. Therefore, storage at all three T was tested under both oxic and anoxic atmospheres. The development of ammonium and nitrate concentrations under all tested conditions (Figure 2) and the underlying processes will be discussed in detail in the following paragraphs.

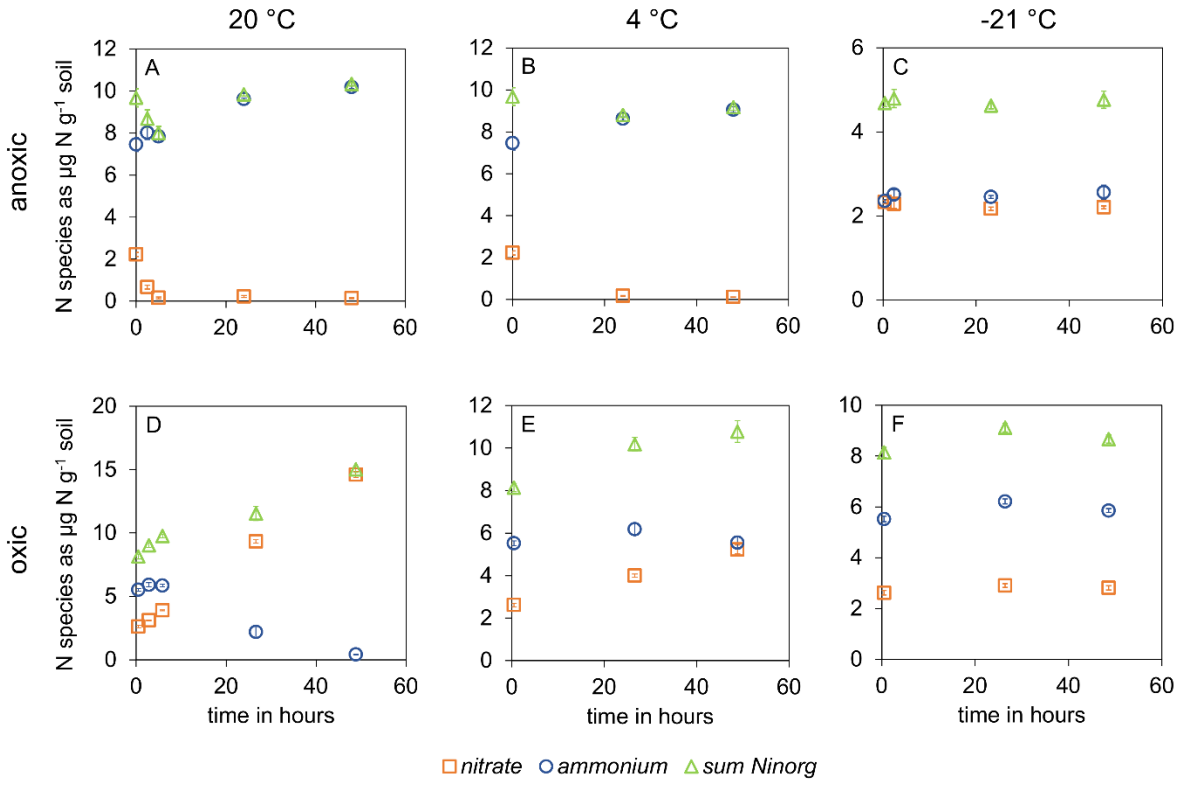

***Figure 2**: Concentrations of inorganic nitrogen species nitrate (orange squares) and ammonium (blue circles) and the sum of both (sum N_{inorg}, green triangles) are shown for all tested conditions: storage at oxic and anoxic conditions and at three different temperatures (20 °C, 4 °C - 21 °C). Concentrations were determined after 24 and 48 hours for all samples and additionally after 2.5 hours for storage at -21 °C (only anoxic) and 20 °C and after 5 hours for storage at 20 °C. Concentrations at zero hours represent the concentrations in the sample right after the spike. Mean values and standard errors of three replicate extractions are displayed for nitrate and ammonium. Note the different ranges of the y scales.*

The findings from all six tested conditions for both inorganic nitrogen species are summarized in Table 2. It was found that both ammonium and nitrate concentrations are instable at 20 °C storage temperature. At -21 °C both species are stable for at least 48 h. At 4 °C nitrate is instable whereas ammonium is well preserved over 48 h. Anoxic or oxic storage of the soil samples alone does not guarantee a sufficient sample preservation. Storage under frozen conditions on the other hand offers a very effective way of proper sample preservation.

***Table 2**: Stability of nitrate and ammonium in soil samples during 48 h storage at three different temperatures (20 °C, 4 °C and -21 °C) under oxic and anoxic conditions. i = instable, s = stable.*

Nitrate	20 °C	4 °C	-21 °C
anoxic	i	i	s
oxic	i	i	s

Ammonium	20 °C	4 °C	-21 °C
anoxic	i	i	s
oxic	i	s	s

Storage at anoxic conditions

Under anoxic conditions at 20 °C (Figure 2A) and 4 °C (Figure 2B), nitrate is completely degraded after 5 h and 24 h, respectively. At the same time a 1.4-fold ($p < 0.05$) and a 1.2-fold ($p < 0.05$) increase in ammonium is observed after 48 h at 20 °C and 4 °C, respectively. At -21 °C slight but insignificant ($p > 0.05$) variations of the concentrations of ammonium and nitrate occurred (Figure 2C). Frozen sample storage guaranteed sample stability over at least 48 h.
Additionally, the sum of ammonium and nitrate (sum N_{inorg}) is depicted and can be used to infer the possible N turnover processes going on at 20 and 4 °C (Figure 2A, B, C). As nitrate is consumed and ammonium is formed, the possible processes are (i) dissimilatory nitrate reduction to ammonium (DNRA) and (ii) a combination of denitrification or DNRA and mineralization of organic nitrogen (N_{org}) to ammonium. DNRA is a 1:1 molar conversion of nitrate into ammonium with the intermediate product NO_2^- (Rütting et al., 2011). Nitrite concentrations ranged between 0.02 and 0.3 µg N g^{-1} soil and were therefore neglected in the mass balance. After storage for 48 h at 20 °C, the amount of formed ammonium 1.2 times exceeds the consumed amount of nitrate and 88.8 % of ammonium is formed between 5 and 24 h while already 90 % of the nitrate was consumed after 5 h. At 4 °C, less ammonium is formed than nitrate is consumed, but ammonium concentrations are still rising between 24 and 48 h by 0.5 µg N g^{-1} soil, whereas nitrate only decreases by 0.05 µg N g^{-1} soil and hence, ammonium is not converted to nitrate at a 1:1 molar ratio. Therefore, a combination of denitrification or DNRA for the loss of nitrate with the mineralization of N_{org} to ammonium is hypothesized as ongoing processes. The identity of the processes of nitrate consumption could be assessed by further analyses of nitrogen and oxygen stable isotopes (Kendall, 1998), of the abundance and expression of functional genes or in isotopic labelling studies.

Storage at oxic conditions

Under oxic conditions, at -21 °C concentrations of all measured species are stable and slight variations ($p > 0.05$) do not show a trend and are parallel for nitrate and ammonium, which can be interpreted as a concentration variation in the subsamples taken for the extractions (Figure 2F). So, the conclusion can be drawn that frozen sample storage preserves inorganic nitrogen concentrations also under oxic conditions.

At 20 °C, however, a 5.6-fold increase of nitrate from 2.6 µg N g^{-1} soil in the initial spiked soil sample to 14.6 µg N g^{-1} soil at 48 h ($p < 0.05$) can be observed (Figure 2D). The increase follows a linear trend ($R^2 = 0.9995$). At the same time, ammonium is nearly fully consumed within 48 h. The ammonium decrease does not start immediately. Concentrations at 0, 2.5 and 5 h only show insignificant variations ($p > 0.05$), but the decrease is obvious at 24 and 48 h ($p < 0.05$). The sum of nitrate and ammonium (sum N_{inorg}) is not stable, in the beginning it is dominated by the higher ammonium concentrations and increases together with increasing nitrate concentrations after 24 and 48 h.
At 4 °C, nitrate concentrations as well increase with a linear trend ($R^2 = 0.9998$), but the increase is slower than at 20 °C: concentrations only double within 48 h ($p < 0.05$). Ammonium concentrations show slight variations, that do not reveal any trend ($p > 0.05$). Sum N_{inorg} shows an increasing trend which is triggered by the increase of nitrate.
For the oxic conditions as well, the data allows to make assumptions about the turnover processes. At 20 °C, nitrate production exceeds ammonium loss. Together with the linear trend of the nitrate increase this indicates, that nitrification of the originally present ammonium cannot be the only source for nitrate but that there must be another source, which is unlimited over the time of the experiment. Mineralization of N_{org} to ammonium and immediate nitrification is the suggested process. The development of both inorganic nitrogen species at 4 °C is similar to the development in the first 5 h in the experiment at 20 °C. It is hypothesized that similar processes occur, but they are slowed down due to the lower temperature.

2.5 Conclusions

Accurate assessment of the concentrations of nitrate and ammonium in soils is important for determining fertilizer need, redox dynamics or microbial turnover processes. As both ammonium and nitrate are involved in complex transformation processes, it is important to ensure the stability of both compounds in soil samples during sampling, storage and extraction.

In the presented study, it was shown, that 2 M KCl as extractant allows to vary the extraction time of standard 30 min from 15 to at least 180 min under both oxic and anoxic conditions. With 0.0125 M $CaCl_2$ as extractant, good results concerning sample stability were achieved for extraction under oxic conditions. At anoxic conditions however, the extraction time must not exceed 30 min on the shaker plus approx. 25 to 30 min for centrifuging and filtration, as longer extraction times led to instabilities of both nitrate and ammonium.
The efficiency of frozen storage (-21 °C) for the preservation of nitrate and ammonium was confirmed for a period of 48 h. On the contrary, even short periods (2.5 h) of unfrozen storage can lead to substantial changes of nitrate and ammonium concentrations. This study extended the knowledge on the methodology of inorganic nitrogen extraction with respect to the effects of availability or absence of oxygen during sample storage: storage under oxic or anoxic conditions alone did not function as appropriate storage method. The corresponding processes

of nitrate and ammonium turnover start to proceed within hours or days at temperatures above 0 °C.

Derived from these experiments, it is recommended to immediately freeze soil samples in the field, e. g., on dry ice, to store them frozen and to extract inorganic nitrogen within two days from sampling. Thawing of the samples before the extraction should be strictly avoided. As 0.0125 M $CaCl_2$ only captures dissolved ammonium and 2 M KCl additionally extracts sorbed ammonium, both methods combined could be used to determine and to distinguish between these two pools of ammonium. The decision, which of the extractants should be used in a certain study depends on the purpose and the questions to be answered and remains subject to the respective experimenter. If the use of 0.0125 M $CaCl_2$ is planned, it is recommended to test the sample stability under 0.0125 M $CaCl_2$ extraction for every new sample location and sample matrix.

Outlook

In the presented study, soil samples from one location were tested. In order to investigate, if the knowledge gained in the presented experiments can be generalized or is dependent on the soil type or soil parameters, the experiments should be repeated with a variety of soils of different type, texture, or mineralogical and elemental composition (e. g., organic matter or clay mineral content).
The study by Esala (1994) hypothesized that an extraction with 2 M KCl for 20 hours led to diffusive release of ammonium from clay mineral interlayers. Thus long-lasting extractions with 2 M KCl should be investigated further to test Esala's hypothesis and if the pool of interlayer ammonium can be quantified this way.

3 Heavy rainfall following a summer drought stimulates soil redox dynamics and facilitates rapid and deep translocation of glyphosate in floodplain soils

Johanna Schlögl, Benedikt Wimmer, Lena Cramaro, Johannes Wirsching, Christian Poll, Holger Pagel, Ellen Kandeler, Carolin Huhn, Christian Griebler, Christine Stumpp, Stefan B. Haderlein

Status in the publication process: Manuscript published.
Schlögl, J. et al., 2022. Heavy rainfall following a summer drought stimulates soil redox dynamics and facilitates rapid and deep translocation of glyphosate in floodplain soils. Environmental Science: Processes & Impacts, 24(5): 825-838. https://doi.org/10.1039/D1EM00527H

Author contributions:
Johanna Schlögl: Conceptualization, Methodology, Investigation*), Data curation, Formal analysis, Validation, Visualization, Writing – original draft preparation; **Benedikt Wimmer**: Conceptualization; Methodology; Investigation, Formal analysis, and Visualization of the glyphosate data; Writing – original draft: Method description glyphosate analysis; Writing – review and editing; **Lena Cramaro**: Conceptualization, Methodology, Investigation, Data curation; **Johannes Wirsching**: Conceptualization, Methodology, Investigation, Writing – review and editing; **Christian Poll**: Conceptualization, Methodology, Investigation, Funding acquisition, Writing – review and editing; **Holger Pagel**: Conceptualization, Methodology, Funding acquisition, Writing – review and editing; **Ellen Kandeler**: Conceptualization, Methodology, Funding acquisition, Writing – review and editing; **Carolin Huhn**: Conceptualization; Methodology; Investigation and Formal analysis of the glyphosate data; Funding acquisition, Writing – review and editing; **Christian Griebler**: Conceptualization, Methodology, Investigation, Funding acquisition, Project administration, Resources, Supervision, Writing – review and editing; **Christine Stumpp**: Investigation and Formal analysis of the δ^2H data; Writing – original draft: method description δ^2H measurement and isotope mass balance; Writing – review and editing; **Stefan B. Haderlein**: Conceptualization, Methodology, Funding acquisition, Project administration, Resources, Supervision, Writing – review and editing.

*) with the help of: Michelle Engelhardt, Bernice Nisch, Marc Jantz and Hartmut Schulz

3.1 Abstract

We present field data on the effects of heavy rainfall after drought on the mobility of glyphosate and redox conditions in a clayey floodplain soil. By applying glyphosate together with deuterated water as conservative tracer in combination with time resolved in situ redox potential measurements, the spatial and temporal patterns of water infiltration and pesticide transport as well as the concomitant changes of the redox conditions were revealed. Our findings demonstrate that shrinkage cracks in dry soils can serve as effective transport paths for atmospheric oxygen, water and glyphosate. The rainfall intensity of a typical summer storm event (approx. 25 mm within one hour) was sufficient to translocate deuterated water and glyphosate to the subsoil (50 cm) within 2 hours. Soil wetting induced partial closure of the shrinkage cracks and stimulated microbial activity resulting in pronounced dynamics of in situ soil redox conditions. Redox potentials in 40 to 50 cm depth dropped permanently to strongly reducing conditions within hours to days but fluctuated between reducing and oxidizing conditions in 10 to 30 cm depth.

Our findings highlight the close link between the presence of macropores (shrinkage cracks), heavy rainfall after drought, redox dynamics and pesticide translocation to the subsoil and thus call for further studies addressing the effects of dynamic redox conditions as limiting factor for glyphosate degradation.

3.2 Introduction

Floodplains are landscape elements of high biogeochemical activity and turnover of natural and anthropogenic compounds (Lair et al., 2009; Venterink et al., 2003). Periodic changes of the water regime induce variations of redox conditions, of the availability of electron acceptors and donors (e. g., oxygen, iron) and thus the sequestration or remobilization and turnover of redox inert (e. g., phosphorus) (Coby et al., 2011) and redox sensitive nutrients (e. g., pentavalent nitrogen in nitrate) and pollutants (Venterink et al., 2003). Floodplain soils in mid-latitudes show pronounced seasonal water dynamics with waterlogged and oxygen-depleted conditions throughout the cold season and extended periods of unsaturated and oxic conditions during summer (Baldwin & Mitchell, 2000; Hefting et al., 2004). Under waterlogged conditions, long residence times for both percolating water and solutes are expected. During and after drought periods in summer and fall, gas exchange with the atmosphere and transport of matter from the surface to the subsoil is facilitated by the formation of shrinkage cracks. Due to climate change with increasing incidents of extreme droughts and precipitation (Coumou & Rahmstorf, 2012; Horton et al., 2016; Perkins et al., 2012), the switch between dry and waterlogged conditions will occur more frequently and with shorter periods also within a season. This will impact not only the water regime in soils but likely also the mobility and transformation of nutrients and agrochemicals in the pedosphere (Borch et al., 2010; Peiffer et al., 2021). The impacts of a rapid wetting after drought due to heavy rainfall on pesticide transport in floodplain soils, however, have rarely been studied and are not well understood.

Macropores such as shrinkage cracks may enhance rapid and irregular infiltration of water, solutes, and particles (Beven & Germann, 2013; Jarvis et al., 2016) as well as gas exchange with the atmosphere. Factors relevant for the occurrence of preferential flow in macropores include pore size, pore continuity and tortuosity (Beven, 1981; Bouma, 1981; Flury et al., 1994; Nimmo, 2021; Skopp, 1981) as well as intensity and quantity of irrigation or precipitation (Bouma & Dekker, 1978). Dry soils initially exhibit a low capacity to take up water which favors water flow in macropores (Hardie et al., 2011; Jarvis et al., 2016; Nimmo, 2012).
Transport along preferential flow paths can be an important pathway for pesticide mobility (Beven et al., 2006; Ciglasch et al., 2005; Flury, 1996; Kasteel et al., 2013). As pesticides largely differ in their physico-chemical properties such as water solubility and affinity to adsorb to the surface of soil mineral particles (Schwarzenbach et al., 2017), their susceptibility to preferential flow also varies (Larsson & Jarvis, 2000). Due to its strong sorption to soil mineral particles (Gimsing & Borggaard, 2002; Gulu Zada, 2021; Sprankle et al., 1975), glyphosate was long regarded to be fairly immobile in topsoil and little susceptible towards leaching to the subsurface (Borggaard & Gimsing, 2008). Nevertheless, significant leaching of glyphosate from soils to tile drains was reported (Kjær et al., 2011; Kjær et al., 2005; Norgaard et al., 2014; Rosenbom et al., 2015; Stone & Wilson, 2006) and the question arises if and under which conditions macropores such as shrinkage cracks facilitate its rapid transport to the subsoil.

As for nutrients and pesticides, also oxygen transport is facilitated through air-filled macropores (Haberer et al., 2012), a process which largely impacts the type and dynamics of biogeochemical conditions in fine-grained soils. Rapid oxygen transport through shrinkage cracks to the subsoil under dry conditions, however, can be terminated by precipitation as shrinkage cracks close due to swelling of clays. In combination with aerobic microbial activity this triggers oxygen consumption, thus lowering soil redox state especially in loamy floodplain soils rich in organic carbon. The presence or absence of molecular oxygen is a key factor for the functioning of microbial communities carrying the metabolic potential for pesticide degradation (Alexander, 1999).

Beside molecular oxygen, floodplain sediments contain alternative electron acceptors for microbial respiration such as iron(oxy)hydroxides. Alternating redox conditions in such soils are often signified by redoximorphic marks in the solid matrix caused by precipitation of redox-active iron minerals (Blume et al., 2016). In contrast to iron(oxy)hydroxides, iron containing clay minerals and soil organic matter (SOM) have only recently come into focus as redox-sensitive soil components (Lau et al., 2015; Tratnyek et al., 2011; Usman et al., 2018). They are capable of reversibly accepting and releasing electrons without leaving visible redoximorphic features and without dissolution or the formation of secondary phases (Aeschbacher et al., 2010; Byrne James et al., 2015; Gorski et al., 2012). Furthermore, SOM and Fe-species are highly redox-active towards commonly used redox probes (Aeschbacher et al., 2011; Sander et al., 2015). Thus, in the presence of such redox sensitive phases, field monitoring

of redox potentials (E_H) provides meaningful information on the redox state and the redox dynamics despite the well-known problems of interpreting measured E_H values due to mixed potential formation and redox disequilibria (Patrick et al., 1996; Peiffer et al., 1992; Zhang & Furman, 2021).

We hypothesize that (i) shrinkage cracks are preferential pathways for water and for glyphosate (as a model compound for strongly sorbing pesticides) leaching into the subsoil, and (ii) their closure during wetting of the soil controls oxygen supply and thus the dynamics of redox potentials. As biodegradation of glyphosate is strongly impaired under anoxic conditions (Kanissery et al., 2015; Sørensen et al., 2006), it is important to understand the interplay of shrinkage crack dynamics, oxygen supply and glyphosate leaching to assess the fate of glyphosate in subsoils.
We applied glyphosate to a dry Gleysol exhibiting a network of shrinkage cracks that developed after summer drought periods. We simulated a heavy rainfall event with irrigation water that was labelled using deuterated water (D_2O) as conservative tracer to quantitatively follow water infiltration. Glyphosate concentrations and the hydrogen isotope ratios (δ^2H) of soil pore water were determined along soil cores (50 cm) taken at spots with and without shrinkage cracks present at the soil surface. Changes of redox conditions indicating the dynamics of oxygen supply and consumption were recorded in situ by means of permanently installed and spatially resolved sensors. We present data on soil water dynamics together with glyphosate concentrations along soil cores immediately after irrigation and the response of in situ redox measurement to the simulated precipitation for 14 days.

3.3 Materials and Methods

Field site

The field site was in the Ammer valley floodplain approx. 7 km west of Tübingen (TÜ), SW Germany (lat. 48.521266, long. 8.972687, 394 m a.s.l.). The Ammer catchment is located in the South-Western German Escarpment within the geological units of the Middle and Upper Triassic. The west of the floodplain is dominated by limestones from the Muschelkalk units, the east lies within Keuper units mainly comprising terrestrial sediments such as sand-, mud- and dolostones including gypsum (Geyer et al., 2011; Grathwohl et al., 2013; Martin et al., 2020; Schwientek et al., 2013).
The floodplain with the field test site is in the eastern part of the catchment. It is stretched in a west-east direction and is enclosed by Keuper hills on its northern and southern rims. The hydrostratigraphy comprises (from top to bottom) a regional aquitard (Upper Clay Aquitard), a confined aquifer made of tufa sediments (Tufa Aquifer), another regional aquitard (Lower Clay Aquitard) and another aquifer made of mainly gravel and clay sediments (Gravel Aquifer) (Martin et al., 2020). The Upper Clay Aquitard, which comprises the investigated soil, consists of fine-grained clay mineral-rich alluvial sediments from the surrounding Keuper hills (Landesamt für Geologie Rohstoffe und Bergbau Baden-Württemberg, 2021a, 2021b). On

average it is 2 m thick and water-saturated in its lower half throughout the year (Martin et al., 2020). The soil is characterized as Gleysol (Landesamt für Geologie Rohstoffe und Bergbau Baden-Württemberg, 2021a) and some cores from the study from Martin et al. (2020) showed typical gleyic properties (personal communication with S. Martin), i. e., color-distinguishable oxidized and reduced horizons (IUSS Working Group WRB, 2015) (Figure A18, Appendix A, Section A1). With the cores (50 cm) taken for the presented study, only the Ah and the Go horizons were sampled.
The soil has a uniform texture of 11 ± 4 wt% of sand, 56 ± 6 wt% of silt and 32 ± 4 wt% of clay over the first 50 cm of depth (Figure A19, determined following DIN EN ISO 17892-4 (DIN Deutsches Institut für Normung e. V., 2017), detailed protocol see Appendix A, Section A2) and a soil organic matter (SOM) content (quantified as total organic carbon (TOC)) of 2 – 2.5 wt% in the upper 15 cm and around 1 wt% between 20 and 50 cm depth (Figure A20, for details on the methodology see Appendix A, section A3). The soil pH varied from 7.0 to 7.3. It was measured on six samples, two each from depth segments 0-10 cm, 20-30 cm and 40-50 cm from irrigated plots. The pH was determined after 30 min of stirring in a 1:1 (v:w) mix of deionized water and soil.

We performed the experiment on a plot of arable land immediately after the harvest of summer barley during summer 2019 (more details in Sections "Meteorological conditions" and "Plot treatment"). Information on prior use and treatment comes from personal communication with the farmer: during winter 2018/19, a catch crop (radish and mustard) was cultivated on the agricultural field and in February 2019 after frost, it was incorporated 10 cm deep with the cultivator. Additionally, during winter 2018/19, the field was fertilized with horse manure (20 t ha^{-1}), and in spring 2019, 300 kg ha^{-1} of calcium ammonium nitrate fertilizer (27% N) was applied. During the cultivation of summer barley, the field was treated with the herbicide Ariane-C (active ingredients: 100 g L^{-1} Fluroxypyr (as Methylheptylester 144 g L^{-1}), 80 g L^{-1} Clopyralid + 2,5 g L^{-1} Florasulam). The field had not been treated with glyphosate for 10 years before our study. Residues of glyphosate from previous applications or spray drift were not detected in prior samples.

Meteorological conditions

The experimental site lies in a region of temperate oceanic climate with a long-term mean precipitation of 720.9 mm y^{-1} and a mean annual temperature of 9.4 °C (German Meteorological Sevice (DWD), 2021). Weather data (hourly precipitation and temperature, Figure A21) was retrieved from a station in TÜ-Unterjesingen (lat. 48.52950, long. 8.98380, 439 m a.s.l., which is 45 m higher than the actual experimental site) (Agrarmeteorologie Baden-Württemberg, 2021): The experiment took place from 15th of July to 30th July 2019. The two-weeks period before the experiment was dominated by maximum temperatures above 20 °C on all but two days and rainfall events on three days (9.1, 5.1, and 33.1 mm, respectively). All of them were of moderate rainfall intensity according to the

classification of the American Meteorological Society (American Meteorological Society, 2021). During the experiment, minimum temperature was 10.2 °C during the night (night average 17.7 °C) and maximum temperature was 36.3 °C during daytime (day average 24.5 °C). Reference evapotranspiration (ETo) for the whole month July 2019 was calculated as 4.2 mm day^{-1} with the ETo calculator of the Food and Agriculture Organization of the United Nations (FAO) following the FAO guideline (Allen et al., 1998) including data on temperature (in °C, monthly min, max, and mean), relative humidity (in %, monthly min, max, and mean), and solar radiation (in Wh m^{-2}, monthly mean) (Appendix A, Section A5, Table A4). Between 15th and 31st July, we recorded 12 days with T_{max} > 25 °C, from which 6 had T_{max} > 30 °C. Throughout the experiment, only two natural rainfall events occurred with a short rainfall event on 21st July 2019 from 2:00 until 5:00 am (2.5 mm) and a heavy rainfall event between 26th July 2019 8:00 pm and 27th July 2019 5:00 am with in total 24.7 mm of precipitation (Figure A21). During both events, the dry control plots were covered by plastic covers.

Experimental setup

Plot design

The experimental area (Figure 3) was divided into nine experimental plots, which were arranged as a Latin square with three different treatments. All plots were of 2.4 m lateral length and were separated by 50 cm stripes to allow access. The plots were shielded by plastic edges to prevent runoff from irrigated plots to dry control plots. Within each plot, an inner sampling area of 2 m x 2 m was defined to exclude boundary effects.

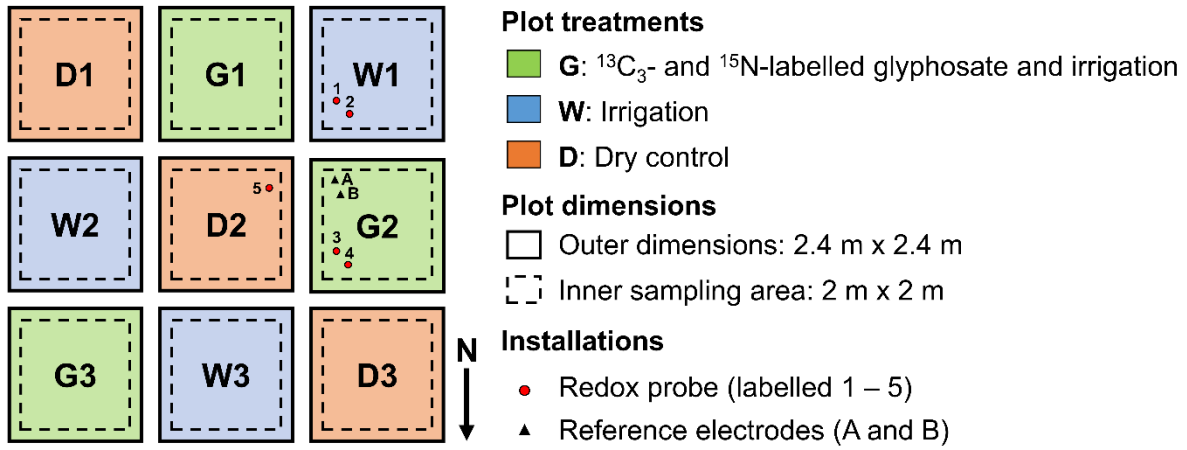

***Figure 3**: The experimental area comprised nine plots with three different treatments arranged as a Latin square: dry control plots (D1-3, orange), plots with a simulated heavy rainfall event (water ^2H-labelled) and two weeks of light irrigation (non-labelled) (W1-3, blue) and plots with a single application of glyphosate one day before the simulated heavy rainfall event and the two-week irrigation period (G1-3, green). Five redox probes (red circles 1-5) and two reference electrodes (black triangles, A and B, where B served as control for the system) were installed for in situ monitoring of redox potentials.*

Three different plot treatments were realized (Figure 3): i) G plots were sprayed with glyphosate and 24 h later G and ii) W plots were artificially irrigated to simulate a heavy rainfall event after a drought period; iii) dry plots (D) without any treatment served as controls (see details in Section "Plot treatment").

Plot treatment

The irrigation took place from the 16th to 30th July 2019 according to the irrigation scheme in Figure 4. The day of the simulated heavy rainfall event (16th July) was defined as Day 0 of the experiment. All plots were covered one week before the start of the irrigation to secure dry soil conditions at start. One day before the start of the irrigation, 215 mg m^{-2} of $^{13}C_3$-^{15}N-glyphosate, which is equivalent to 2.1 kg ha^{-1}, was sprayed directly onto the soil surface on the G plots (Figure 3) with a manual sprayer (Schachtner, Ludwigsburg, Germany) to allow sorption equilibration on the soil mineral particles to take place before irrigation. The use of ^{13}C- and ^{15}N-labelled glyphosate allowed to distinguish between potential residual and experiment-associated glyphosate.

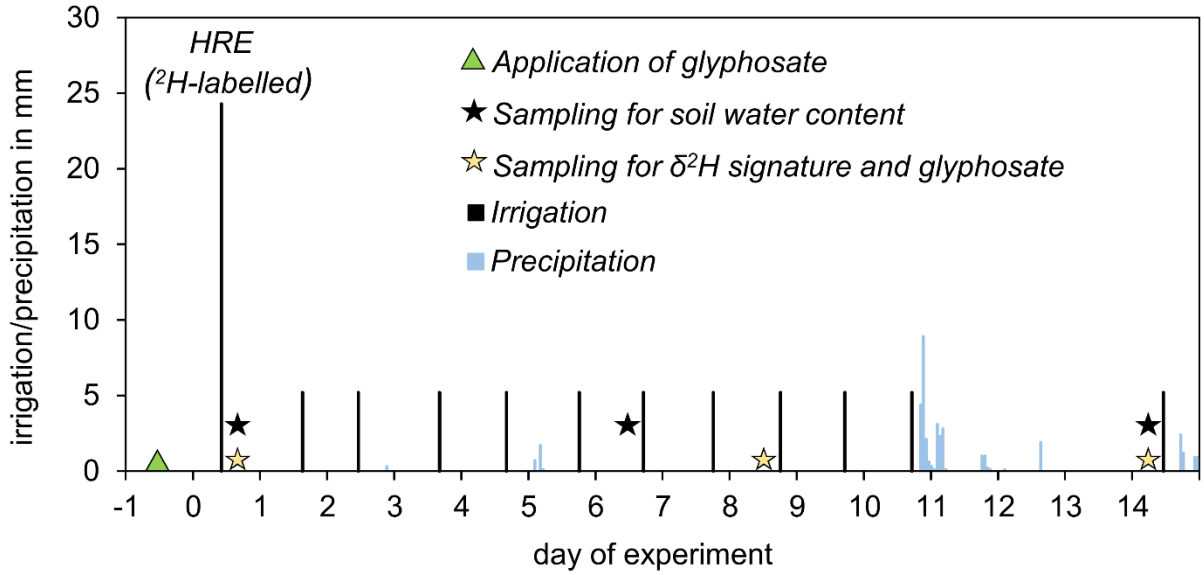

Figure 4: *Irrigation and sampling scheme. The experimental procedure included a 14-day irrigation period with application of glyphosate on particular plots on Day -1 (green triangle) and a simulated heavy rainfall event (HRE) with ²H-labelled irrigation water on Day 0 followed by light daily irrigation with non-labelled water (black bars; height indicates irrigation intensity). Natural precipitation is shown as light blue bars; height indicates intensity). Sampling days for different analytes and parameters are labelled with black and golden stars (see legend).*

After 24 h, a heavy rainfall event (defined by a rainfall intensity of 7.6 to 50 mm per hour (American Meteorological Society, 2021)) was simulated on G and W plots by irrigation with 24.3 mm deionized water over approx. 1 hour using watering cans. The irrigation water of the initial heavy rainfall event was labelled with deuterated water (D_2O) serving as conservative tracer. 2 L of deuterated water (99.9 atom%, Carl Roth, Germany) were added to the irrigation water (1000 L) resulting in an input isotope signature of δ^2H = 12730‰ vs. Vienna Standard

Mean Ocean Water (VSMOW). During the subsequent 10 days and on Day 14, 5.2 mm day^{-1} of deionized water without D_2O spike were irrigated as indicated in Figure 4. The repeated small daily irrigations together with the natural precipitation at Days 11 to 13 were meant to compensate the daily evapotranspiration to maintain closure of large shrinkage cracks.

Samples

Soil cores were collected with a soil corer probe (Humax/GreenGround, Hasle-Rüegsau, Switzerland) and retrieved within polyvinyl chloride (PVC) liners of 50 cm length and 3.5 cm in diameter. The resulting holes were filled with bentonite. The first soil core samples were taken two hours after the simulated heavy rainfall event. Samples from all plots were either taken from sites where shrinkage cracks were initially visible directly at the surface or at a distance of at least 25 cm from the next crack in the bulk soil ("sampling type"). The course of the initially present shrinkage cracks was marked before the onset of the experiment, so that in later stages of the experiment, the distinction between the two sampling types was still possible. Of course, even when shrinkage cracks were not visible at the soil surface, shrinkage cracks entering the core from the side may still be present. This issue will be addressed in more detail in the Discussion.
Sample labelling included the treatment (glyphosate (G), irrigation (W), dry (D)), where experimental triplicates of each treatment were denoted with numbers 1, 2, and 3, respectively (Figure 3). Further sample labelling included the "sampling type" (at a shrinkage crack (c) or in bulk soil (b)), and sampling day (T + number) (Table 3). As an example, *G1bT3* refers to a sample from the glyphosate + water plot 1 taken from bulk soil at the time point of Day 3. *GbT3* refers to a set of values from all plot triplicates or the mean value of the three replicate G plots taken from bulk soil on Day 3, depending on the context.

***Table 3**: Code for samples from the different treatments and of different sampling types.*

treatment	
water + glyphosate	G
water	W
dry	D
sampling type	
bulk	b
shrinkage crack	c
time/day	T + number

For the analysis of soil water δ^2H ratios, cores were taken from W plots along shrinkage cracks and from G plots in bulk soil on Days 0, 8, and 14 (WcT0/8/14 and GbT0/8/14). Additionally, soil cores were taken from D plots to determine the natural background δ^2H (DcT0/8/14). The cores of the first day with glyphosate applied (GbT0) were also analyzed for glyphosate in the

depth intervals 0 – 10 cm, 20 – 30 cm and 40 – 50 cm. Soil water content was determined on cores from W and D plots taken along shrinkage cracks on Days 0, 6 and 14 (W/DcT0/6/14). The analysis of grain size distribution and SOM was conducted on cores DcT10 and WcT14. In the field, all cores were stored on dry ice immediately after sampling to minimize further chemical or microbial processes. Soil cores were stored in the lab at -80 °C until analysis for soil water δ^2H and glyphosate and at -20 °C for grain size and SOM analysis.

In situ monitoring of redox potentials

To monitor in situ soil redox potentials, multilevel redox probes (PaleoTerra, Oijen, The Netherlands) were installed on plots of all three treatment types (Figure 3). The probes had a total length of 1.20 m and consisted of fiberglass and epoxy tubes with in total 10 platinum (Pt) redox electrodes each. For installation, we first drilled a hole with a 2 mm smaller diameter than the probes vertically into the ground. The probes were then installed with the first Pt electrode at a depth of 5 cm, followed by distance intervals of 10 cm below ground level (bgl). Two redox probes each were installed on plots W1 and G2 at a distance of 20 cm (Figure 3). After installation, the readings of neighboring probes were in close agreement.
Redox potentials were measured as E_{meas} versus an Ag/AgCl field reference electrode (KCl sat., E^0 = 0.199 V) (PaleoTerra, Oijen, The Netherlands) and are reported versus the standard hydrogen electrode (SHE, E^0 = 0 V, by definition) as $E_{in\ situ} = E_{meas} + E^0_{KCl,sat}$. Measurement precision was ± 10 mV. A temperature correction was not done as (i) no conversion factors were available for the used reference electrodes and (ii) the estimated change of E_{meas} due to temperature correction lies within the measurement precision and is thus small compared to the expected redox dynamics. Redox probes and electrodes were connected to a CR 1000 data logger (Campbell Scientific, Logan, Utah, US), which logged redox potentials in all depths every 30 minutes throughout the experiment. A second reference electrode was installed as control for the system (E_{meas} = 0 ± 10 mV). We will use the following ranges of measured E_H values to characterize the overall soil redox conditions at circumneutral pH: oxidizing (> +400 mV vs. standard hydrogen electrode), weakly reducing (+400 to +200 mV), moderately reducing (+200 to -100 mV) and strongly reducing (< -100 mV) (Mansfeldt, 2003).

Soil water content

Soil water content was determined gravimetrically for irrigated (W) and dry (D) plots. To this end, soil cores were taken vertically including shrinkage cracks and cut in 5 cm intervals between 0 and 10 cm and in 10 cm intervals between 10 and 50 cm. Samples were weighed in triplicates of approx. 1.500 g (scale accuracy ± 0.001 g) of field wet soil samples before and after freeze drying. The ratio of water loss to dry sample (g g^{-1}) was calculated. The soil water content on the dry plots on Day 0 was used as a reference and denoted "initial soil water content".

δ^2H signature of soil water

Hydrogen (δ^2H) isotope ratios of pore water in the soil samples were measured using H_2O(liquid)–H_2O(vapor) pore water equilibration and cavity ring-down laser spectroscopy (Picarro L2120-i and L2130-i) (Wassenaar et al., 2008). Frozen core samples (50 cm, core set GbT0) were sliced into 10 cm segments. For the determination of the background value the uppermost core segment (0 – 10 cm) was ignored as it could have been impacted by wind drift of water vapor from irrigation water or evaporation. Aliquots of these segments (between 66 g and 170 g) were placed into 1 L Ziploc Freezer bags, double-bagged and stored at 4°C in the laboratory. For analysis, the bags were filled with dry air in the laboratory and equilibrated for three days before analysis. This allows establishing an isotopic equilibrium between the water vapor in the headspace and the pore water. Three sample measurements were bracketed by the analysis of internal standards for calibration (10 mL water with known isotopic composition in freezer bags). Each sample analysis was monitored over up to 30 min until reaching a plateau indicating stable conditions within the expected measurement accuracy. The average value for the last minute was recorded with stable conditions defined as standard deviations of < 1.0‰ for δ^2H for water vapor. Stable isotope values are given as isotope ratios relative to the international standard (VSMOW) and presented in the delta notation in ‰, δ ‰ $= ((R_{sample} - R_{standard})/R_{standard}) * 1000$, with R as the isotope ratio $^2H/^1H$ of the sample and the VSMOW standard.
Afterwards, the samples were dried at 105°C until reaching constant weight to determine the soil water content gravimetrically comparing wet and dry weight. These data on gravimetric water content were also used for the following mass balance calculations.

Water mass balance

A water mass balance approach was used to calculate the contributions of the 24.3 mm heavy rainfall event to the profiles and individual depth segments assuming that the irrigation mainly causes a change in water storage and leaching below 50 cm is small. The amount of water volume change was calculated from measured gravimetric water contents in cores from W, G and D plots on Day 0 which were converted into volumetric water contents from known bulk densities in the individual depths. This will give the increase in water content and thus the increase in water volume per m² due to irrigation compared to the dry plots.

Isotope mass balance

To assess the penetration depth of the irrigation water 2 hours after the irrigation event, the fraction of D_2O-labelled irrigation water in soil water present in every i-th depth segment ($f_{IW,zi}$), was calculated using a two-component mixing approach (i. e., isotope mass balance):

$$f_{IW,z_i} = \frac{\delta^2 H_{z_i} - \delta^2 H_0}{\delta^2 H_{IW} - \delta^2 H_0}$$

where δ^2H_{zi} is the measured isotope ratio of the *i*-th depth segment, δ^2H_{IW} is the isotope ratio of the heavy rainfall event water (i. e., 12730‰) and δ^2H_0 is the background average δ^2H before irrigation (i. e., -47.6‰). The amount of irrigation water in each depth interval was calculated from the water volume $V_{w,zi}$ multiplied by the fraction of irrigation water $f_{IW,zi}$ in each depth interval. The water volume was determined from the analysis of the gravimetric water content in the cores used for isotope analysis converted to volumetric water contents from known bulk densities in the different depths.

Elemental composition

Si and Al were extracted by alkaline fusion (DIN Deutsches Institut für Normung e. V., 2003). Ca, Cu, Fe, K, Mg, Mn, P were extracted by aqua regia dissolution (VDLUFA, 2011). Concentrations were determined from the extraction solutions by ICP-OES (inductively coupled plasma optical emission spectroscopy, Agilent 5110, Waldbronn, Germany).

Glyphosate Analysis

For glyphosate analysis, representative subsamples from the respective core sections (see Section "Samples") were lyophilized. Two aliquots of 200 mg of the freeze-dried sample were extracted with 0.5 mL of an aqueous solution containing 50 mM of both NaOH and Na_2HPO_4 upon sonication. This newly developed method is described in detail elsewhere (Wimmer et al., 2022). To quantitate $^{13}C_3$,^{15}N-glyphosate applied to the field, non-labelled glyphosate was added to the extraction medium with a final concentration of 0.5 mg L^{-1}. After centrifugation, the supernatant was acidified with aqueous HCl, precipitates were removed by centrifugation and the remaining supernatant was injected for analysis by capillary electrophoresis-mass spectrometry (Wimmer et al., 2020). Separation was accomplished on a bare fused silica capillary of 68 cm length at a separation voltage of -30 kV and 50 mbar pressure. The background electrolyte was made of 175 mM formic acid titrated to pH 2.8 with ammonia; mass spectrometric detection was accomplished in negative ionization mode. The final concentration was calculated using the signal area of labelled and non-labelled glyphosate considering the liquid-solid ratio (0.5 mL : 200 mg) chosen for the extraction.

3.4 Results and Discussion

Shrinkage crack dynamics and water infiltration pattern

The soil at the studied field site showed numerous shrinkage cracks with a horizontal extension of several decimeters and widths of up to 1 to 2 cm at the start of the experiment (Figure 5A) due to a dry period over several weeks before the onset of our experiment. Such shrinkage cracks form preferential flow paths enabling fast and deep penetration of irrigation water, solutes, and fine particles (Beven & Germann, 2013; Jarvis et al., 2016; Nimmo, 2021). Major structural heterogeneities and thus preferential flow paths at the soil surface were

absent from Day 3 on (Figure 5B). The high clay content of the soil resulting from weathering of Keuper bedrocks (Landesamt für Geologie Rohstoffe und Bergbau Baden-Württemberg, 2021a, 2021b) led to a fast swelling of the soil upon wetting. During the following days, only narrow surficial shrinkage cracks formed during daytime as a result of the diurnal evaporation (Figure 5C). These small shrinkage cracks closed rapidly after the daily irrigations of 5.2 mm (Figure 5D).

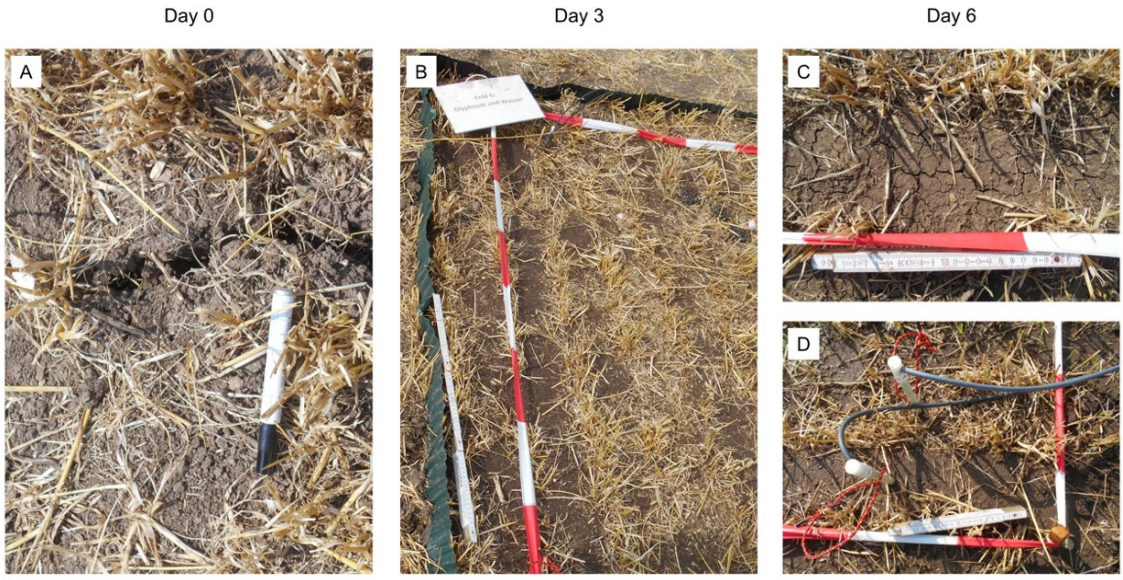

Figure 5*: Dynamics of shrinkage cracks during the experiment.* ***A****. Shrinkage cracks (approx. 1 cm wide) on Day 0 at a dry control plot.* ***B****. Disappearance of surficial shrinkage cracks on Day 3, following the irrigation scheme in Figure 4 (length of red bands of the barrier tape is 20 cm).* ***C*** *and* ***D****. Recurring formation of narrow shrinkage cracks (few mm wide) during daytime due to high water evaporation rates (panel C) and immediate closure of these cracks (panel D) during a daily 5.2 mm irrigation event on Day 6 (length of metering rule is 24 cm).*

The dynamics of opening and closure of shrinkage cracks are in line with the gravimetric soil water content, which we determined for Days 0, 6 and 14 from soil cores taken along shrinkage cracks comparing results for irrigated (W and G) and dry (D) plots (Figure 6): due to the drought period preceding the irrigation experiment, the initial gravimetric soil water content was low throughout the profile as shown in Figure 6 exemplarily for the dry plots on Day 0 (dataset DcT0), with lowest values (0.12 ± 0.03 g g^{-1}) in the top 5 cm. The water content increased rapidly with depth and was almost twice the value of the top interval in the section 10 – 20 cm and below reaching 0.20 ± 0.02 g g^{-1}. On the dry plots the water content further decreased by 0.03 – 0.04 g g^{-1} until Day 14 (DcT14) at all observed depths due to high temperatures and evapotranspiration.

On the irrigated plots, the gravimetric water content in the uppermost section (0 – 5 cm) was 0.26 ± 0.02 g g^{-1} on Day 0 (WcT0) and thus more than twice the initial soil water content (DcT0). Water content increased by 1/3 compared to DcT0 in the following section 5 – 10 cm (0.23 ± 0.02 g g^{-1}) due to heavy irrigation on Day 0 (Figure 6). Subsequent light daily irrigation (5.2 mm day^{-1}) slightly increased the water content of the uppermost section to 0.31 g g^{-1} ± 0.01 g g^{-1} until Day 6 (WcT6) when it reached a stable value despite continued light daily irrigation

(WcT14). The G plots (GbT0) showed a similar behavior (Figure 6). The strong increase in water content induced swelling of the soil and closure of the shrinkage cracks (Figure 5). Generally, on W and G plots the water content gradually decreased with depth within the upper 10 cm. In deeper layers (20 to 50 cm), water content increased by 0.02 – 0.04 g g^{-1} (WcT0 and GbT0) following the heavy irrigation on Day 0 compared to the initial soil water content (DcT0) but then remained nearly constant during the experiment (WcT6/14) (0.22 ± 0.01 g g^{-1}).

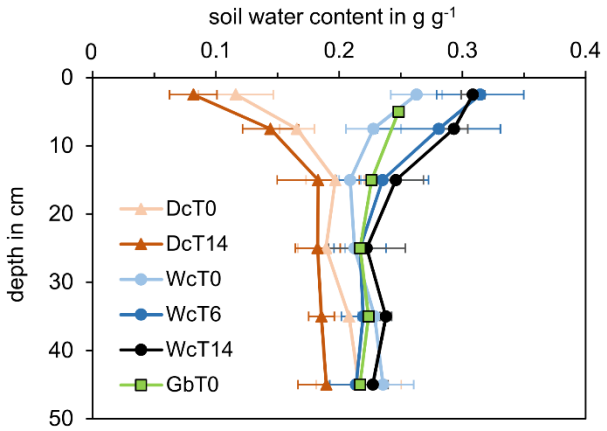

***Figure 6**: Gravimetric soil water contents from spots where shrinkage cracks were visible at the surface of dry plots (Dc, orange triangles) and irrigated plots (Wc, blue circles) and from bulk soil from glyphosate + irrigated plots (Gb, green squares) from Days 0, 6 and 14 (T0, T6 and T14, respectively) are displayed. Standard deviations were calculated from plot triplicates. The color code from light to dark colors represents the time course of the experiment from Day 0 to Day 14.*

The D_2O spike of the irrigation water allowed us to assess the water distribution along the soil profile and to evaluate heterogeneities of the infiltration pathways both in bulk soil and along shrinkage cracks. Note, that the background δ^2H value is -47.6‰ on average. The mean (n = 3) δ^2H isotope values (Figure 7) illustrated the progression of the irrigation water during the experiment. On Day 0, right after the first irrigation pulse, highest δ^2H ratios were present in the top layer, but elevated δ^2H values also were recorded through the entire soil profile. Throughout the irrigation experiment (Day 8 and 14), isotope ratios decreased in the top layers whereas the δ^2H values in the deeper layers of the profile were still clearly showing a labelling (Figure 7A to C). The standard deviations of the averaged (n = 3) δ^2H values decreased from Day 0 to Day 14 and when comparing results for shrinkage cracks vs. bulk samples (Figure 7). This can be rationalized by the pronounced heterogeneity of the initially dry soil structure due to large shrinkage cracks providing an extended network of preferential flow paths. These preferential flow paths led to an uneven water infiltration during the initial heavy irrigation pulse on the dry soil. Upon closure of the shrinkage cracks (Figure 5C and D), the distribution of the tracer in both bulk soil and shrinkage crack samples became more uniform (Figure 7B and C) by mixing of water from the macropore region with the surrounding soil matrix.

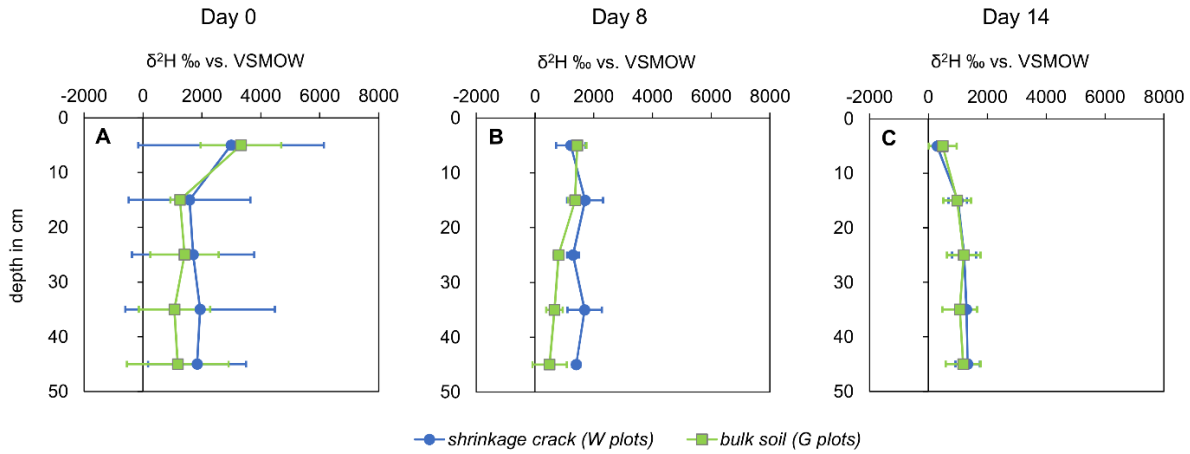

***Figure 7**: δ²H ratios of soil water after the irrigation pulse spiked with D_2O (δ²H = 12730‰ vs. VSMOW). Mean values and standard deviations of three cores each from irrigated plots (W) sampled along shrinkage cracks (blue circles) and from plots treated with glyphosate (G) sampled in bulk soil (green squares) at Days 0, 8 and 14 (Panels A to C). δ²H ratio in soil water on dry plots (i. e., background before irrigation) was on average -47.6‰ vs. VSMOW.*

The water balance (Figure A22A and B) (considering average values from datasets DcT0 and WcT0/GbT0, Figure 6) indicated that on W and the G plots 51.8 % (i. e., 12.6 mm) and 53.4 % (i. e., 13.0 mm) of the 24.3 mm irrigation were present in the segment 0 – 10 cm, respectively, two hours after the simulated heavy rainfall event. The small increases of soil water content of 0.02 – 0.04 g g^{-1} in each of the three 10 cm thick segments between 20 and 50 cm accounted for 12.3 % (approx. 3 mm) of the applied irrigation water per depth segment. In total, 95.4 % (W) and 95.8 % (G) (i. e., 23.2 mm and 23.3 mm) of the irrigation water were recovered in the upper 50 cm two hours after the simulation of the heavy rainfall event on Day 0.

Furthermore, isotope mass balances for individual cores from W and G plots (WcT0 and GbT0) (Figure A22C and D) were determined from the δ²H ratios. Recoveries were 41.5 to 74.4 % of the irrigation water (i. e., 10.1 to 18.1 mm) for 4 out of 6 individual soil cores (from plots W1, W3, G1, and G2). Two cores (from plots W2 and G3), however, showed irrigation water recoveries of 238 and 148 %, respectively (i. e., 57.9 mm and 36.1 mm). The average recovery from the W plots was 26 ± 27 mm (W_avg, Figure A22C) and 22 ± 12 mm (G_avg, Figure A22D) from the G plots. These average values closely matched the applied 24.3 mm and thus, on average, the water and the isotope mass balances agreed well. The high standard deviations, however, reflect the large differences between the individual plots and thus a substantial heterogeneity of the macropore network below ground. In good agreement with the water mass balances, the mean isotope mass balances W_avg and G_avg (Figure A22C and D) also showed that 41 – 57 % (i. e., 10 – 14 mm) of the irrigation water reached depths of 20 to 50 cm within two hours after the simulated heavy rainfall event. These numbers also vary strongly between individual soil cores and corroborate the uneven infiltration along preferential flow paths. The small fraction of the irrigation water that is missing in in some of the cores likely percolated below the sampling depth of 50 cm or escaped the plots by lateral transport through shrinkage cracks as indicated by the high recoveries of 238 % and 148 % in cores W2 and G3.

Vertical distribution of glyphosate and D_2O in individual soil cores after the heavy rainfall event (Day 0)

Glyphosate was sprayed manually on selected plots of the field site 24 h prior to the first irrigation pulse. In Figure 8, we compared glyphosate concentrations (sum of sorbed and dissolved glyphosate) vs. fractions of D_2O-labelled irrigation water in soil water in %.

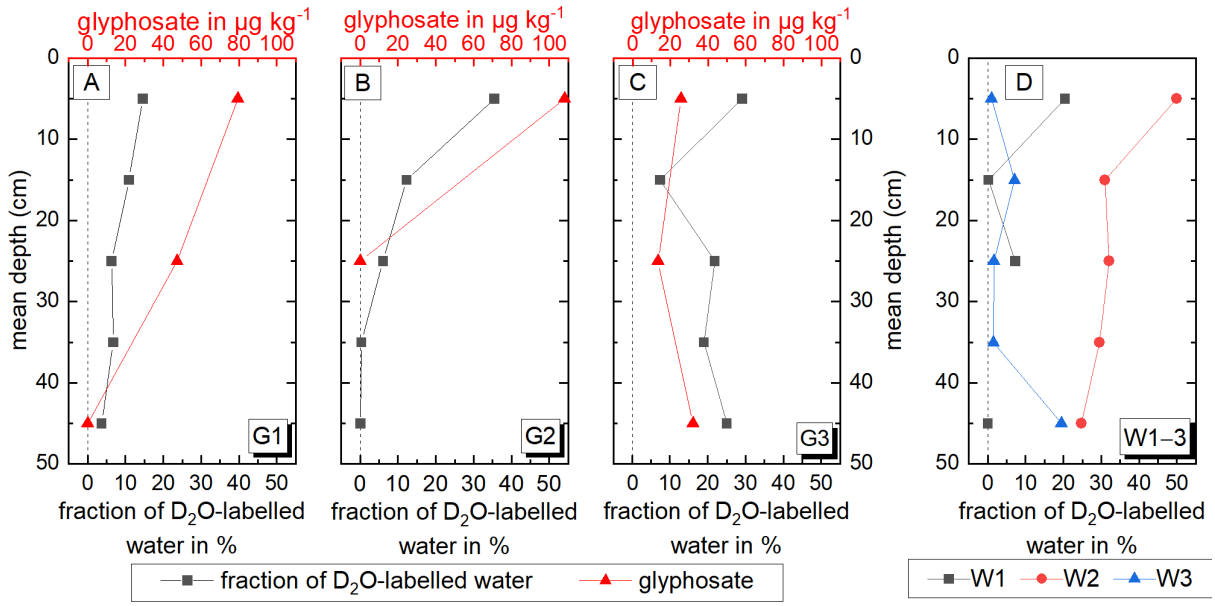

***Figure 8**: **A – C**. Fraction of D_2O-labelled water in soil water in % (black squares, black horizontal axis) and glyphosate concentrations in µg kg^{-1} (red triangles, red horizontal axis) from plots G1, G2 and G3 (from bulk soil) on Day 0 measured in aliquots of the same cores for a direct comparison. **D** (WcT0, but separate data for plots 1-3). Fraction of D_2O-labelled water in soil water in % in cores from all irrigated plots (along shrinkage cracks) on Day 0 (W1, black squares; W2, red circles; W3, blue triangles).*

The depth distributions of the conservative tracer and the pesticide were similar (Figure 8A to C, Figure A23): cores from plots G1 and G2 (bulk soil) showed highest concentrations in the top 10 cm and a steady decrease of concentrations with depth (Figure 8A and B). In contrast, the core from plot G3 (bulk soil) showed an elevated percentage of irrigation water and elevated concentrations of glyphosate in the subsoil at the bottom of the profile (Figure 8C). The cores taken from W plots at spots where shrinkage cracks were visible at the surface (WcT0) also showed elevated percentages of D_2O-labelled water in topsoil (W1 and W2) but also in the subsoil (W2 and W3) shortly after the heavy rainfall event (Figure 8D).

As glyphosate strongly sorbs to the soil matrix (Gimsing & Borggaard, 2002), strong retardation of the compound on the soil surface and in the topsoil is expected when matrix flow is the dominant transport process (Sprankle et al., 1975), both under saturated and unsaturated conditions. However, high glyphosate concentrations occurred in the subsoil already two hours after the first irrigation pulse. The rapid and irregular vertical transport of labelled water together with glyphosate suggests that slow matrix flow through the fine-

grained soil was not the major transport mechanism, because transport through advective flow only, would leave glyphosate in the upper few cm (given a porosity of 0.5 it would be the upper 5 cm).

The depth profiles of D_2O-labelled irrigation water in individual soil cores on Day 0 parallel glyphosate depth profiles (Figure 8, Figure A23). Together with the high standard deviations of δ^2H values on Day 0 (Figure 7) these findings are consistent with the presence of an extended network of macropores in the subsurface both in soil cores that included shrinkage cracks at the surface and in bulk soil cores. The short time span (two hours) between irrigation and detection of labelled water and glyphosate in the subsoil suggests that the large shrinkage cracks initially present (Figure 5) served as preferential flow paths for irrigation water and glyphosate into deeper soil levels following the heavy irrigation. The unknown and irregular distribution of macropores below ground hampers the prediction of glyphosate translocation processes at the centimeter scale. These structural heterogeneities, however, levelled out over space (on the meter scale) and time due to closure of the large shrinkage cracks after initial wetting of the soil (Figure 7).

Although our field data do not provide direct insight into the transport mechanisms of glyphosate, we consider particle-bound transport through the shrinkage crack macropores as the most plausible transport mechanism, because of the strong sorption of glyphosate to soil mineral particles (de Jonge et al., 2000; Gimsing & Borggaard, 2002; Gulu Zada, 2021; Sprankle et al., 1975). Glyphosate leaching from loamy soils triggered by heavy rainfall events has also been observed in a long-term field study in Denmark (Kjær et al., 2011; Kjær et al., 2005; Norgaard et al., 2014; Rosenbom et al., 2015). Glyphosate transport to depths of at least 1 m was shown by monitoring runoff water from tile drains over 8 months after glyphosate application (Kjær et al., 2011) also suggesting preferential flow as the primary transport mechanism. While the Danish study addressed the leaching of glyphosate under long term wet conditions during the winter in a sandy clay loam (Kjær et al., 2011), our study showed, by the correlation of D_2O-labelled water and labelled glyphosate, that the rainfall intensity of a single summer storm was high enough to translocate glyphosate from the soil surface to the subsoil (50 cm depth) even in a dry and more fine grained soil (silty clay loam). The irrigation intensity (24.3 mm per hour) corresponds to rainfall intensity thresholds determined for the transport of other strongly sorbing pesticides (McGrath et al., 2010).

Dynamics of redox conditions

Soil redox conditions, which reflect the presence or absence of oxygen and alternative electron acceptors and are a decisive factor for the fate of glyphosate (Kanissery et al., 2015), were monitored in situ for all three treatments (W, G, D). Given the neutral soil pH (7.0 – 7.3), the measured redox potentials correspond to E_H-values at pH7 and further pH corrections were not made. At 5 cm depth on plots W1 and G2, redox potentials around 600 mV with only slight diurnal fluctuations were observed and indicated oxidizing conditions (Figure 9A and B, Figure A24A and B). Despite closure of shrinkage cracks upon irrigation, oxygen supply to the

uppermost soil layer likely proceeded through the small cracks that opened during the irrigation breaks (Figure 5C and D). The low amplitude of diurnal variations was partly due to the daily irrigation and temperature changes, as they were also visible on the dry plot albeit to a lower extend than on the irrigated plots (Figure 9A, B and C).

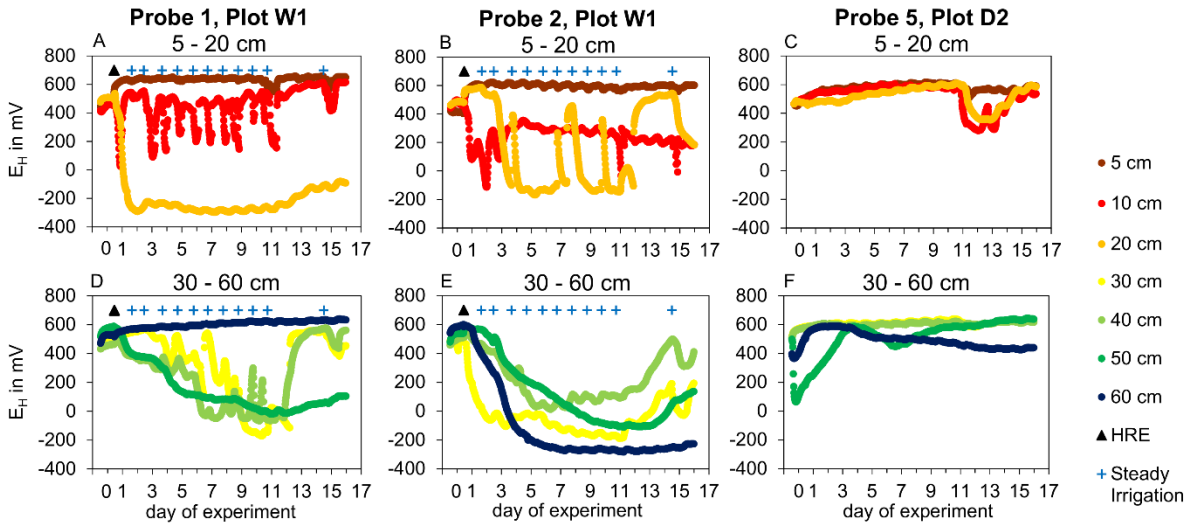

***Figure 9**: In situ redox potentials at pH7, reported in mV vs. SHE. Panels A, B, D, and E show redox potentials measured on a plot treated with water only (W1), panels C and F show potentials measured on a dry control plot (D2). Panels A to C show potentials in the topsoil at depths of 5 cm (brown), 10 cm (light red), and 20 cm (orange). Panels D to F show potentials in the subsoil at depths of 30 cm (yellow), 40 cm (light green), 50 cm (dark green) and 60 cm (blue). The time point of the heavy rainfall event (HRE) on the W plots is labelled with a black triangle and the time points of the weak (daily) irrigation with dark blue crosses. The redox conditions (E_H-values vs. standard hydrogen electrode at pH7) are classified as follows: oxidizing (> +400 mV), weakly reducing (+400 to +200 mV), moderately reducing (200 to -100 mV) and strongly reducing (< -100 mV) (Mansfeldt, 2003).*

Redox potentials rapidly dropped by 400 to 800 mV, i. e., from oxidizing to moderately/strongly reducing conditions on the W1 and G2 plots at 10 and 20 cm depth within a few hours after the irrigation pulse (Figure 9A and B, Figure A24A and B; the deviating behaviors of probe 2 at 20 cm will be discussed later). The probe 4 data set (plot G2, Figure A24B) did not show such a pronounced drop, but redox potentials clearly responded to the irrigation. Swelling of the clay minerals led to the closure of shrinkage cracks and thus to a reduction of the gas phase. In 30 to 60 cm depth, changes of similar magnitude (400 to 800 mV) were recorded on the W1 plot but with a lag time of 1 to 5 days (Figure 9D and E) due to the interruption of diffusive oxygen supply from ground surface (Haberer et al., 2012). Clearly, redox conditions changed from oxidizing to moderate or even strongly reducing propagating from top to bottom along the soil profile triggered by the irrigation pulse. Anoxic groundwater influence can be excluded given that the sampling was well above capillary fringe, which reached to about 1 m bgl (Martin et al., 2020). In general, the response of redox potentials at 30 to 60 cm on the G2 plot was less strong and slower than on W1 (Figure A24). It only reached weakly reducing conditions most of the time (see discussion below).

After the initial decrease, redox potential changes in the W1 and G2 plot data sets revealed three domains (1, 2a and 2b) with different characteristics: (1) between 10 cm and 20 cm (partially also at 30 and 40 cm, compare Figure 9D), redox potential fluctuations between oxidizing and weakly to moderately reducing conditions (amplitudes up to 600 mV) occurred with frequencies of around 24 hours. This diurnal pattern (Figure 9A and B, 10 cm; Figure A24A and B, 10 cm, 20 cm) was likely driven by the daily irrigation and desiccation cycles. Irregular fluctuations of redox potentials on the other hand (Figure 9B, 20 cm) might be linked to a penetration of oxygen through macropores affected by local shrinkage phenomena, root channels or the redox probe itself. In the second domain (2a) between 30 to 60 cm on plot W1, the redox potentials after their initial drop to reducing conditions of 0 to -200 mV vs. SHE did not show further pronounced fluctuations (Figure 9D and E). Hence, oxygen exchange with the atmosphere via shrinkage cracks was absent. In contrast, in domain 2b, identified at 30 to 60 cm on the G2 plot (Figure A24C and D) and at 60 cm on the W1 plot (probe 1, Figure 9D), the drop of redox potentials was strikingly less pronounced (lowest reading approx. +250 mV; Figure A24D, 50 cm and Figure A24C, 30 cm) and indicated oxic or weakly reducing conditions most of the time. This behavior suggests that at least parts of the vertical network of macropores was still present so that oxygen supply to the subsoil was not completely interrupted throughout the irrigated plots. As all plots were separated by segments of 50 cm width staying dry, gas exchange through some remaining lateral macropores connections is conceivable. An alternative explanation is, that even if there is enough SOM available for microbial respiration (Figure A20), microbial activity in some places in the deeper layers is too low (Loeppmann et al., 2016; Niemi et al., 2005; Stock et al., 2019) to initiate a drop of redox potentials even under oxygen shortage.

The redox-active components in the soil with substantial redox capacity were SOM (Figure A20), iron(hydr)oxide minerals and iron-containing clay minerals with a total soil iron content of approx. 2.5 % (Table A5). Both SOM and iron-bearing clay minerals can reversibly take up and release electrons and are electrode active (Aeschbacher et al., 2010; Gorski et al., 2012). As these compounds can function as geobatteries (Klüpfel et al., 2014; Peiffer et al., 2021), they might contribute to the dynamics of daily redox potential fluctuations observed in the topsoil. However, the observed diel E_H-changes in the topsoil can be well explained by diel temperature variations (Dorau et al., 2021). In contrast, the rapid drop of redox potentials after closure of the shrinkage cracks can be rationalized by aerobic microbial respiration using SOM as an electron donor. At that point, the reversible electron donating capacity of geobatteries was exhausted by the extended dry and oxic period prior to the irrigation event.

Redox potentials of the dry D plots (Figure 9C and F) down to 40 cm indicated oxidizing conditions throughout the soil columns with only small changes during the experiment as expected. One exception was the sudden drop of E_H values at 10 and 20 cm between Days 11 and 13, in response to a natural summer rainstorm (24.7 mm) on the evening of Day 10 reaching plot D2 as its plastic cover was blown away by strong winds. This incident showed that also a natural heavy rainfall event induces a response of the redox conditions in 10 and 20

cm depth. The redox conditions in deeper soil layers (30 cm and below) did not react to the rainfall.
Overall, the redox data demonstrated that irrigation (artificial or natural) induced a drop of redox potentials, although the magnitude of the drop differed between different spots. On the dry plots without irrigation, the atmospheric oxygen supply was unaffected and oxidizing conditions prevailed throughout the entire experiment.

Consequences of dynamic redox conditions in subsoils for sorption and bioavailability of glyphosate

The highly dynamic redox potential profiles as well as the presence of deuterated irrigation water and glyphosate in the subsoil suggest that in the beginning of the experiment the pronounced spatial heterogeneities in the soil in the form of shrinkage cracks reached deep into the subsoil, thereby acting as transport paths for water, glyphosate and oxygen. Once glyphosate had entered the subsoil, it could be exposed to changes in soil redox conditions which can affect its fate. At low redox potentials, microbial or abiotic reduction of Fe(III) to Fe(II) may partially dissolve Fe(III) minerals (Cornell & Schwertmann, 2003). Dissolution of such strong sorbents for glyphosate (Gimsing & Borggaard, 2002; Sprankle et al., 1975) will increase its dissolved fraction and thus should increase its mobility and bioavailability in anoxic soils. Enhanced desorption of glyphosate in anoxic compared to oxic soil incubations was reported but glyphosate desorption did not enhance biodegradation (Kanissery et al., 2015). While biotransformation of glyphosate to ((aminomethyl)phosphonic acid) (AMPA) or sarcosine under oxic conditions in the field has often been reported (Sviridov et al., 2015; Zhan et al., 2018), anoxic conditions strongly retard (Kanissery et al., 2015) or even impede (Sørensen et al., 2006) glyphosate biodegradation. Increased desorption in combination with inhibited biodegradation could increase persistence of the compound in the subsoil and could also impose the risk of glyphosate leaching into groundwater or – via tile drains (Kjær et al., 2011; Kjær et al., 2005; Norgaard et al., 2014) – into surface water bodies.

3.5 Conclusions

In the light of increasing incidents of extreme drought and precipitation events due to climate change, it is imperative to understand their influence on the fate of agrochemicals in highly structured soils. The experimental approach presented here enabled us to study the effects of heavy rainfall after a drought period on the mobility of glyphosate and the redox dynamics in a clayey floodplain soil. By applying glyphosate together with deuterated water as conservative tracer in a field experiment in combination with time resolved in situ redox potential measurements the spatial and temporal patterns of water infiltration and pesticide transport as well as the concomitant changes of the redox milieu under field conditions were revealed.

Shrinkage cracks proved to be the key structural soil features controlling physical and biogeochemical processes including water infiltration and redox conditions. Our results demonstrate that shrinkage cracks in dry soils can serve as effective transport paths for atmospheric oxygen, water and even strongly sorbing pesticides like glyphosate. The rainfall intensity of a typical summer storm event (approx. 25 mm in 1 h) was sufficient to transport water and the model pesticide glyphosate to the subsoil (50 cm) before closure of the shrinkage crack network through swelling of the clay. Further light irrigation resulted in an interruption of the oxygen supply to the depth, which entailed the decrease of soil redox potentials to strongly reducing conditions that potentially impair biodegradation of glyphosate. Given its high application rates worldwide, future research should focus on the fate of glyphosate under highly variable redox conditions.

4 Dynamics of inorganic nitrogen cycling, redox conditions, and microbial community composition in a floodplain soil induced by a heavy rainfall after summer drought

Johanna Schlögl, Clemens Karwautz, Lena Cramaro, Wolfgang Wanek, Judith Prommer, Theresa Böckle, Andreas Kappler, Stefan B. Haderlein, Christian Griebler

Status in the publication process: Manuscript in preparation

Author contributions:
Johanna Schlögl: Conceptualization, Methodology*), Investigation*) ***), Data curation*), Formal analysis*), Validation*), Visualization**), Writing – original draft preparation; **Clemens Karwautz**: Data curation (microbial communities), Formal analysis (microbial communities), Visualization (microbial communities), and Writing – original draft preparation (microbial communities), Writing – review and editing; **Lena Cramaro**: Conceptualization, Methodology, Investigation (microbial communities, extracellular enzymes), Data curation (microbial communities); **Andreas Kappler**: Funding acquisition, Writing – review and editing; **Wolfgang Wanek**: Investigation and formal analysis for data on extracellular enzymes, Writing – review and editing; **Judith Prommer**: Investigation (extracellular enzyme activities), Formal analysis (extracellular enzyme activities) ; **Theresa Böckle**: Investigation (extracellular enzyme activities), Formal analysis (extracellular enzyme activities); **Stefan B. Haderlein**: Conceptualization, Methodology, Funding acquisition, Project administration, Resources, Supervision, Writing – review and editing; **Christian Griebler**: Conceptualization, Methodology, Funding acquisition, Project administration, Resources, Supervision, Writing – review and editing.

*) except of microbial communities and extracellular enzymes
**) except of microbial communities
***) with the help of: Michelle Engelhardt, Bernice Nisch, Marc Jantz, Hartmut Schulz, Ellen Röhm and Franziska Schädler

4.1 Abstract

Climate change increases the frequency of droughts and heavy rainfall events in temperate climates of Central Europe. This study examined the impacts of such extreme weather events on the transport of water and inorganic nitrogen species, the main processes governing inorganic nitrogen turnover, and the dynamics of the soil microbial community in loamy floodplain soils. To this end, we conducted a field experiment simulating a heavy rainfall event applying isotopically (^2H) enriched water on a plot of arable land with fine-textured soil after a prolonged dry period. Subsequently the experimental plots were irrigated with non-labeled water. 50-cm deep soil cores were collected from irrigated and dry control plots at different time points (day 0, 6/8 and 14) and investigated for soil nitrate and ammonium content, soil water content, ^2H-enrichment of soil water, microbial DNA and RNA as well as extracellular enzyme activities. Furthermore, redox potentials were recorded in situ along the soil profile on dry and irrigated plots. Whereas the irrigation water of the simulated heavy rainfall event penetrated at least 50 cm deep into the soil along preferential flow paths after only two hours, ammonium and nitrate values remained fairly constant at 50 cm depth despite a significant decrease of nitrate in the topsoil after irrigation. This suggests that some nitrate might have been transported rapidly below 50 cm depth in contrast to ammonium, which is rather immobile in soils due to strong sorption to clay minerals. In general, ammonium behaved very conservatively and only increased significantly in the topsoil (0-5 cm) in response to the wetting of the dry soil ("Birch effect"). At day 6 and day 14 of the experiment, the non-labeled irrigation water of the daily recurrent low irrigation doses resided in the topsoil layer (0-5 cm depth) and only a small fraction penetrated to the subsoil, because the shrinkage cracks present at the beginning of the experiment had closed. In parallel, the in situ redox potential dropped from > +400 mV to below -100 mV relative to the standard hydrogen electrode. Soil nitrate contents decreased when redox potentials were below +100 mV and vice versa. This implies that nitrate formation and consumption after the initial rewetting was governed by soil redox conditions instead of processes induced by the rewetting after drought. Microbial community composition analysis showed no significant differences between the active fraction of the community (RNA) on irrigated and dry plots. Diversity indices on the RNA-level were somewhat higher on dry than on wet plots, although not significantly, which suggests that drying and the following rewetting selected for more adapted taxa. Overall, the heavy rainfall event had only a minor effect on the turnover of inorganic nitrogen species. Inorganic nitrogen turnover was mainly governed by redox conditions. The presence of pronounced shrinkage cracks formed after a drought period before the heavy rainfall event, however, allowed for rapid nitrate dissipation into the subsoil and eventually to the underlying aquifer. Our study also showed that the soil microbial community in temperate climates may ultimately be re-shaped to represent more resilient taxa regarding drying and rewetting cycles.

4.2 Introduction

Floodplains are important landscape compartments when it comes to nitrogen turnover (Lair et al., 2009; Venterink et al., 2003). Often, floodplain soils are exposed to recurrent inundation and dry periods or they are influenced by alternating groundwater levels throughout the year (Baldwin & Mitchell, 2000; Coby et al., 2011). In both cases, they experience alternating oxygen availability and thus fluctuating redox conditions. The availability of oxygen determines which nitrogen turnover processes dominate (Baldwin & Mitchell, 2000; Hefting et al., 2004). Inorganic nitrogen in the form of ammonium is released during the mineralization of organic matter. Ammonium is relatively stable under reducing conditions but is nitrified under oxidizing conditions. Under reducing conditions, nitrate is mainly denitrified to N_2 via nitrite, NO_2^-, and nitrous oxide, N_2O (Thamdrup, 2012).

Climate change increases the frequency and amplitude of weather extremes such as drought periods and heavy rainfall events (Coumou & Rahmstorf, 2012; Horton et al., 2016; Perkins et al., 2012). Heavy rainfall after summer drought triggers important hydrological and biogeochemical processes, particularly with fine-textured, loamy soils. First of all, drought causes the formation of shrinkage cracks of substantial width and depth, that allow for preferential flow (Beven & Germann, 2013; Jarvis et al., 2016; Nimmo, 2021) and thereby vertical solute and particle-bound transport of nutrients and agrochemicals (Bronswijk et al., 1995; Kelly & Pomes, 1998; Schlögl et al., 2022) during a following heavy rainfall event. The two inorganic nitrogen species ammonium and nitrate differ strongly in their chemistry and biogeochemical behavior in soils. Ammonium as a cation is prone to sorption to the mostly negatively charged soil mineral particles whereas nitrate as an anion is little sorbed in soils and therefore more mobile in pore water (Blume et al., 2016) and can thus be lost from the soil system by leaching. The fate of ammonium and nitrate during rewetting of dry soils is also determined by the so-called Birch effect. This effect describes the occurrence of a temporary flush of inorganic nitrogen after the rewetting of dry soil, that was observed in both lab (Birch, 1958, 1960) and field experiments (Cui & Caldwell, 1997). This flush of inorganic nitrogen is caused by microbial lysis, mineralization of dead microbial biomass, and by decomposition of osmoregulatory substances released by microorganisms upon rewetting (Fierer & Schimel, 2002; Jarvis et al., 2007; Saetre & Stark, 2005; Unger et al., 2010). The effect can last up to several days in the field with the main fraction of nitrogen mineralized in the first three days after wetting (Cui & Caldwell, 1997). Despite the potential importance of the Birch effect on inorganic soil nitrogen cycling, it is only triggered by severe drying-rewetting cycles. After this pulse of nitrogen seizes it is later expected that the "usual" redox-driven processes dominate soil inorganic nitrogen cycling, including mineralization, nitrification and denitrification.

Inorganic nitrogen turnover processes are largely microbiologically driven in soils. The soil microbial community adapts to regular drying and rewetting cycles (Armstrong et al., 2016; Fierer et al., 2003; Veach & Zeglin, 2020). In mid-European temperate climates such as at our study site, drying and rewetting cycles might become more frequent in the future due to

climate change (Coumou & Rahmstorf, 2012; Horton et al., 2016; Perkins et al., 2012). It is therefore important to understand their effects on microbial community composition and related changes in soil nitrogen cycling.

The objectives of our study were (i) to evaluate the water flow and solute transport during a drying-rewetting event induced by heavy rainfall following a summer drought in a fine-textured floodplain soil, (ii) to examine the temporal transition from pulse-driven nitrogen cycling (the Birch effect) upon soil rewetting towards redox-driven nitrogen turnover processes, and (iii) to assess the impact of drying and rewetting on soil microbial community structure and activity. To this end, we conducted a field experiment simulating a one-hour heavy rainfall event followed by recurrent moderate daily rainfall for 14 days on a Gleysol that exhibited pronounced shrinkage cracks after summer drought. The water of the heavy rainfall event was spiked with deuterated water as a conservative hydrological tracer, that allowed us to quantify water infiltration depth and distribution. We monitored depth-resolved in situ redox potentials using permanently installed sensors and took soil cores to 50 cm depth from irrigated and dry control plots on day 0, i. e., two hours after the heavy rainfall simulation, on day 6/8, and on day 14. The soil samples were analyzed for vertical changes in soil water content, in isotopic signatures (δ^2H) of the pore water, in extractable ammonium and nitrate concentrations, in total (DNA-level) and active (RNA-level) microbial community composition, as well as in extracellular enzyme activities.

4.3 Materials and Methods

Study site

The study site was located in the Ammer valley floodplain, approx. 7 km West of Tübingen in SW Germany (lat. 48.521266, long. 8.972687, 394 m a.s.l.). The catchment of river Ammer is situated in the South German Escarpment in the geological units of the Middle and Upper Triassic. The west of the catchment lies within the Muschelkalk unit whereas the eastern part lies within Keuper units, which mostly consist of terrestrial sediments, such as sand-, mud- or dolostones (Geyer et al., 2011; Grathwohl et al., 2013; Martin et al., 2020; Schwientek et al., 2013).

The floodplain with the study site lies in the eastern part of the catchment and is defined by Keuper hills at its southern and northern rim. The hydrostratigraphy within the floodplain comprises from bottom to top: Keuper rocks as basement, an aquifer mainly made of gravel and clay (gravel aquifer), a regional aquitard (lower clay aquitard), a confined aquifer made of calciferous tufa sediments (tufa aquifer) and another regional aquitard (upper clay aquitard) (Martin et al., 2020). The upper clay aquitard comprises the investigated soil. On average, it is 2 m thick and consists of fine-grained, clay mineral-rich alluvial sediments from the surrounding Keuper hills. The bottom half of this aquifer is water saturated throughout the year. The soil is characterized as Gleysol, showing the typical gleyic properties such as color-distinguishable reduced and oxidized horizons (Figure B25, Appendix B, Section B1) (Martin

et al., 2020). In the presented study, the cores of 50 cm depth only sampled the Ah and the Go horizon. The soil has an organic matter content (quantified as total organic carbon (TOC), for methodological details see Appendix B, Section B2) of 2-2.5 wt-% in the upper 15 cm and of 1 wt-% at 15 to 50 cm depth (Figure B26). It has a uniform soil texture of 11 ± 4 wt% of sand, 56 ± 6 wt% of silt and 32 ± 4 wt% of clay within the upper 50 cm (Figure B27, see Appendix B, Section B2 for methodological details). The soil pH varied between 7.0 and 7.3 and was determined on six samples from irrigated plots, two each from soil depths of 0-10 cm, 20-30 cm and 40-50 cm, after stirring the sample in a 1:1 (v:w) mix with deionized water for 30 min. The experiment was conducted on a plot of arable land after summer barley harvest and after a prolonged dry period during summer (see Section "Meteorological conditions" for more details). Information about the previous use of the plot was provided by personal communication with the farmer: During winter 2018/19 before cropping of summer barley a catch crop (radish and mustard) was planted and in February 2019 this green manure was incorporated into the soil with a cultivator. The plot was fertilized with horse manure in winter 2018/19 and with calcium ammonium nitrate fertilizer (27% N) in spring 2019. During cultivation of summer barley, the herbicide Ariane-C (active ingredients: 100 g L^{-1} Fluroxypyr (as Methylheptylester 144 g L^{-1}), 80 g L^{-1} Clopyralid + 2.5 g L^{-1} Florasulam) was applied.

Meteorological conditions

The climate in the region of the experimental site is temperate oceanic with a long-term mean annual precipitation of 718 mm and a mean annual temperature of 9.4 °C (1981-2010, (German Meteorological Service (DWD), 2024)). From a weather station in Tübingen Unterjesingen (lat. 48.52950, long. 8.98380, 439 m a.s.l., close to the actual experimental site) meteorological data were retrieved (Agrarmeteorologie Baden-Württemberg, 2021) (Appendix B, Section B4). The experiment was conducted from 16th to 30th July 2019. In the two weeks preceding experimental start, temperatures well above 20 °C dominated on all but two days and three moderate (according to the classification of the American Meteorological Society (2012)) rainfall events occurred (9.1, 5.1, and 33.1 mm, respectively). During the experiment, a minimum temperature of 10.2 °C was reached during night (night average 17.7 °C) and a maximum temperature of 36.3 °C during day time (day average 24.5 °C). On 12 days, temperatures > 25 °C and on six of these temperatures > 30 °C were measured. Following the FAO guideline (Allen et al., 1998), the reference evapotranspiration ETo for July 2019 was calculated as 4.2 mm day^{-1} (see Appendix B, Section B5 for details on the calculation). From 16th to 30th July 2019, two natural rainfall events occurred, one on the 21st July from 2:00 to 5:00 am (2.5 mm) and a heavy rainfall event from 26th July 8:00 pm to 27th July 5:00 am (24.7 mm) (Appendix B, Section B4). During both of these events, the dry control plots were covered by plastic foils.

Experimental setup

Plot design

The plot design comprised nine plots that were arranged as a Latin Square with three different treatments (Figure 10). All plots were of 2.4 m lateral length and separated by 50 cm stripes to allow access. Within each plot, a sampling area of 2 m x 2 m was defined to exclude boundary effects. Three different treatments were realized, but only two are relevant for the study presented here: (i) W plots were artificially irrigated to simulate a heavy rainfall event (HRE) after a dry period, (ii) D plots remained dry and served as controls. The third treatment included the application of glyphosate before irrigation. Results from these plots are presented in other publications (Schlögl et al., 2022; Wirsching et al., 2022).

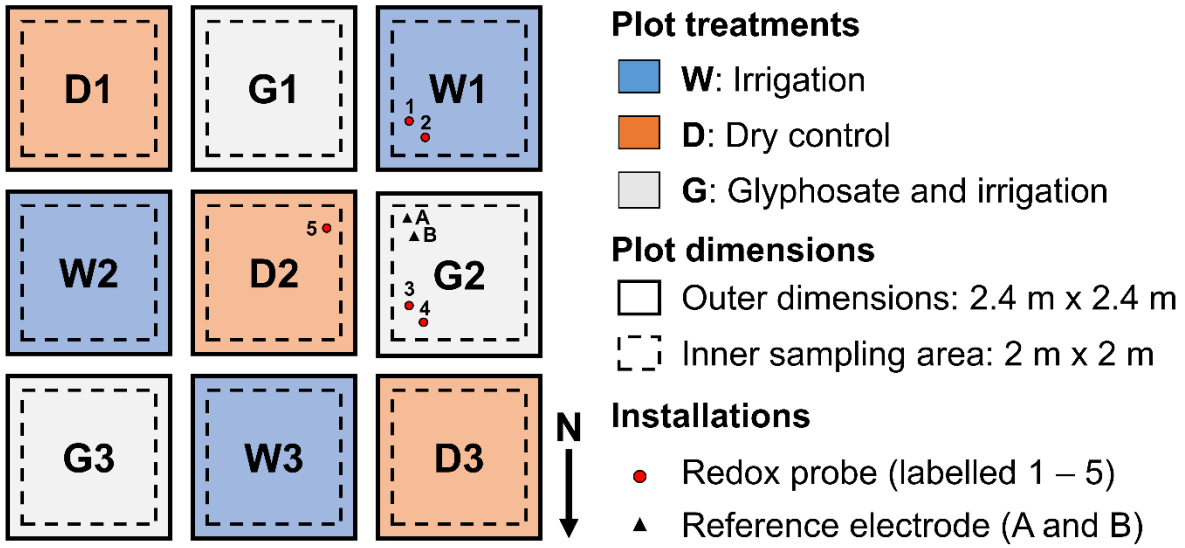

***Figure 10**: Plot design and treatments in the field experiment. Nine plots of 2.4 m x 2.4 m lateral length were arranged as a Latin Square and three treatments were realized in triplicates: A heavy rainfall event was simulated at day 0 and light daily irrigation followed for 14 days (W plots, blue). D plots (orange) remained dry and served as control plots. G plots (grey) were treated with glyphosate before they received the same rainfall treatment as W plots. An inner sampling area (dashed line) was defined to minimize boundary effects. For the in situ monitoring of redox potentials, redox sensors (red circles) were installed on plots W1, D2 and G2, and two reference electrodes (black triangles A and B, where B served as control for the system) were installed on plot G2 approx. in equidistance to all redox sensors.*

Plot treatment

Irrigation took place from the 16th to 31st July 2019 with the day of the simulated heavy rainfall event (16th July) defined as day 0 (T0) (Figure 11). All plots were covered for one week before the experiment to guarantee dry initial conditions. The heavy rainfall event (defined as 7.6 to 50 mm per hour by the American Meteorological Society (2012)) was simulated by irrigation with 24.3 mm deionized water for approx. one hour with watering cans. The water was labeled with deuterated water (D_2O) as a conservative tracer. Two liters of deuterated water (99.9 atom%, Carl Roth, Germany) were mixed with the irrigation water (1000 L) which resulted in

an input δ^2H signature of 12 730 ‰ vs. Vienna Standard Mean Ocean Water (VSMOW). On days 1 to 10 and on day 14, light irrigation with non-D_2O-labeled water was conducted with an irrigation rate of 5.2 mm day^{-1} to keep the soils moist and to force closure of shrinkage cracks to investigate the development and influence of in situ redox potential on nitrogen turnover processes and on the microbial community.

Sampling

Sampling was done with a stainless steel soil corer (Humax, Hasli-Rüegsau, Switzerland). The soil cores were retrieved within PVC liners of 50 cm length and 3.5 cm diameter and immediately put on dry ice. In the lab, they were stored at -80 °C (microbiological analyses, enzyme analyses, δ^2H analyses) and at -21 °C (inorganic nitrogen species) until further analysis. The holes in the field were filled with bentonite.
The sampling scheme comprised sampling for inorganic nitrogen species, soil water content, analyses of the δ^2H signature of the pore water, the microbial community, and enzymes (Figure 11). For the analysis of soil water δ^2H, cores were taken from W plots along shrinkage cracks. Additional samples were taken from D plots to determine the natural δ^2H background. Samples for inorganic nitrogen species, soil water content and microbiological analyses were taken from W and D plots along shrinkage cracks.

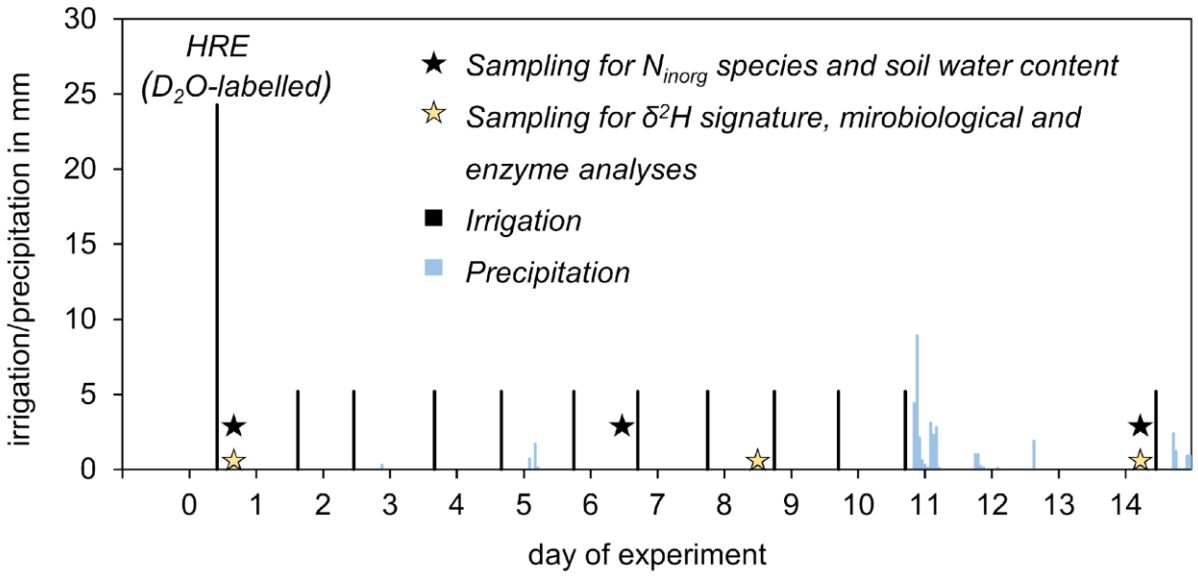

***Figure 11**: Irrigation and sampling scheme. Irrigation (black bars, length indicates intensity) included a simulated heavy rainfall event (HRE) with D_2O-labeled water on day 0 followed by light daily irrigation on W plots. Natural precipitation is indicated by light blue bars, which was excluded from D plots but not from W plots. Sampling for inorganic nitrogen species (N_{inorg}) and soil water content took place on days 0, 6 and 14 (black stars), samples for analyses of δ^2H signature, microbial communities and enzymes were retrieved on days 0, 8 and 14 (golden stars).*

The initial shrinkage cracks were marked before the first irrigation so that during later stages of the experiment, their course was still recognizable. Sample codes in the following text are as follows: treatment of the respective plot (dry (D), irrigated (W)) followed by the respective

experimental replicate number (1, 2 or 3) as well as the time point T + number, where the number expresses the day. For example, W1T8 refers to the irrigated plot W1 sampled at day 8, while WT8 refers to all three replicate W plots on day 8.

In situ monitoring of redox potentials

To evaluate the redox potential as a controlling factor of the microbial turnover of the two inorganic nitrogen species, nitrate and ammonium, in situ soil redox potentials were measured on a plot irrigated with water (plot W1) with two independent redox sensors (sensor 1 and 2) and on a dry control plot (plot D2) with one sensor (sensor 5) (Figure 10). The multilevel redox sensors (PaleoTerra, Oijen, The Netherlands) were made of fiberglass and epoxy tubes and were of 1.20 m length. Each sensor had 10 platinum (Pt) electrodes. For the installation of the sensors, we first drilled a vertical hole into the soil that was 2 mm smaller in diameter than the sensors, so that after sensor installation, the contact between the electrodes and the soil was given. Then the sensors were installed in a way that the first electrode was placed 5 cm below ground level (bgl) and the further electrodes at 10 cm intervals bgl. Two Ag/AgCl reference electrodes (A and B) (KCl sat.; E^0 = 0.199 V) were installed on plot G2 (Figure 10). One of them served as the reference electrode for the measurements, the other as a control for the system. Measured redox potentials (E_{meas}) are reported vs. the standard hydrogen electrode (SHE; E^0 = 0 V, by definition) as $E_H = E_{meas} + E_{KCl,sat}$. Measurement precision was ± 10 mV. The sensors and the reference electrodes were connected to a data logger (Campbell Scientifc, Logan, Utah, US) which stored the redox potentials at 30 minute intervals throughout the experiment. The characterization of the in situ soil redox conditions will be based on the following categorization (Mansfeldt, 2003) of E_H values at circumneutral pH: oxidizing (> +400 mV vs. SHE), weakly reducing (+400 to +200 mV), moderately reducing (+200 to -100 mV) and strongly reducing (< -100 mV).

Soil water content

For the assessment of gravimetric soil water content on irrigated (W) and dry (D) plots, the 50-cm cores were cut into increments of 5 cm for 0-10 cm depth and into increments of 10 cm for 10-50 cm depth. From these increments, triplicates of approx. 1.5 g of field wet soil (scale precision 0.001 g) were weighed (small pebbles were rejected) before and after freeze drying. The gravimetric water content (g g^{-1}) was calculated as the ratio of water loss to dry weight. The soil water content of the D plots on day 0 was used as reference and is hereafter referred to as “initial soil water content”.

Chemical and isotopic analyses

δ^2H signature of soil water

The δ^2H signature of the soil pore water was determined by H_2O(liquid)-H_2O(vapor) pore water equilibration and cavity ring-down laser spectroscopy (Picarro L2120-i and L2130-i) (Wassenaar et al., 2008). To this end, frozen core samples (cores WT0/8/14 and DT0) were sliced in 10 cm segments and aliquots of 66 to 170 g of those segments were double-bagged in 1 L Ziploc Freezer bags and stored at 4 °C. Before analysis, the bags were filled with laboratory dry air and the bags were stored for 3 more days to let the pore water equilibrate with the headspace water vapor. Each analysis lasted up to 30 minutes until the signal plateaued, that is, stable conditions within the expected measurement accuracy were reached (i. e., standard deviation < 1.0‰ for δ^2H of the water vapor). The average signal over the last minute of the analysis was recorded. After every third sample, an internal standard (water of known isotopic composition in a freezer bag) was measured for calibration. The isotopic signatures are reported as isotope ratios relative to the international standard (Vienna Standard Mean Ocean Water, VSMOW) in delta notation in ‰ ($\delta‰ = ((R_{sample} - R_{standard})/R_{standard})*1000$), where R is the isotope ratio $^2H/^1H$ of the sample and the standard, respectively. For the determination of δ^2H background values on cores from DT0, the upper-most segment was ignored to avoid corruption by wind drift or water vapor from irrigation. Additionally, the gravimetric water content of each analyzed segment was determined by the weight difference before and after drying at 105 °C. These values were used for the isotope mass balance calculation.

Water mass balance

To assess how much of the total irrigation plus natural precipitation on W plots received until day 0, 6 and 14 (24.3 mm, 60.0 mm and 115.0 mm, respectively) reached the different depth segments of the profile, a water mass balance was calculated. It was assumed that irrigation only led to a water storage change and that hardly any leaching below 50 cm occurred. The measured gravimetric soil water contents from WT0/6/14 and DT0 were converted to volumetric water contents using bulk densities of individual depth segments. With these volumetric water contents, the amount of water volume change was calculated and the increase of water content, i. e., water volume per m² on irrigated plots, at each day was assessed by comparison with dry plots on day 0.

Isotope mass balance

The irrigation water of the simulated heavy rainfall event on day 0 (Irr_{HRE}) was labeled with D_2O. A two-component (i. e., isotope mass balance) mixing approach was used to calculate the fraction of Irr_{HRE} in every i-th depth segment ($f_{IW,zi}$):

$$f_{IW,z_i} = \frac{\delta^2 H_{z_i} - \delta^2 H_0}{\delta^2 H_{IW} - \delta^2 H_0}$$

where $\delta^2 H_{zi}$ is the measured isotope ratio in the *i*-th depth segment, $\delta^2 H_{IW}$ is the isotope ratio of the simulated heavy rainfall event on day 0 (i. e., 12 730‰) and $\delta^2 H_0$ is the background average δ^2H of the pore water before irrigation (i. e., -47.6‰). For the calculation of the amount of Irr_{HRE} in each depth segment, the volumetric water content calculated as described in the Section "Water mass balance" was multiplied by the fraction of irrigation water $f_{IW,zi}$.

Extraction and analysis of inorganic nitrogen

Changes in the content of inorganic nitrogen compounds nitrate and ammonium allow to follow redox transformations induced by the heavy rainfall event. Inorganic nitrogen was extracted from approx. 1.2 g of frozen soil aliquots with 12 mL 2 M KCl (p.a., Honeywell, Germany) prepared in ultrapure water (GenPure Pro UV-TOC, Thermo Fisher Scientific, Germany). Samples were shaken for 30 minutes on a horizontal shaker (IKA, Germany) with 160 motions per minute (mpm) and then centrifuged at room temperature for 15 min at 5 000 x *g* (centrifuge 5430 R, Eppendorf, Germany) and filtered (0.2 µm, regenerated cellulose, Sartorius, Germany). The extracts were stored at 4 °C until analysis and were analyzed within maximum three days. Ammonium and nitrate were analyzed in these extracts by continuous flow analysis (CFA) using an AA3 HR AutoAnalyzer System from Seal Analytical (Germany). All chemicals used were purchased from Sigma Aldrich, Germany, and were of ACS grade. Standard curve range was from 0 to 7.5 mg N L^{-1} for both analytes, giving a high linearity (R^2 between 0.999 and 1.000). Nitrate determination followed the ISO 13395 standard methodology where nitrate is reduced to nitrite by hydrazine, which then reacts with sulfanilamide and NEDD forming a pink complex, which is measured at 550 nm. Potentially present nitrite in the original sample is determined independently without hydrazine addition and subtracted from nitrate concentration. Ammonium was determined according to the ISO 11732 standard methodology where it reacts with salicylate and dichloroisocyanuric acid to form a blue complex which is measured at 660 nm. To account for signal shifts due to the sample matrix of 2 M KCl, standards were also prepared in 2 M KCl for both compounds.

Nitrate and ammonium mass balance

Measured nitrate and ammonium concentrations (mg N L^{-1}) were corrected for baseline and blank values and the mass of nitrate and ammonium in the extraction solution was calculated. The original weight of the frozen sample was corrected to dry weight by the gravimetric water content and the mass of ammonium-N and nitrate-N per gram of dry soil was calculated. Including bulk density of the soil and the sample volume at different depths of the soil core, the mass of ammonium-N and nitrate-N at each depth interval and for the whole core was calculated.

Microbiological Analyses

Molecular Analysis

For molecular analysis of bacteria and archaea, soil cores were stored on dry ice immediately after sampling. Soil cores were stored in the lab at -80°C until analysis. The frozen cores were cut into segments ranging from soil depth 0-10 cm, 20-30 cm and 40-50 cm using a sterilized (2% sodium hypochlorite solution) electric saw. For nucleic acid extraction representative subsamples (10-15 g) of the soil samples were defrosted at room temperature, homogenized with a sterile spatula, and finally duplicate aliquots of 400 mg of each subsample were used for DNA extraction.

DNA extraction was conducted with the DNeasy PowerSoil Kit (Qiagen, Hilden, Germany) according to the manufacturer's protocol. RNA was extracted using the modification of a commercial DNA extraction kit according to Tournier et al. (2015) combining the FastDNA SPIN™ kit for soil (MP Biomedicals) and the RNaid® Kit (MP Biomedicals, LLC, Illkrich, France). Instead of the standard weight of 0.25 g, 0.5 g soil was used to increase the mass of RNA. RNA was purified with the RNeasy Micro Kit (Qiagen). Residual DNA was removed with DNAse I and the RNA was transcribed to cDNA using the RevertAid RT Reverse Transcription Kit (Thermo Scientific) with a random hexamer primer. A primer combination of 515F (5′-GTGYCAGCMGCCGCGGTAA-3′) and 806R (5′-GGACTACNVGGGTWTCTAAT-3′), annealing to the V4 region of the 16S rRNA was used for gene amplification, following the PCR protocol as described by Pjevac et al. (2017). Sequencing was performed on a MiSeq platform (Illumina, San Diego, CA, USA), using a v3, 600 cycle chemistry (2 × 300 b paired-end sequences) in two separate runs.

Raw reads were processed in R (version 4.1.1,) with DADA2 (v. 1.20.0) as outlined in Callahan et al. (2017). Amplicon Sequence Variants (ASVs) were inferred across all samples in pooled mode (details on sequence trimming, and quality filtering is outlined in Pjevac et al. (2017)). ASV sequences were subsequently aligned and classified using SINA version 1.7.2 and the SILVA database SSU Ref NR 99 release 138.1 using default parameters. ASVs classified as archaea, eukaryotes, mitochondria, or chloroplasts, as well as ASVs not classified at the domain level, were removed from the dataset prior to downstream analysis. Statistical data analysis was performed with R and plots were created using the package ggplot2. Alpha and beta diversity indices were calculated (vegan) and compared. Non-metric multidimensional scaling (NMDS) analysis of Aitchinson distances was used for ordination.

Extracellular Enzyme Activities

Potential activities of three soil hydrolytic enzymes, i. e., β-glucosidase (BG), N-acetylglucosaminidase (NAG; exochitinase) and acid phosphatase (AP) were measured fluorometrically with artificial substrates (Tian et al., 2023). The following 4-methylumbelliferyl (MUF) based substrates were used to measure the enzyme activities: MUF-β-D-glucopyranoside for BG, MUF-N-acetyl-β-D-glucosaminide for NAG, and MUF-

phosphate for AP. Soil slurries (1:100 (w:v)) were prepared in 50 mM sodium acetate buffer (pH 5) by ultrasonication (energy input ~350 J). Substrates were added to soil slurries in black microplates in five replicates and incubated in the dark for 180 min with repeated measurements of sample fluorescence. Microplates were read by a TECAN Infinite® M200 spectrophotometer at an excitation wavelength of 365 nm and an emission wavelength of 450 nm. Sample fluorescence was corrected for quenching and the concentrations of MUF released by enzymatic activity were calibrated by respective standards added to soil slurry.

4.4 Results

Soil water content and in situ redox potentials

Water and ^{2}H-isotope mass balances were calculated for days 0, 6 and 14 and 0, 8 and 14, respectively (Figure 12A and B) to reveal flow pathways of the irrigation water. Mean values were calculated from the triplicate experimental plots for each depth section. For the water mass balance on T14 and the isotope mass balance on T8, mean values were only calculated from two individual plots due to sample loss. The water mass balance (Figure 12A) included the sum of all irrigation and natural precipitation water during the experiment (Irr_{tot}) whereas the isotope mass balance (Figure 12B) only included the recovery of the D_2O-labeled heavy rainfall event (HRE) water (Irr_{HRE}).

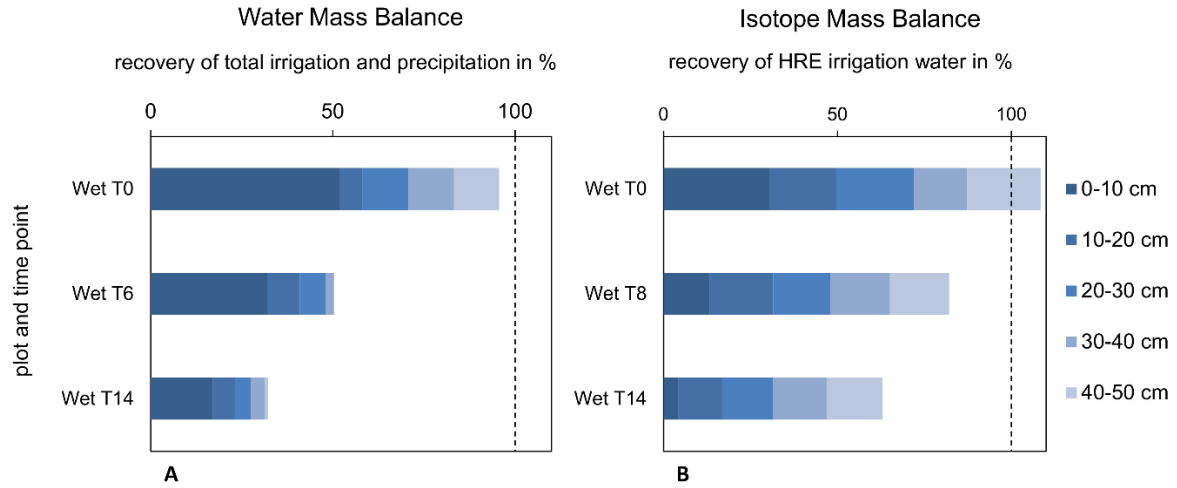

***Figure 12**: **A**. Water mass balance for days 0, 6, and 14 (T0, 6, and 14) in five 10-cm soil depth sections. Recovery of the water is given in relation to the total amount of water that had reached the plots by irrigation and natural rainfall at the respective time point (Irr_{tot}, represented by the 100% line). **B**. Isotope mass balance for days 0, 8 and 14 (T0, T8 and T14) in five 10-cm depth intervals. Recovery of heavy rainfall water is given in relation to the amount of deuterium-labeled irrigation water of the simulated heavy rainfall event (Irr_{HRE}) on T0. The color gradient from dark to light blue indicates the depth from top (0-10 cm) to bottom (40-50 cm) of the soil profile.*

The water mass balance was calculated as the percentage of Irr_{tot} recovered in the soil at days 0, 6 and 14 (T0, T6, T14) on irrigated (W) plots (Figure 12A) after subtracting pre-event water levels measured on samples from dry plots. Irr_{tot} was 24.3 mm at T0, 60.0 mm at T6, and 115.0

mm at T14 which is represented as the 100% line in Figure 12A. The recovery of irrigation plus precipitation water was 95.6% at T0, 50.3% at T6, and 32.1% at T14, and thus steadily decreased during the experiment.
In the following, the dynamics of irrigation and precipitation water recovery are described as percentages of the amount of recovered water at the time points T0, T6, and T14, respectively. At T0, 2 hours after the simulated heavy rainfall event, 54.2% of the recovered irrigation water was found in the top 10 cm. 19.9% of the recovered water was found at a depth of 10-30 cm. A substantial fraction (25.9%) however, was already present in the subsoil (30-50 cm depth). Also at T6 and T14, more than 50% of the recovered irrigation water was found in the upper 10 cm. At 10-30 cm depth, the percentage of recovered water increased to 31.6% and 32.6% at T6 and T14, respectively. However, the absolute amount of Irr_{tot} at 10-30 cm depth decreased compared to T0. At T6 and T14, only small fractions of the recovered water (4.7% and 14.4%, respectively) were found at 30-50 cm depth.

While the irrigation water of the heavy rainfall event (HRE) at T0, Irr_{HRE}, carried a ^{2}H-label, the irrigation water of the following moderate daily rainfalls was unlabeled. Thus, the recovery of the HRE water could be assessed via an isotope mass balance at T0, T8 and T14 from the soil water content, the fraction of the recovered ^{2}H-label, and the amount of simulated heavy rainfall event irrigation water, Irr_{HRE}, (24.3 mm). The recovery was calculated for 10-cm layers of the 50-cm soil cores. The isotope mass balance is presented as the percentage of the simulated heavy rainfall event (24.3 mm) recovered in the soil on days 0, 8, and 14 (T0, T8, T14) on W plots (Figure 12B). The recovery of Irr_{HRE} was 108% at T0, 82% at T8 and 63% at T14. In the following, the development of the recovery is described as the percentages of the amount of recovered irrigation water from the heavy rainfall event. At T0, the biggest fraction of HRE irrigation water (30%) was found in the upper 10 cm of the soil. The rest of the irrigation water was fairly evenly distributed throughout the soil profile: each of the 10-cm depth intervals from 10 to 50 cm containing 15-22% of the recovered irrigation water. On T8 and 14 only 13% and 4% of the recovered Irr_{HRE} were found in the top 10 cm, respectively. Also in the deeper segments the recovery decreased during the experiment but less pronounced compared to the top 10 cm.

The in situ redox potentials were measured at different depths from 5 cm below ground to 60 cm below ground (Figure 13). In the beginning of the measurements (T0), the in situ redox conditions were oxidizing (> 400 mV vs. SHE) at all depths. In situ redox potentials responded to the irrigation at all measurement points on W plots. In the topsoil layers (0-20 cm below ground) redox potentials mostly declined to reducing conditions within 24 h after the simulated heavy rainfall. In the subsoil (30-50 cm below ground), redox potentials declined more slowly, in most cases within three days.
At 10, 20 and 30 cm soil depth, after the first decline, we observed high temporal and spatial (among sensors) variations in the redox potentials, ranging between oxidizing and moderately

reducing conditions, whereas at a depth of 40 to 60 cm below ground, the decline of in situ redox potentials after the irrigation was more constant.

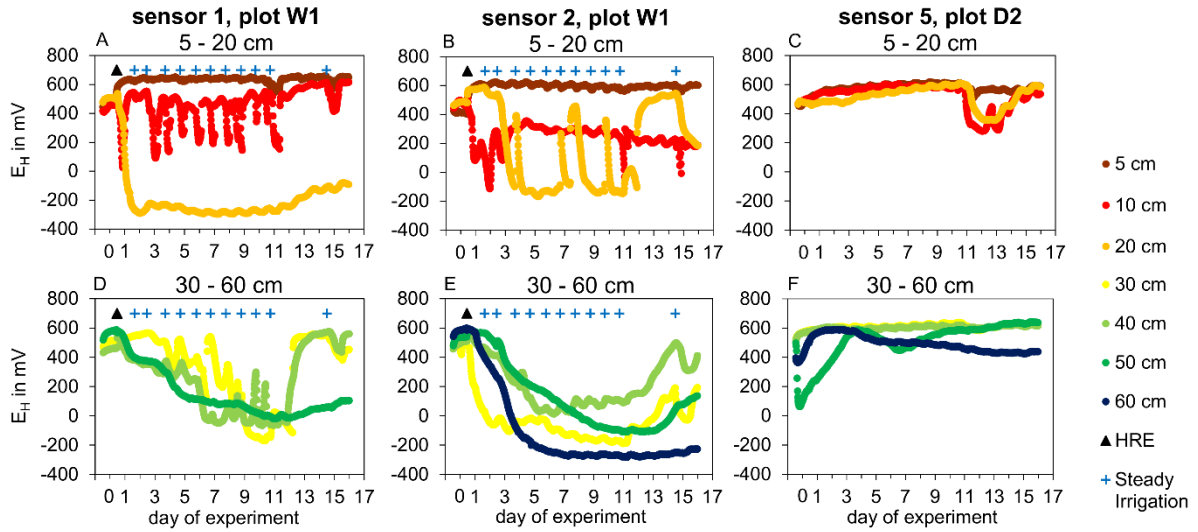

***Figure 13**: In situ redox potentials (reported as E_H at pH7 in mV vs. SHE) were measured on plot W1 (irrigated with water, sensor 1 and 2, panels A, B, D and E) and on plot D2 (dry control, sensor 5, panels C and F) in depths of 5, 10, 20 cm (panels A to C) and 30, 40, 50, and 60 cm (panels D to F). The measurements started at experiment day T -1 and are presented until T16. For plot W1, the time points of the simulated heavy rainfall event (HRE, black triangle) and the steady light irrigation (blue crosses) are depicted (panels A, B, D and E).*

Especially in sensor 1 at a depth of 10 cm (Figure 11A), the daily irrigation and drying of the soil led to sharp diurnal changes of the redox potentials between oxidizing and moderately reducing conditions (200 mV to -100 mV). Between day 10 and 14, the daily irrigation of 5.2 mm was interrupted and redox potentials rose well into weakly reducing or oxidizing conditions even at soil depths of 30 to 50 cm. At the dry plot (plot D2, Figure 11C and F), the redox potentials remained oxidizing throughout the experiment, except of 10 and 20 cm soil depth at day 10 to 14, when a natural heavy rainfall event hit the experimental plots and removed the protecting foil from plot D2 around the redox sensor (but not the other dry treatment plots).

Nitrogen Cycle

Ammonium and nitrate mass balances were calculated to evaluate the nitrogen solute transport and the turnover of the two inorganic nitrogen species. Dry control plots on day 0 (DT0) represent the initial state of the soil inorganic nitrogen before irrigation. A comparison of DT0 with irrigated plots on day 0 (WT0), 2 h after the irrigation, therefore indicates the impact of the irrigation on the inorganic nitrogen species in the soil profile.

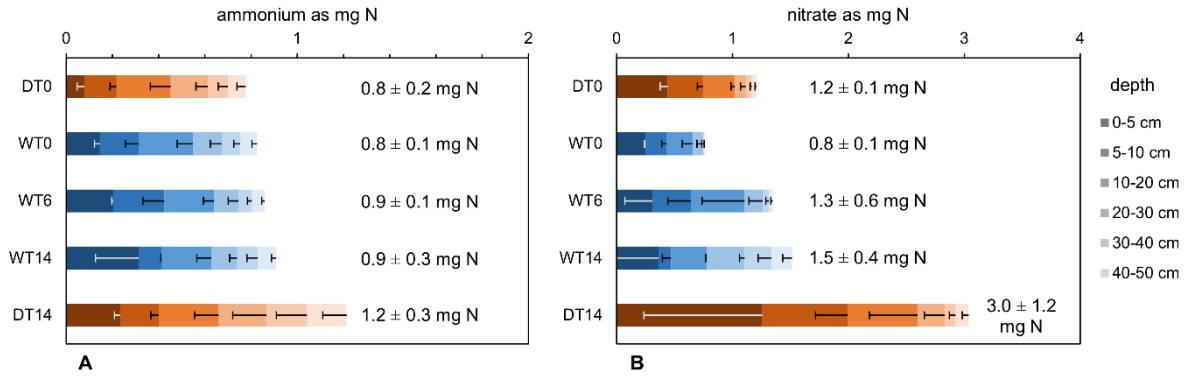

***Figure 14**: Mass balance of ammonium (panel A) and nitrate (panel B) (each as mg N per core segment) in cores from dry plots on day 0 and day 14 (orange bars, DT0 and DT14) and on irrigated plots on days 0, 6 and 14 (blue bars, WT0, WT6, WT14). Color shading from dark to light symbolizes increasing depth of the core segments. Displayed are the means of three experimental triplicates and their standard deviations. The sum of ammonium and nitrate content together with the standard errors in each 50-cm core are displayed on the right of the bars.*

Two hours after the simulated heavy rainfall, ammonium (Figure 14A) had doubled in the top horizon (0-5 cm), from 0.08 ± 0.03 mg N (DT0) to 0.15 ± 0.02 mg N (WT0) ($p < 0.05$). On W plots at 0-5 cm depth, the ammonium contents further increased to 0.20 ± 0.01 mg N at T6 ($p = 0.058$) and 0.3 ± 0.2 mg N at T14 ($p > 0.05$). Below 5 cm soil depth, only minor changes in soil ammonium content occurred during the experiment, the sum of ammonium over the entire 50-cm soil profile therefore being very similar at DT0, WT0, WT8 and WT14 (0.8-0.9 mg N). However, the sum of ammonium in DT14 (1.2 ± 0.3 mg N) was nearly twice as high as in DT0 ($p > 0.05$). From DT0 to DT14, ammonium mass increased at all depths, three-fold at 0-5 cm ($p < 0.05$) and 1.1-fold to 2.2-fold at greater depth (all $p > 0.05$).

Nitrate mass in the whole profile (Figure 12B) decreased by one third shortly after irrigation (1.2 ± 0.1 mg N in DT0 vs. 0.8 ± 0.1 mg N in WT0, $p < 0.05$). This was mostly caused by a 40% decrease at 0-5 cm and 5-10 cm soil depth (both $p < 0.05$) and an 18% decrease at 10-20 cm depth ($p > 0.05$). From WT0 to WT14, during ongoing moderate daily irrigation (5.2 mm day^{-1}), the whole-profile nitrate mass almost doubled from 0.8 ± 0.1 mg N to 1.5 ± 0.4 mg N ($p < 0.05$). From WT0 to WT6 nitrate increased at 0-5 cm, 5-10 cm and 10-20 cm while there were no relevant changes below 20 cm depth. From WT6 to WT14, nitrate increased at 0-5 cm and below 20 cm, and decreased at 5-10 cm and 10-20 cm (all $p > 0.05$).
On D plots, the sum of nitrate mass showed a 2.5-fold increase from T0 (1.2 ± 0.1 mg N) to T14 (3.0 ± 1.2 mg N) ($p > 0.05$) (Figure 12B). This strong increase of nitrate was mainly due to a strong increase in the upper soil layers: a nearly 3-fold increase in the top segment (0-5 cm) ($p > 0.05$) and a 2.4- and 2.2-fold increase at 5-10 cm ($p < 0.1$) and 10-20 cm ($p > 0.05$), respectively.

Microbial community and extracellular enzymes

To assess the effect of a heavy rainfall after a summer drought and the following changes in soil redox potentials on soil microbial community composition and activities, the depth- and time-resolved in situ redox potentials (E_H) were recorded as well as total (on DNA level) and

active (on RNA level) soil microbial community composition at depths of 0-10 cm, 20-30 cm and 40-50 cm from dry (D) and wet (W) plots on days 0, 8 and 14.

The 16S rRNA amplicon sequencing resulted in a mean number of 7 401 reads per sample for DNA and 6 970 reads per sample for RNA. Due to the great range of reads per sample (DNA: min: 3 531; max: 13 706, and RNA: min: 8; max: 18 224) we selected only samples with at least 300 reads, thereby reducing the RNA dataset from 54 to 46 samples. These samples contained on average 1 334 different Amplicon Sequence Variants (ASVs) (richness) (Figure 15).

The microbial community composition of the different experimental treatments revealed high heterogeneity between sample plots. The soils were dominated by the phyla *Proteobacteria* (mean: 17.4% SD: 4.7), *Acidobacteriota* (mean: 14.5% SD: 4.9), *Actinobacteriota* (mean: 13.5% SD: 7.4) and *Verrucomicrobiota* (mean: 11.5% SD: 5.2). These were the most abundant phyla independent of wetting, soil depth, and the day of the experiment (Appendix B, Section B6). At a finer taxonomic resolution, *Pedosphaeraceae* (*Verrucomicrobiota*), unclassified *Vicinamibacterales* (*Acidobacteriota*), *Xiphinematobacteraceae* (*Verrucomicrobiota*) and *Nitrosomonadaceae* (*Gammaproteobacteria*) were the top four bacterial families found throughout all samples with the mean relative abundances varying between 4.6 and 3.2%.

The common alpha diversity parameters (RNA-fraction) showed only minor differences between dry and wetted soils. Dry soils revealed a little higher diversity compared to the water treated soils (Figure 15). The Shannon diversity of the active (RNA-fraction) prokaryotic communities in dry and wet soils was not significantly different (p = 0.956). The DNA and RNA based community data suggest that microbial communities did not change with depth and treatment in terms of composition and active fractions (Figure 16).

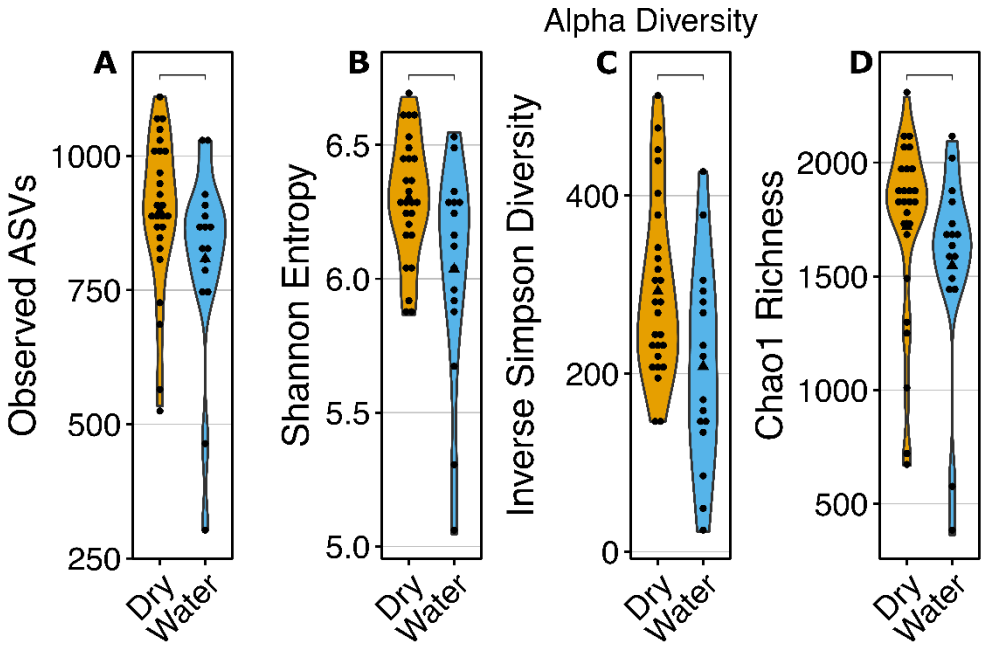

***Figure 15**: Observed amplicon sequence variants (ASVs) (panel A) and different alpha diversity indices (panels B, C and D) of microbial communities (RNA) on dry (orange) and watered (blue) plots. Differences between the treatments were not significant (p > 0.05) (brackets without asterisk above violins).*

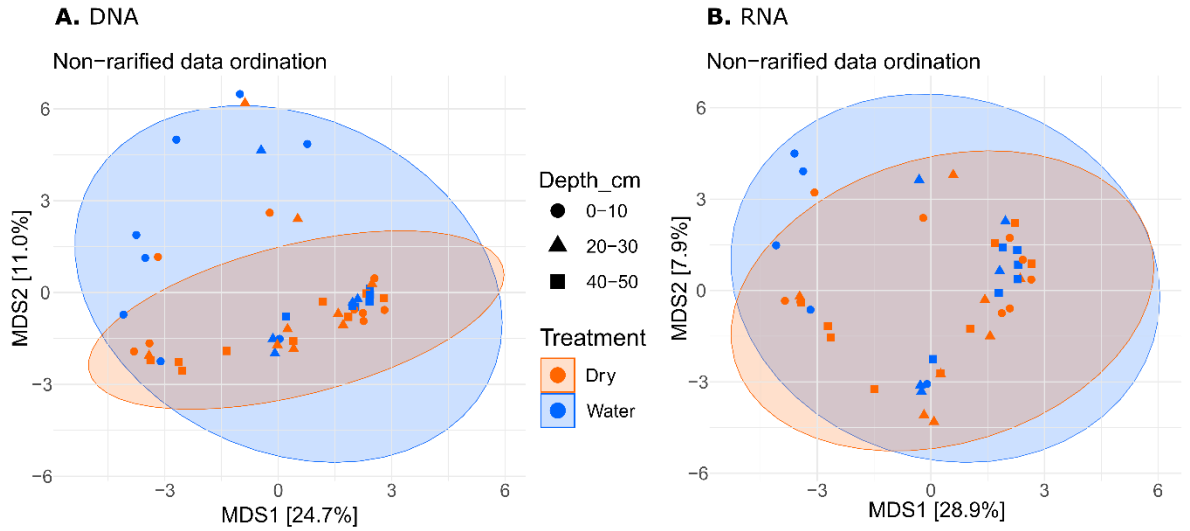

***Figure 16**: Non-metric multidimensional scaling plots of the microbial community composition (A) on the DNA-level and (B) on the RNA-level at three soil depths (0-10 cm: dots, 20-30 cm: triangles, 40-50 cm: squares) on dry (orange) and irrigated (blue) plots.*

The activities of the extracellular enzymes β-glucosidase, exochitinase and acid phosphatase decreased with depth ($p < 0.05$) (Figure 17).

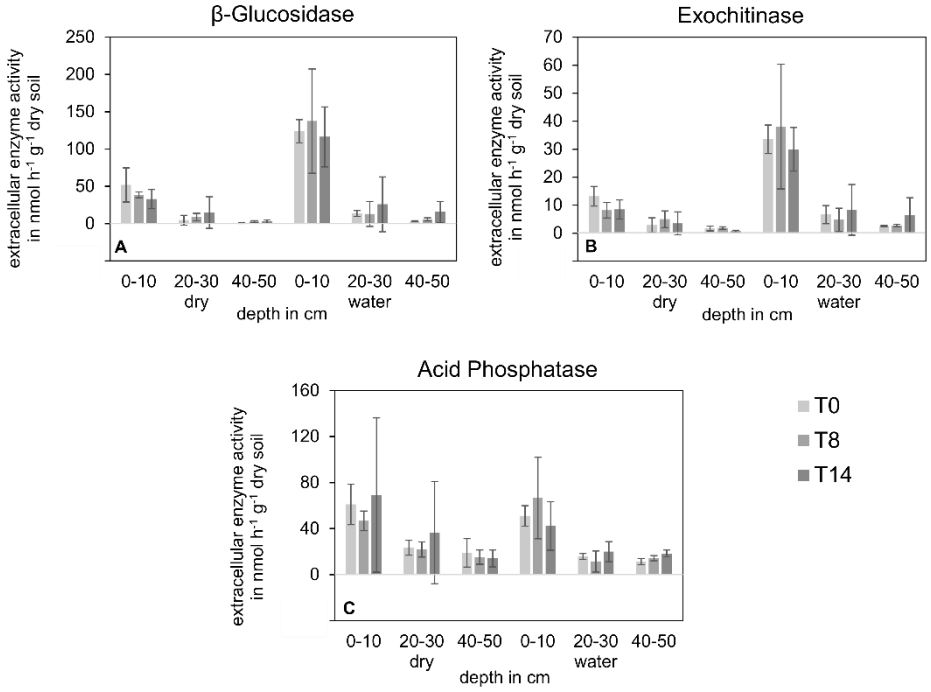

***Figure 17**: Extracellular enzyme activities of β-glucosidase (panel A), exochitinase (panel B) and acid phosphatase (panel C) at three soil depths on dry and watered plots. The measurement time points day 0, 8 and 14 (T0, T8, T14) are indicated by grey shading from light to dark. Error bars indicate standard deviations of three replicate plots.*

β-glucosidase and exochitinase showed significantly higher activities on wet plots than on dry plots ($p < 0.05$), whereas the activities of acid phosphatase did not respond to the irrigation

treatments ($p > 0.05$). Time after rewetting by heavy rainfall was non-significant for all three enzymes ($p < 0.05$), indicating that treatment effects occurred very rapidly. The significant interaction of treatment and soil depth ($p < 0.05$, two-way ANOVA) for β-glucosidase and exochitinase reflects that the wetting treatment effect (stimulation) was strongest in topsoils (0-5 cm) and declined with depth.

4.5 Discussion

Water flow and solute transport

Both the water and the isotope mass balance show that at T0 almost all of the irrigation water was recovered within the profile (Figure 10A and B). It is remarkable that shortly (2 h) after the simulated heavy rainfall, only about half of the irrigation water resided in the topsoil (0-20 cm) while the rest already had reached the subsoil (below 20 cm depth) (Figure 10A). This rapid deep infiltration was facilitated by the pronounced network of shrinkage cracks, which formed in the fine-textured soil due to the preceding drought (Schlögl et al., 2022).
The water mass balance (Figure 10A), following the recovery of the sum of irrigation water and precipitation during the whole experimental period (Irr_{tot}), showed that Irr_{tot} decreased from 96% at T0 to 50 and 32% at T8 and T14, respectively (Figure 10A). This strong loss of irrigation water can be explained by high evaporation rates (ETo = 4.2 mm day^{-1}, calculation see Table B6, Appendix B, Section B5) during the course of the experiment. While during the simulated heavy rainfall at T0 (24.3 mm), parts of the irrigation water penetrated down to 50 cm soil depth or even deeper through shrinkage cracks, the continued daily irrigation scheme (5.2 mm day^{-1}) did not penetrate into the subsoil to a larger extent as the shrinkage cracks and thus the preferential flow paths closed after initial wetting as shown in Schlögl et al. (2022). The water of subsequent moderate daily irrigations was trapped close to the soil surface and was thus subject to high evaporation rates (4.2 mm day^{-1}). The pronounced impact of evaporation is supported by the isotope mass balance (Figure 10B), which shows the recovery of the ^{2}H-labeled irrigation water from the simulated heavy rainfall event at T0 (Irr_{HRE}). Over the entire 50 cm soil profile, the isotope mass balance indicates somewhat lower losses than shown by the water mass balance but as well shows most pronounced losses in the top 10 cm of the soil (56% and 86% at T8 and T14 compared to T0, respectively). Thus, the irrigation rate of 5.2 mm day^{-1} was not high enough to balance the losses by evapotranspiration and seepage during the experimental period as indicated by the decreasing values of the water mass balance with time.

The vertical distributions of ammonium (Figure 14A) and nitrate (Figure 14B) on irrigated and dry plots were affected by solute transport during the simulated heavy rainfall event in different ways. Nitrate as a weakly sorbing anion in soils is expected to travel in seepage water without noticeable retardation (Blume et al., 2016). Moreover, rapid transport of dissolved nitrate along preferential flow paths has been shown in earlier studies (Bronswijk et al., 1995;

Kelly & Pomes, 1998) and could be the cause of initially decreasing nitrate contents in the topsoil in our experiment (loss of 0.37 mg nitrate-N in the top 20 cm) as evident by the comparison of nitrate in the soil profiles at DT0 (initial state) to WT0 (2 h after the heavy rainfall event) (Figure 14B). However, even though D_2O-labeled water from the simulated heavy rainfall event was found in the subsoil two hours after the event and accompanying hydrological export of nitrate from the topsoil is very likely, we did not observe an accumulation of nitrate in the subsoil. Denitrification is probably not the reason for the disappearance of nitrate at WT0, as the redox potentials in the subsoil were still around 560 ± 30 mV at two hours after the heavy rainfall simulation (Blume et al., 2016). Given that crops had been harvested before the start of the experiment and residual roots therefore were inactive, plant root uptake of nitrate (Cui & Caldwell, 1997) was likely not the cause for the profile-level decrease in nitrate mass. The gradual microbial immobilization of nitrate following severe drought within 2 hours of rewetting could have contributed, but cannot be responsible for such large nitrate "losses". Moreover, this would occur at a time when the Birch effect indicates a flush of microbial metabolites and enzymes into the soil environment, i. e., loss of carbon and nitrogen mass from the microbial community instead of uptake and immobilization. For this reason, most likely the unaccounted nitrate mass was transported below the zone investigated in this study (> 50 cm soil depth) via preferential flow. Directly beneath the upper 2 m clay layer, which comprises the investigated part of the soil profile, the shallow tufa aquifer is located (Martin et al., 2020). Moderately to strongly reducing conditions prevail in the tufa aquifer (Martin et al., 2020), so denitrification would take place, which could lead to the formation of N_2O, a greenhouse gas, or the loss of inorganic nitrogen from the system in form of N_2 gas. Constant nitrate input in the groundwater would ultimately lead to a consumption of the reduction capacity of the tufa aquifer and thus to increasing nitrate concentrations in the aquifer. Therefore, nitrate leaching along preferential flow pathways during rewetting after drying can substantially threaten groundwater quality (Sánchez Pérez et al., 2003).

Ammonium (Figure 14A) is subject to cation exchange at negatively charged mineral surfaces including clay minerals. Ammonium therefore is less prone to hydrological (downward) transport in soils compared to nitrate (Blume et al., 2016). This retardation prevented rapid loss of ammonium from topsoils by percolating irrigation water. The low mobility of ammonium in the soil profile was confirmed when comparing the ammonium mass profiles at DT0 (initial state) to WT0 (2 h after the heavy rainfall event, Figure 14A) with very similar total ammonium contents and depth distributions in both.

Nitrogen turnover processes

Soil nitrate and ammonium contents showed a high variability between the three replicate experimental plots; thus, the trends observed in space and time were often not statistically significant (Figure 14). This reflects the high spatial heterogeneity of the distribution of inorganic nitrogen compounds in soils that was also observed by Hergert et al. (1995). At our

field site, the heterogeneous distribution (quantified in terms of coefficients of variation) of the simulated heavy rainfall event water was governed by the presence of shrinkage cracks (Schlögl et al., 2022). In the beginning of the experiment, pronounced cracks (up to 1 cm width) were visible at the soil surface and the coefficients of variation of deuterium enrichment of soil water were high. These cracks closed in later states of the experiment while the coefficients of variation of isotope signatures decreased. The coefficients of variation of nitrate and ammonium, however, showed different patterns (Figure B31, Appendix B, Section B7). For nitrate, the coefficients of variation on the W plots in the top 10 cm were much lower on day 0 than on day 6 and day 14 (Figure B31), reflecting the opposite trend in variance as for the deuterium-enrichment of soil water. For ammonium, no clear trends of the coefficients of variation existed in space and time. The spatial and temporal heterogeneity of the distribution of ammonium and nitrate was therefore not governed by the presence of shrinkage cracks.

The irrigation of the dry soil stimulated the mineralization of organic nitrogen (N_{org}) which is reflected by the doubling of ammonium concentration in the topsoil (0-5 cm depth) from DT0 to WT0 (Figure 14A). This increase is in line with the observations made by H. Birch, who described intense nitrogen release upon rewetting of dry soils (Birch, 1958, 1960). The Birch effect is induced by the mineralization of dead microbial biomass and of osmoregulatory substances that are released by microorganisms upon rewetting (Fierer & Schimel, 2002; Jarvis et al., 2007; Saetre & Stark, 2005; Unger et al., 2010). This is supported by the significant and immediate increase of two extracellular enzymes (β-glucosidase and exochitinase) in soils of W plots compared to D plots within two hours of heavy rainfall simulation (Figure 17), which indicates the release of intracellular compounds (including enzymes) by lysis of a fraction of the microbial cells due to irrigation (Khan et al., 2019). The prolonged increase of ammonium in the topsoil at T6 and T14 (0.05 mg ammonium-N and 0.10 mg ammonium-N, respectively) can be explained by continued net mineralization of organic matter in cropland soils (Booth et al., 2005), by bulk atmospheric deposition of ammonium (average of 0.011 mg ammonium-N wk^{-1} on the cross sectional area of a sample core (Beyn et al., 2014), for calculation see Table B7, Appendix B, Section B8) and further nitrogen release due to daily drying and rewetting (Birch, 1958; Fierer & Schimel, 2002). Nitrogen fixation as a potential ammonium source was likely negligible, as no legumes were grown at this field site prior to the experiment. At a soil depth of 10 cm and below, ammonium contents, however, did not respond much to irrigation. The reasons can be that (i) there is less labile organic matter at soil depths below 10 cm (Appendix B, Section B2) and thus less ammonium can be released from mineralization of organic compounds or (ii) that most ammonium present is strongly sorbed to clay minerals and thus is not accessible for nitrification or other microbial-driven processes (Buss et al., 2004; Cavalli et al., 2015). Ammonium can either be bound as exchangeable cation at the surface of clay minerals (Blume et al., 2016; Buss et al., 2004) or it can enter the 2:1 clay mineral interlayer (Buss et al., 2004), rendering interlayer ammonium largely recalcitrant to microbial utilization. The high clay and silt content of the studied soils (Appendix B, Section B3) highlights the high cation-exchange capacity triggered by high surface area and high negative charge density of the clays for ammonium sorption. Alternatively, (iii) ammonium contents can remain

relatively constant if the ammonium that is produced per time step is consumed by microbial uptake or oxidized to nitrate under oxic conditions during the same period.
On the W plots, the increase of nitrate mass in the topsoil (0-5 cm) from T0 to T6 and to T14 (by 0.061 mg nitrate-N and 0.05 mg nitrate-N, respectively) (Figure 14B) cannot fully be explained by bulk atmospheric nitrate deposition (0.007 mg nitrate-N wk^{-1} on the cross sectional area of a sample core (Beyn et al., 2014) for calculation see Table B8, Appendix B, Section B9). The increase of nitrate mass at 0-20 cm soil depth at T6 and below 20 cm depth at T14 (Figure 14B) can thus be explained by nitrification (oxidation) of ammonium under oxic conditions (Figure 13) (Cui & Caldwell, 1997). The redox potentials in W plots showed great variations at 10 and 20 cm depth (Figure 13A and B), which occurred between sensors (spatial variations) and between time points in single sensors (temporal variations) (Figure 13B). The spatial variations can be explained by oxic and anoxic microsites in otherwise anoxic and oxic environments, respectively (Dorau et al., 2023; Kuzyakov & Blagodatskaya, 2015). Moderate daily fluctuations (e. g., at all sensors at 5 cm), were potentially induced by temperature changes (Dorau et al., 2021). The stronger temporal variations (e. g., sensor 1 at 10 cm (Figure 13A)) followed the daily irrigation and were thus most likely the result of rapid changes between air- and water-filled pore space. Following these changes in oxygen availability, the nitrification rates likely fluctuated. For most of the experimental time, the redox conditions remained above +100 mV, a threshold above which nitrification is active (Hansen et al., 1981), and during these periods we observed an increase in nitrate mass at 5-10 cm and 10-20 cm soil depth at T6. Below 20 cm depth at T6, nitrification did not substantially occur because redox potentials (Figure 13) were below +100 mV, disfavoring the process. At T14, however, due to the pause in daily light irrigation from the T10 to T14, redox potentials below 20 cm depth rose above the threshold for nitrification related to increased nitrate contents at T14. Nitrate and ammonium mass changes were therefore partially coupled and nitrate accumulation under oxic conditions was related to ammonium draw down and/or continued mineralization of N_{org} across the whole soil profile.
In summary, the observed nitrogen turnover processes were initially governed by the rewetting of the dry soil and the so-called “Birch effect”, which is known to be a short-term effect (Birch, 1958; Cui & Caldwell, 1997; Unger et al., 2010). After approximately one week of the experiment, the nitrogen turnover processes switched from the pulse-driven regime after rewetting to the “usual” redox-driven nitrogen cycling regime governed by oxygen availability as reflected by the drop of in situ redox potentials at greater depth.

The 1.5-fold and 2.5-fold increase of ammonium and nitrate, respectively, on D plots between T0 and T14 is remarkable. The D plots were covered with greenhouse foil between T10 and T14 to prevent wetting by a natural heavy rainfall on the evening of T10 and the following three days. Temperatures below the plastic foil might have increased and thereby microbial turnover processes were activated though we did not observe a shift in microbial community composition on D plots on T14. Prolonging the experimental drought period prior to irrigation of the dry plots by another two weeks, such as happened on the D plots, might have critically

amplified the drying effects on microbial functioning, and therefore have induced a stronger cellular water deficit and soil microbial turnover and death, with concomitant releases of organic and inorganic nitrogen (Figure 14). Alternatively, constant evaporation on D plots during the experimental period might have induced the rise of soil water transporting dissolved species such as nitrate upwards. On W plots, this effect was interrupted by the recurring irrigation.

Microbial communities and activities

Environmental conditions such as temperature, pH, oxygen availability and moisture directly affect soil microbes and thereby affect biogeochemical processes such as nitrogen turnover. The use of stable isotope labeled substrates has shown that soil microbial communities consist of a dynamic fraction that can be activated by rewetting (Aanderud et al., 2015). Revealing these processes and changes in community structure remains challenging. Nucleic acids can persist in the soil environment for long time spans (Carini et al., 2016) hampering diversity estimations. This "inactive" DNA has been linked to either dormant cells (Aanderud et al., 2015) resembling a seed bank or to extracellular nucleic acids that may play a role in other processes (Lennon et al., 2018). In this study, the more short-lived RNA has been used as a proxy of the "active" microbial community fraction. However, we did not find any significant differences between sampling treatments, depth or the length of the experiment (Figure 16). Populations of soil bacteria vary over space, time and in response to environmental changes. Their spatial variation can occur at the micro-scale (Vos et al., 2013), in relation to soil microstructure and organic matter distribution and thus it can be difficult to depict differences between samples. The increase in activities of the extracellular enzymes β-glucosidase and exochitinase (Figure 17) and of ammonium (Figure 14) on W plots nevertheless indicated an activation of microbial cells by the rewetting.

In dry soils, microbial communities display reduced metabolic activity due to a combination of desiccation stress and reduced diffusion of substrates (Schimel et al., 2007). Our data indicate higher microbial diversity (RNA) in the dry than in irrigated soils (Figure 15), although the differences in diversity were not significant. While precipitation and rewetting of soils have been shown to increase microbial metabolism (Blazewicz et al., 2014; Fierer & Schimel, 2002) they may, on the other hand, induce stress to the microbial communities (Barnard et al., 2013; Schimel, 2018) and by this they can cause the elimination of microbial taxa not adapted to dry-wet cycles (Armstrong et al., 2016; Fierer et al., 2003; Veach & Zeglin, 2020). Microbial communities in our tested soil were not particularly pre-adapted to drought and rewetting, so such a functions-related selection process within the various taxa present during rewetting of the soil seems plausible. The reasons for this selection process – from microbial death to soil chemistry as driver – are still in discussion (Schimel, 2018). In our experiment, the induced osmotic stress has most likely driven the shift in the microbial community.

4.6 Conclusions

Due to climate change, the frequency of droughts and heavy precipitation is increasing in temperate climates. In our study, we investigated the effects of a heavy rainfall event after a summer drought in a loamy floodplain soil on (i) water flow and solute transport of inorganic nitrogen species, (ii) the occurrence of the Birch effect and the transition towards redox-driven nitrogen turnover processes, and (iii) the soil microbial community structure.

Our study showed, that (i) during the heavy rainfall event, water including dissolved nitrate penetrated into the subsoil along preferential flow paths. This bears the risk of nitrate leaching into the underlying aquifer. (ii) Upon rewetting, an increase in inorganic nitrogen (ammonium) occurs as described by the Birch effect. The study confirms that this effect is a short-term effect that lasts for several days at the most until the usual redox-driven nitrogen cycling dominates again. (iii) The soil microbial community composition did not respond much to irrigation on both DNA and RNA level. Lower diversity indices on irrigated vs. dry plots however indicate, that the stress induced by rewetting leads to a certain shift in the microbial community to better adapted taxa.

The leaching of nitrate into shallow aquifers upon heavy rainfall events and the shift of the microbial community in temperate climate soils of Central Europe should be studied in more detail in follow-up studies.

5 General Discussion

In the following, the results of the three studies and their methodological and environmental implications are discussed in order to answer the research questions introduced in Chapter 1.

5.1 Methodological aspects for the extraction of inorganic nitrogen from soil samples

Information about the concentration of the two inorganic nitrogen species nitrate and ammonium is important for many applied and scientific questions, e. g., for the determination of the amount of fertilizer an agricultural field needs in the beginning of the cultivation season or for the study of soil redox processes. Preliminary tests (extraction with 0.0125 M $CaCl_2$) with the soil studied in the presented thesis gave implausible results (unpublished), which implicated that an alteration of the concentrations of nitrate and ammonium might have taken place during sample handling or extraction. Therefore, experiments were conducted to assess sample stability and extraction efficiency during the extraction process and sample stability during sample storage under different conditions (Chapter 2) at both oxic and anoxic conditions. The results are summarized and discussed in the following paragraphs and recommendations for sampling, sample storage and handling as well as the extraction procedure are given.

Stability of inorganic nitrogen concentrations under different sample storage conditions

During field campaigns, usually many soil samples are taken and they are stored until they are further processed in a laboratory. Until this point, it has to be made sure, that no alteration of nitrate and ammonium concentrations takes place during storage. To preserve the samples, they could be dried, stored cool, i. e., at 4 °C or frozen, i. e., -21 °C or 80 °C. In the presented study, samples were stored at room temperature, cooled (4 °C) and frozen (-21 °C) for up to 48 h. Frozen samples were put into the extraction solution when still frozen and were not thawed prior to extraction. The study showed that only frozen storage at -21 °C was able to preserve both nitrate and ammonium during a storage period of 48 h. In another study (Ma et al., 2005), thawing of samples and intensive sample preparation before the extraction led to changes of ammonium and nitrate concentrations and should therefore be avoided.

Sample stability and extraction efficiency during inorganic nitrogen extraction with two different extraction solutions

Nitrate and ammonium were extracted from soil samples with two different extraction solutions (0.0125 M $CaCl_2$ and 2 M KCl) under both oxic and anoxic conditions for 15, 30, 60 and 180 min. The extraction with 2 M KCl yielded stable ammonium and nitrate concentrations for all tested conditions and extraction periods, whereas the extraction with 0.0125 M $CaCl_2$

did so only under oxic conditions. Under anoxic conditions, however, nitrate concentrations decreased and ammonium concentrations increased when the extraction lasted 60 min and longer. The higher salinity of 2 M KCl was able to inhibit microbial activity and, thus, nitrate and ammonium turnover during extraction (Oren, 2001) and therefore led to more stable results than the 0.0125 M $CaCl_2$ solution.
Additionally, the extraction efficiency of both solutions was tested and it was found that 2 M KCl consistently yielded higher ammonium concentrations than 0.0125 M $CaCl_2$, when applied to the same sample. Because the potassium cation has a similar ionic radius and the same charge as the ammonium cation (Kuderna et al., 1993), 2 M KCl targets the sorbed and the dissolved ammonium whereas 0.0125 M $CaCl_2$ only targets the dissolved ammonium. This fact can be used to distinguish between these two ammonium pools. For nitrate, there is no difference in the extraction efficiency, because nitrate does not sorb to soil mineral particles and is thus easily dissolved in both extraction solutions.

Implications for sampling, sample handling and the extraction of inorganic nitrogen species from soils

The results of the study have several technical implications. Field samples should be frozen immediately after retrieval as otherwise it is very likely that nitrate and ammonium concentrations undergo severe alterations and the results of extractions will not reflect the in situ state of the sample. Thawing of samples during storage should be avoided by all means. For the extraction of nitrate and ammonium, samples should be kept frozen as long as possible and the subsamples should be added to the extraction solution when still frozen. The selection of the extraction solution depends on the research question of the respective study, e. g., if the dissolved or the dissolved *and* sorbed ammonium pools are of interest. It should always be kept in mind, that with 0.0125 M $CaCl_2$ as extractant, the extraction period should be kept as short as possible (max. 30 min) to minimize the possibility of concentration alterations of nitrate and ammonium.

5.2 Effects and processes in floodplain soils induced by a heavy rainfall event after summer drought

Floodplains are important landscape compartments for the biogeochemical turnover of nutrients and pollutants (Coby et al., 2011; Lair et al., 2009; Venterink et al., 2003). They are influenced by alternating water saturation due to rising and falling groundwater levels or water stagnation during winter and severe drying during the summer season. In fine-textured floodplain soils, shrinkage cracks of substantial width and depth can form during summer drought periods. As the frequency of these drought periods as well as following heavy rainfall events rises with ongoing climate change (Coumou & Rahmstorf, 2012) this thesis studied pesticide transport, inorganic nitrogen turnover and effects on the microbial community

composition in floodplain soils induced by a simulated heavy rainfall event after a summer drought in a field experiment (Chapter 3 and 4).

Water infiltration patterns, preferential flow and the transport of dissolved and sorbed compounds

The floodplain soil at the studied site was dry and exhibited a network of shrinkage cracks of 1 to 2 cm width, several decimeters in horizontal and likely also vertical extension in the beginning of the experiment. The water, that was used for the simulated heavy rainfall event, was spiked with deuterated water (D_2O) as a hydrological tracer. It allowed to follow the water infiltration pattern during the whole experiment (Chapter 3 and 4). During the simulated heavy rainfall event 24.3 L m^{-2} were applied to the experimental field within one hour. Two hours after the end of the heavy rainfall event, 50-cm soil cores were retrieved. The isotopic signature of the pore water revealed that during and after the heavy rainfall event, 50 % of the event water resided in the top 20 cm but the other 50 % of the water were found evenly distributed at 20 to 50 cm. This finding shows that the shrinkage cracks served as preferential flow paths and as such could also allow for the transport of particle-bound (Chapter 3) and dissolved compounds (Chapter 4).

In literature, several studies describe surprising findings of strongly sorbing pesticides that were found in soil pore water (Kasteel et al., 2010) or drainage pipes (Kjær et al., 2011; Norgaard et al., 2014). Glyphosate shows a strong sorption to mineral particles (Gimsing & Borggaard, 2002; Sprankle et al., 1975; Wimmer et al., 2023) but nevertheless in the presented study, it was associated with findings of the deuterium-labeled heavy rainfall event water in the subsoil two hours after the simulated heavy rainfall event (Chapter 3). This suggests particle-bound transport of glyphosate along preferential flow paths and can explain the unexpected mobility of glyphosate in soils during storm events. Glyphosate has two known degradation pathways, to AMPA ((aminomethyl)phosphonic acid) and sarcosine, respectively, and it is said to be readily degraded in soils (Sviridov et al., 2015). However, once leached to the subsoil, it may reach oxygen-depleted and less dense microbially populated soil layers (Preusser et al., 2021) which might impair glyphosate degradation. As glyphosate strongly sorbs to mineral particles, the nature of these particles affects glyphosate's mobility under reducing conditions. For example, iron-containing clay mineral particles remain stable if iron is reduced and glyphosate would be kept sorbed, but iron(oxy)hydroxides partially dissolve when Fe(III) is reduced to Fe(II) (Cornell & Schwertmann, 2003) thereby releasing glyphosate. The degradability of glyphosate under anoxic conditions is not yet well studied. A companion study on the same experimental setup as presented in this thesis found that glyphosate is still degraded by fungi and bacteria in the subsoil, but degradation is slower compared to the topsoil (Wirsching et al., 2022). This would result in an accumulation of glyphosate or ultimately its degradation products, sarcosine and AMPA, in the subsoil. Sarcosine as amino acid is readily taken up by organisms, but AMPA as a well soluble and

thus mobile organic compound can ultimately end up in and pollute groundwater resources (Sviridov et al., 2015).

Besides particle-bound transport, this thesis also investigated solute transport of nitrate during a heavy rainfall event (Chapter 4). As nitrate is highly soluble in water it is expected to leach along preferential flow paths (Franklin et al., 2021; Kelly & Pomes, 1998). In the presented study a decrease of nitrate in the top 20 cm of the soil was observed after the simulated heavy rainfall event. As the summer barley, that was cultivated on the field, was harvested before the experimental period, nitrate uptake by plant roots (Cui & Caldwell, 1997) can be excluded as reason for the nitrate loss in the topsoil. Microbial immobilization of the nitrate might have contributed but cannot account for the full nitrate loss in the topsoil. Thus, part of the nitrate must have leached to depths below 50 cm, as no accumulation of nitrate was observed in the soil above 50 cm, i. e., the maximum depth of the sample cores. Nitrate leaching from soils into groundwater during heavy rainfall events has been observed in other studies (Bauwe et al., 2015; Kennedy et al., 2012). At the herein described study site, right below the 2 m thick Gleysol lies an aquifer (calcareous tufa with imbedded peat layers (Martin et al., 2020)). Although in this aquifer, reducing conditions would promote nitrate attenuation by denitrification, the leaching of nitrate into the aquifer should be prevented as the electron donors in the aquifer (mainly bisulfide and organic matter (Klingler et al., 2020; Martin et al., 2020)) may be used up at some point and nitrate would accumulate in the aquifer. The pollution of groundwater with nitrate is a wide-spread problem (van Grinsven et al., 2012) and therefore additional pathways for nitrate input into groundwater should be thoroughly studied and quantified.

Drivers of inorganic nitrogen turnover – the role of the "Birch effect" and dynamic redox conditions

This thesis studied the impacts of a heavy rainfall event after summer drought on the soil inorganic nitrogen turnover (Chapter 4). Two different drivers of these processes are known: The rewetting of dry soils usually evokes mineralization of dead microbial biomass and osmoregulatory substances and thus a pulse of CO_2 and inorganic nitrogen (nitrate and ammonium) (Birch, 1958, 1960; Fierer & Schimel, 2002; Unger et al., 2010). On the other hand, the rewetting leads to a swelling of clay minerals and thus a closure of the shrinkage cracks and a limitation in oxygen supply (Haberer et al., 2012), which then leads to redox-driven nitrogen turnover. In the presented study, both processes were followed by the measurement of nitrate and ammonium concentrations as well as in situ redox conditions.

At day 0 of the field experiment, soil cores were taken from irrigated and dry control plots two hours after the simulated heavy rainfall event. The results from the dry control plots at day 0 were interpreted as the initial state of the soil and the results from the irrigated plots reflected the immediate effects of the heavy rainfall event. In the top 5 cm of the soil, a statistically significant doubling of the ammonium content on irrigated plots is a sign for the occurrence of the Birch effect, i. e., a pulse of inorganic nitrogen. Studies on the Birch effect also reported an increase of nitrate (Birch, 1960; Cui & Caldwell, 1997). However in the presented study,

nitrate decreased in the top 20 cm during or right after the heavy rainfall event, which was most likely a result from nitrate leaching through macropores (compare discussion in the paragraph above). Therefore, a Birch effect-related nitrate increase could still have occurred but was potentially masked by nitrate leaching.
The in situ redox potentials responded to the heavy rainfall event by decreasing from oxidizing to reducing conditions. The response set in more quickly in the topsoil (within 24 h) than in the subsoil (up to three days) but was more stable in the subsoil than in the topsoil. Subsequently to the heavy rainfall event, the irrigated experimental plots received a light daily irrigation to keep the soil moist and the shrinkage cracks closed. The dynamics of soil nitrate at days 6 and 14 in different depths were in line with the dynamics of redox conditions. The study confirmed, that the Birch effect is a short term effect and the inorganic nitrogen turnover is again driven by redox conditions after a few days. The longer the drying period, the more nitrogen is mineralized upon rewetting (Birch, 1960). Therefore, the effect is stronger in regions with a climate with defined dry and wet periods. However, with an increasing frequency of drought and heavy rainfall in temperate climates such as in Central Europe, the importance of the Birch effect for soil nitrogen cycling will increase.

Microbial community composition

To evaluate the impact of a heavy rainfall event after a summer drought period and subsequent dynamic redox conditions on the soil microbial community, the soil microbial community composition on DNA and RNA-level and extracellular enzyme activities were investigated (Chapter 4). It was expected, that short-term changes due to the rewetting after drying should be more visible on the RNA-level than on DNA-level because microbial growth and replication is much slower than the activation of gene transcription (Göransson et al., 2013; Placella & Firestone, 2013). Surprisingly, no statistically significant difference between the composition of the active fraction of the microbial community neither in dry and irrigated soils nor along a depth or time gradient was found. The heterogeneity between the individual samples was higher than possible effects of the irrigation. However, slightly higher diversity indices were found in the dry soils compared to the irrigated soils, although those differences were not statistically significant. As the rewetting of dry soils imposes stress on microbial communities (Schimel, 2018) these results indicate, that certain taxa in the investigated soil did not endure this stress and died (Armstrong et al., 2016; Fierer et al., 2003; Veach & Zeglin, 2020). Under more frequent dry-wet-cycles in the future, the soil microbial community in temperate climates will be reshaped to be more resilient to these weather extremes.

6 Conclusions and Outlook

This thesis demonstrated that many interdependent processes occur in floodplain soils upon a heavy rainfall event after a summer drought. Its results are important for hydrogeological settings where fine-textured soils lie on top of shallow aquifers.

The general experimental setup of the field study was suitable to study interacting processes occurring upon a simulated heavy rainfall event. The use of deuterium-labeled water as tracer during the simulated heavy rainfall event was successful. It allowed to follow the water infiltration and to show that preferential flow paths in the form of shrinkage cracks enabled a fast penetration of the water into the subsoil. Alongside measurements of glyphosate and nitrate in soil samples taken along shrinkage cracks allowed to compare the traveling behavior of both substances with the water percolation. The revision of the method for determination of inorganic nitrogen compounds in soil samples yielded a robust procedure for the sampling, sample storage, sample handling and the actual extraction of ammonium and nitrate from soil samples. This procedure was followed in the presented study and it produced plausible and reliable results.

On the other hand, the methodology of the field experiment for further investigation of the studied processes could also be improved in certain aspects. First, in this study, the nitrogen turnover processes during the field experiment were described and deduced from mass balances of the main inorganic nitrogen species, i. e., nitrate and ammonium. For a more robust identification of the processes, e. g., an analysis of genes that encode for the hypothesized processes (nitrification, denitrification) or an analysis of the isotopic composition of nitrate and ammonium with respect to $\delta^{15}N$ and $\delta^{18}O$, would be useful. Second, the investigation depth of 50 cm (i. e., length of the soil corer) realized in the presented study, turned out to be too shallow to conclusively study the process of nitrate leaching during the heavy rainfall event. For future studies, I recommend to further investigate the loss of nitrate from the topsoil during heavy rainfall events. It is important to quantify the amount of nitrate, that potentially leached through the shrinkage cracks into the aquifer to assess its significance compared to groundwater nitrate pollution by agricultural usage. To this end, the full soil profile until the shallow tufa aquifer should be studied, e. g., by taking longer soil cores or by using lysimeters which offer the possibility to directly sample the pore water in different depths.

The presented study showed that glyphosate is transported along preferential flow paths during a heavy rainfall event and thus rose the awareness that also strongly sorbing organic micropollutants by this means can quickly reach deep soil layers. Future studies should therefore address other strongly sorbing compounds and test their susceptibility to transport by preferential flow in field studies. In a companion study, it was found, that the glyphosate transported to the subsoil was degraded slower than in the topsoil. Further studies should investigate if this is due to smaller numbers of microbial cells in the subsoil or if the lack of oxygen impairs the degradation. For this, microcosm experiments under controlled conditions could be performed.

Climate change is an ongoing process and its consequences (will) become more and more obvious. From 2018 on, prolonged drought periods occurred in Germany during the summer months. The field study described in this work, took place in 2019. Thus, an evaluation of the effects of repeated droughts on the investigated floodplain soils with respect to inorganic nitrogen turnover and microbial community compositions is considered important.

Appendix A: Supporting Information on Chapter 3

A1 Soil profile and core photos

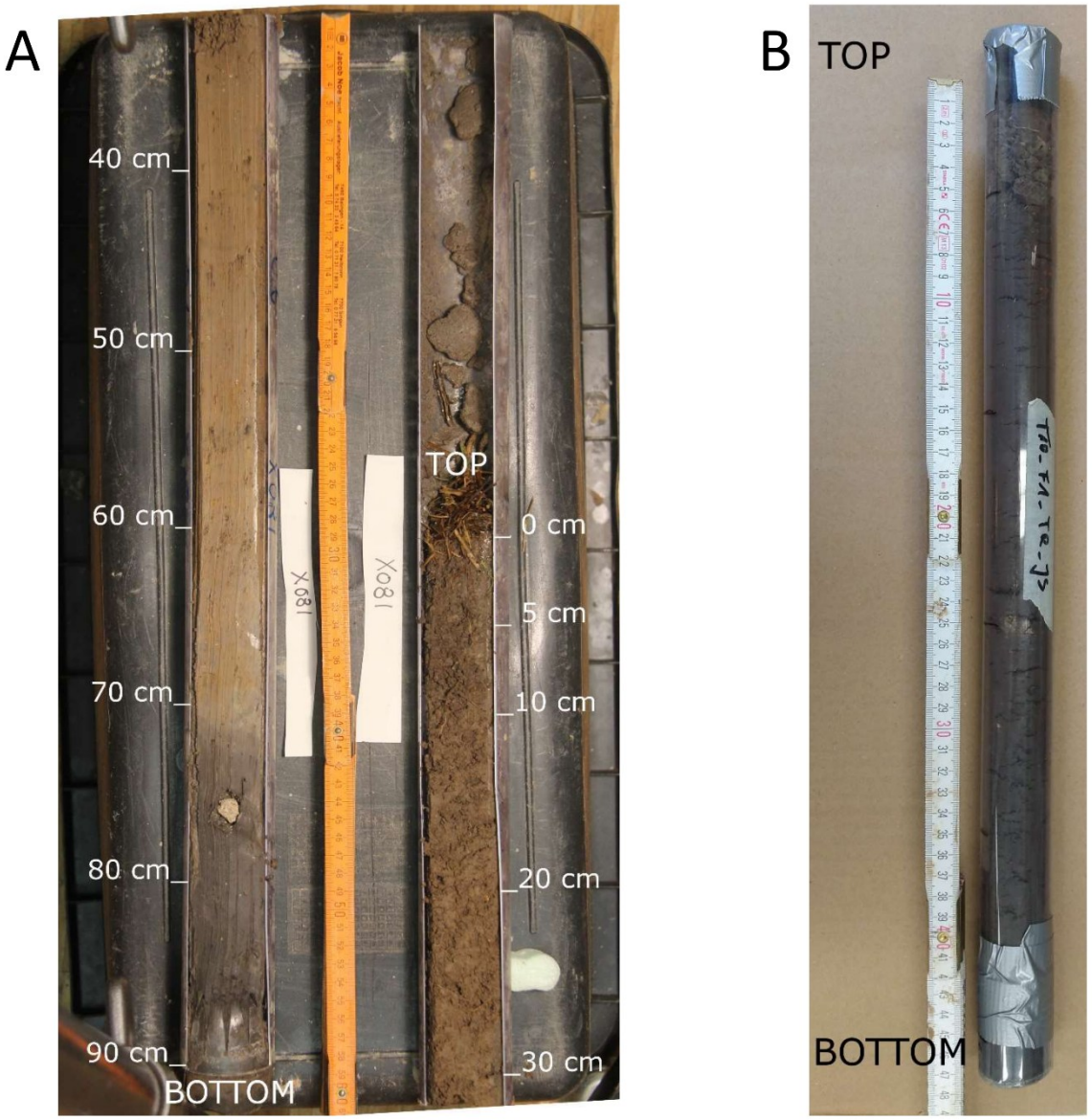

***Figure A18**: **A**. Soil profile from a location 100 m NW' of the experimental site. A 1.20 m core was taken with a direct push unit (6610 DT, Geoprobe, Salina, Kansas, US), the missing 30 cm can be explained by core loss at the bottom of the core. The core liner was cut at 0.6 m for taking the photo. Depth in cm below ground level is depicted besides the core. The top 70 cm of the soil have a red-brown color and comprise the oxidized Go horizon. A color shift towards grey is visible around 71 cm depth and marks the start of the reduced Gr horizon. Sampling depth in the presented study was 50 cm and thus within the Go horizon. (The photo is courtesy of S. Klingler and S. Martin.) **B**. Photo of a 50 cm soil core taken from the Plot D1 at the experimental site of the presented study. The continuous red-brown color in the upper 50 cm is visible through the plastic liner.*

A2 Soil texture

Determination of soil texture

The cores taken for grain size analysis were cut with an oscillating saw into sections from 0 – 5 cm, 5 - 15 cm, 15 – 25 cm, 25 – 35 cm, 35 – 45 cm and 45 – 50 cm. For each section, grain size analysis was performed according to German Standard DIN EN ISO 17892-4 (DIN Deutsches Institut für Normung e. V., 2017). In brief, a representative subsample (50g) was sieved wet trough 2 mm, 1mm and 125 µm sieves to separate the fine-grained fraction below 125 µm. The fraction bigger than 125 µm was dried and sieved dry through 1mm, 500 µm, 250 µm and 125 µm sieves. Dry mass of all fractions was determined by weighting. The fraction smaller than 125 µm was further analyzed by sedimentation analysis using the integral suspension pressure method (ISP) (Durner et al., 2017) using a PARIO device (Meter Group, Munich, Germany).

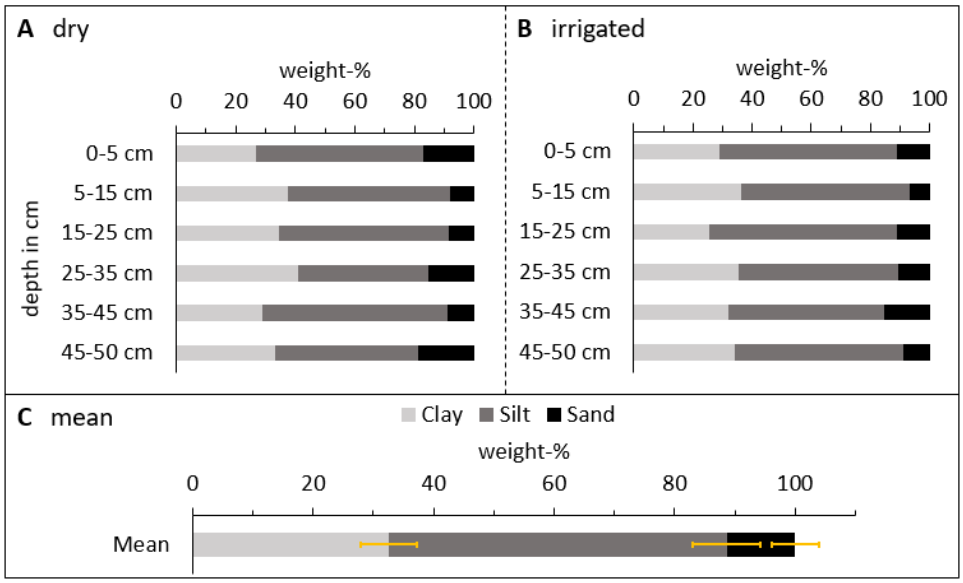

***Figure A19**: **A** and **B**. Grain size distribution for cores from dry (D) (panel A) and irrigated (W) plots (B) are shown for six different depth intervals each. **C**. Soil texture as weight-% of clay (light gray), silt (dark gray) and sand (black). Mean grain size distribution and standard deviations (yellow bars) were calculated from all samples (n = 12). The soil is a silty clay loam.*

A3 Soil organic matter (SOM) quantified as total organic carbon (TOC)

Determination of total organic carbon (TOC)

To analyze total organic carbon (TOC), soil cores (DcT10 and WcT14) were cut with an oscillating saw into sections of 5 or 10 cm length (0 – 5 cm, 5 - 15 cm, 15 – 25 cm, 25 – 35 cm, 35 – 45 cm and 45 – 50 cm). Correlating depth segments from the three replicate D and W cores, respectively, were combined to obtain representative samples. An aliquot of 10 g was freeze-dried (CHRIST ALPHA 1-4, CHRIST, Germany) and ground with a planetary mill to a grain size < 63 µm. For each analysis, 1 g of dry, ground soil was used. Inorganic carbon was removed by decalcification with 16% aqueous HCl. Afterwards, samples were washed with ultrapure water until reaching a minimum pH of 5. The amount of inorganic carbon was estimated by weight loss after drying and independently determined by acid titration of a second subsample. TOC was analyzed from the dried, decalcified sample by elemental analysis in an elemental analyzer (Elementar vario EL, Elementar, Hanau, Germany), with four replicate measurements for each sample. TOC was normalized to the initial dry weight of the soil and expressed as weight-%.

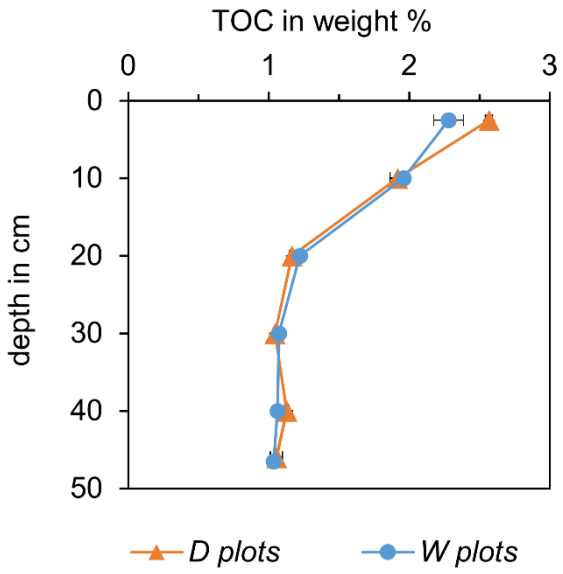

Figure A20: *Organic carbon content as TOC from dry (D, orange triangles) and irrigated plots (W, blue circles) are shown. Mean values and standard deviations were calculated from replicate measurements from the same sample (n = 4).*

A4 Weather data

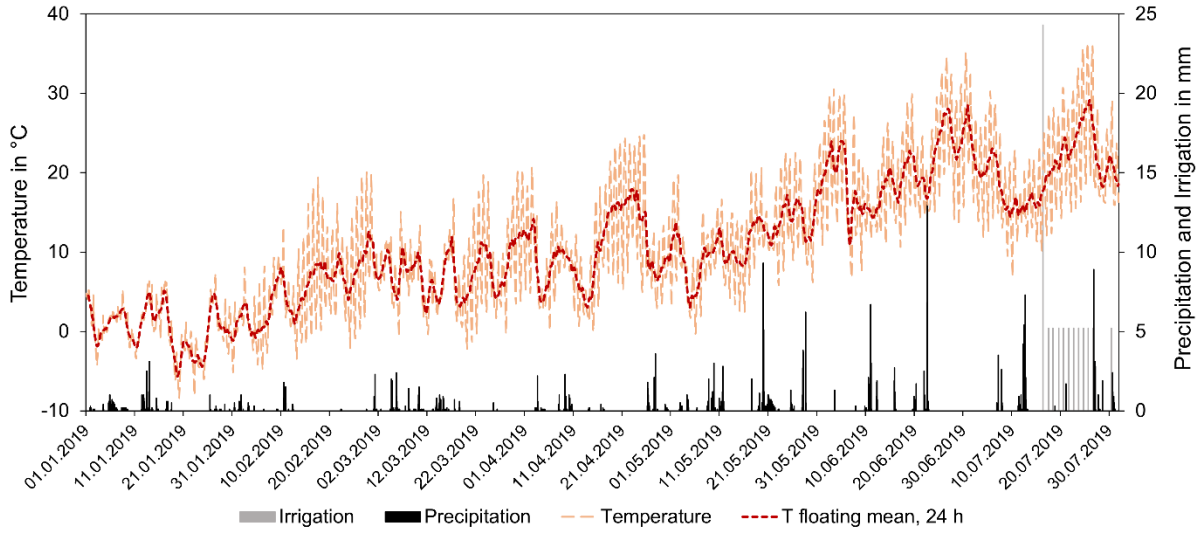

Figure A21: *Hourly data on irrigation (grey bars) and natural precipitation (black bars) in mm as well as temperature (T) in °C from 01.01.2019 until 31.07.2019 (experiment duration 16.07.2019 – 30.07.2019).*

A5 Calculation of reference evapotranspiration ETo according to FAO Irrigation and Drainage Paper No. 56 (Allen et al., 1998)

***Table A4**: Data on temperature (T), relative humidity (RH) and global radiation (Rs) from the weather station in TÜ-Unterjesingen used for the calculation of the reference evapotranspiration ETo for the period 1st to 31st July 2019*

Parameter	Measured value
T_{max} in °C	36.3
T_{mean} in °C	20.4
T_{min} in °C	6.9
RH_{max} in %	100.0
RH_{mean} in %	68.7
RH_{min} in %	26.0
Rs in W m^{-2}	236.0
ETo in mm day^{-1}	4.2

A6 Water balances

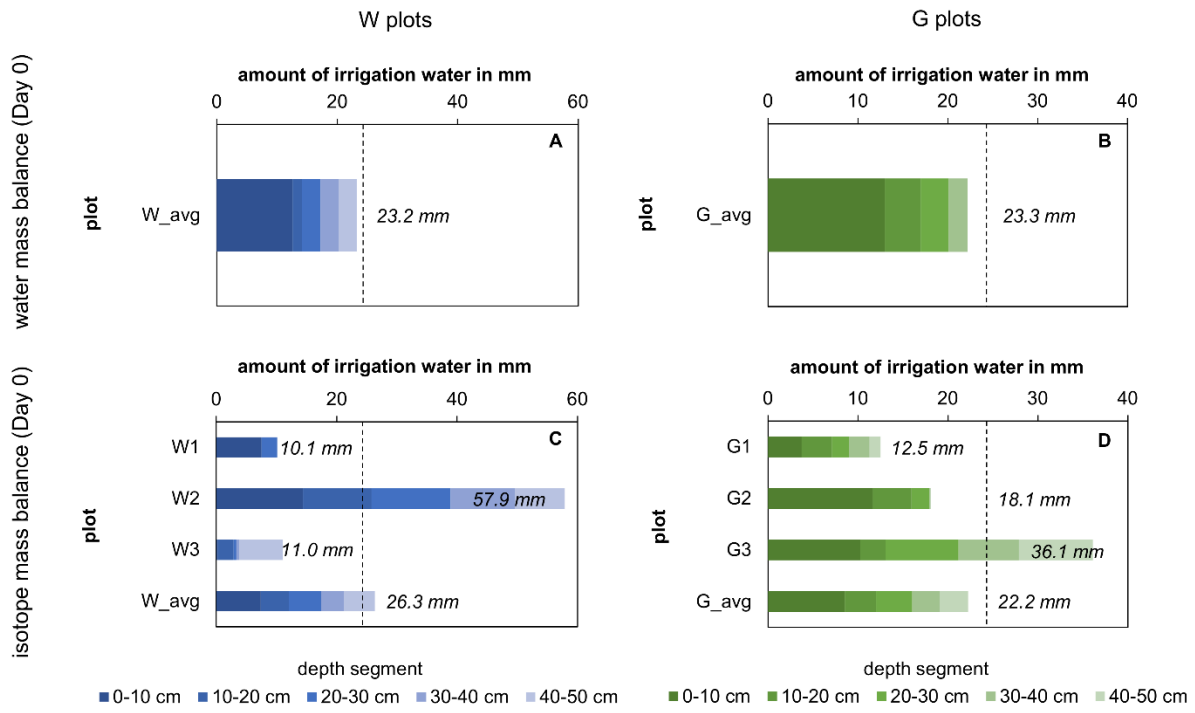

Figure A22: *The amount of irrigation water recovered in the cores right after the simulated heavy rainfall event (Day 0) is shown for all 10 cm depth segments (color gradient) and the sum of 0 - 50 cm depth is displayed close to the bar. The dashed line indicates the 24.3 mm (= 100 %) of irrigation water applied in the heavy rainfall event.* ***A*** *and* ***B.*** *The water mass balances were calculated from the difference between the mean gravimetric water content on D plots vs. W (blue) and G (green) plots, respectively, on Day 0.* ***C*** *and* ***D.*** *The isotope mass balances were calculated from the percentage of D_2O-labeled water and the gravimetric water content for W (blue, panel B) and G plots (green, panel C). Water balances from individual cores (W1 – 3 and G1 – 3) and the mean values are displayed (W_avg, G_avg).*

A7 Glyphosate concentration vs. percentage of irrigation water in soil water

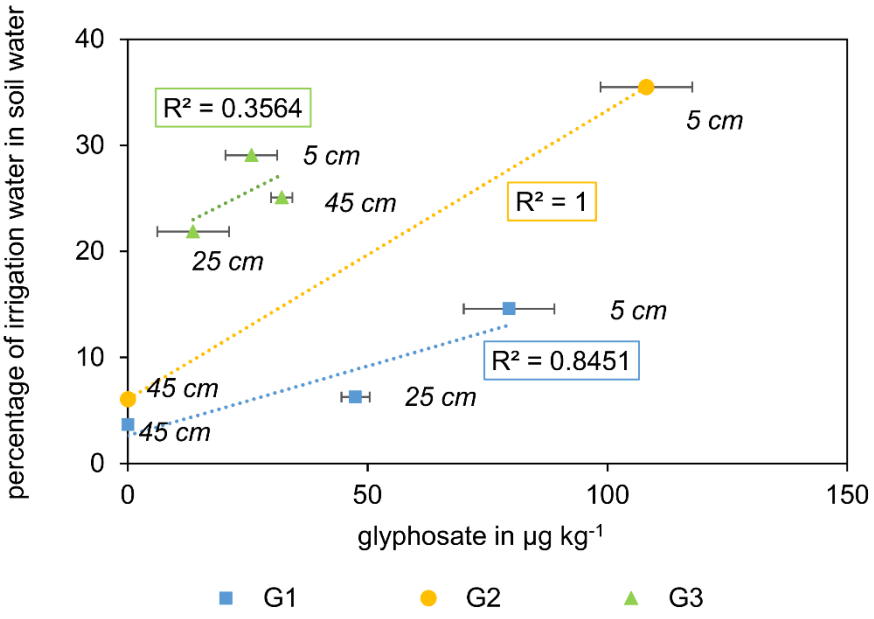

***Figure A23**: Correlation of glyphosate concentrations in the soil (µg kg^{-1}) and percentage of irrigation water in individual cores from plots G1 (blue squares), G2 (yellow circles) and G3 (green triangles). Trend lines and R² are shown in respective colors. Depth below ground level is displayed close to the data points (e. g., "5cm" corresponds to depth segment of 0 – 10 cm).*

A8 Redox potentials on G plots

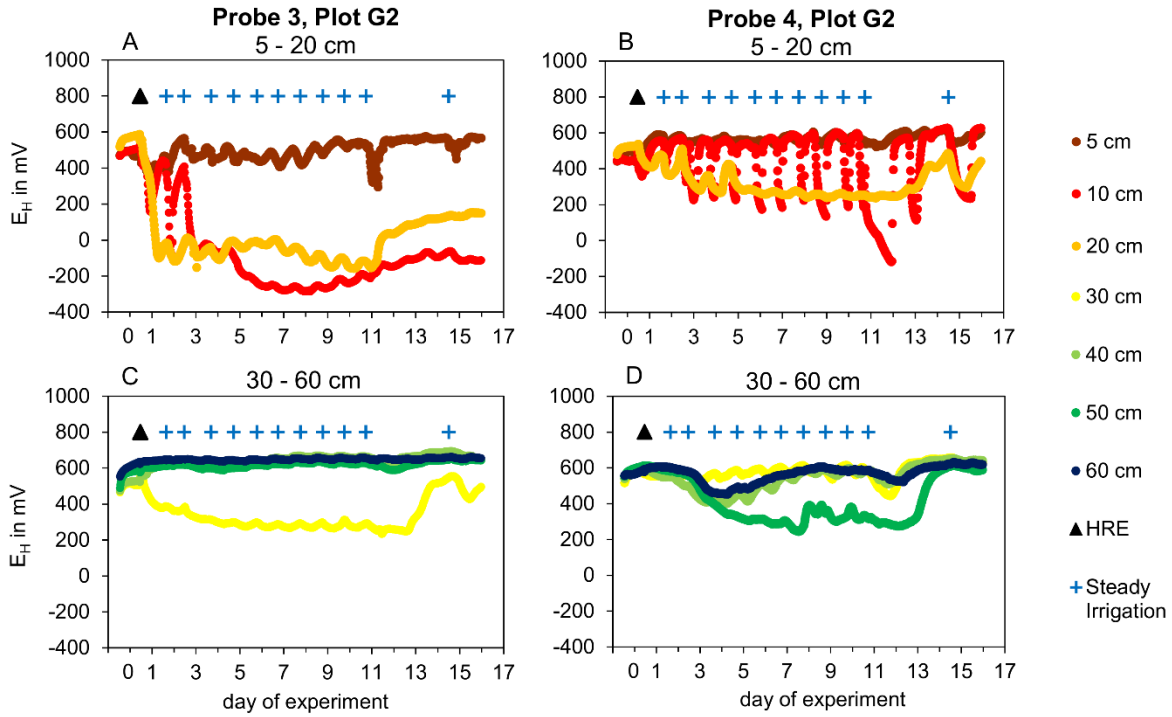

***Figure A24**: In situ redox potentials at ph7 reported in mV vs. SHE from the two redox probes installed on a plot (G2) treated with water and glyphosate. Panels **A** and **B** show potentials in the topsoil at depths of 5 cm (brown), 10 cm (light red), and 20 cm (orange). Panels **C** and **D** show potentials in the subsoil at depths of 30 cm (yellow), 40 cm (light green), 50 cm (dark green) and 60 cm (blue). The time point of the heavy rainfall event (HRE) is labelled with a black triangle and the times of the steady (daily) irrigation are labelled with dark blue crosses. The redox conditions are characterized as follows: oxidizing (> +400 mV vs. standard hydrogen electrode), weakly reducing (+400 to +200 mV), moderately reducing (200 to -100 mV) and strongly reducing (< -100 mV) (Mansfeldt, 2003).*

A9 Elemental composition of the soil

***Table A5**: Elemental composition (Al, Ca, Cu, Fe, K, Mg, Mn, P, Zn) of the soil. Element concentrations are given in g kg^{-1}.*

depth in cm	Al	Ca	Cu	Fe	K
	g kg^{-1}	g kg^{-1}	g kg^{-1}	g kg^{-1}	g kg^{-1}
0-10	33.6 ± 0.2	11 ± 1	0.03 ± 0	26.8 ± 0.1	31.5 ± 0.1
10-20	34.4 ± 0.5	12.9 ± 0.5	0.03 ± 0	27.3 ± 0.1	25 ± 12
20-30	35.4 ± 0.3	17 ± 3	0.027 ± 0.006	27.38 ± 0.09	32.2 ± 0.1
30-40	34 ± 2	29 ± 17	0.027 ± 0.006	27 ± 2	31 ± 2
40-50	34.3 ± 0.8	33 ± 16	0.027 ± 0.006	26 ± 1	31 ± 1

depth in cm	Mg	Mn	P	Zn
	g kg^{-1}	g kg^{-1}	g kg^{-1}	g kg^{-1}
0-10	16.8 ± 0.2	0.27 ± 0.01	1.06 ± 0.05	0.07 ± 0
10-20	17.2 ± 0.2	0.73 ± 0.03	0.9 ± 0.1	0.07 ± 0
20-30	17 ± 1	0.69 ± 0.06	0.71 ± 0.08	0.063 ± 0.006
30-40	15 ± 2	0.62 ± 0.06	0.61 ± 0.07	0.06 ± 0
40-50	14 ± 1	0.60 ± 0.08	0.60 ± 0.05	0.06 ± 0

Appendix B: Supporting Information on Chapter 4

B1 Soil profile in a soil core from the Ammer valley

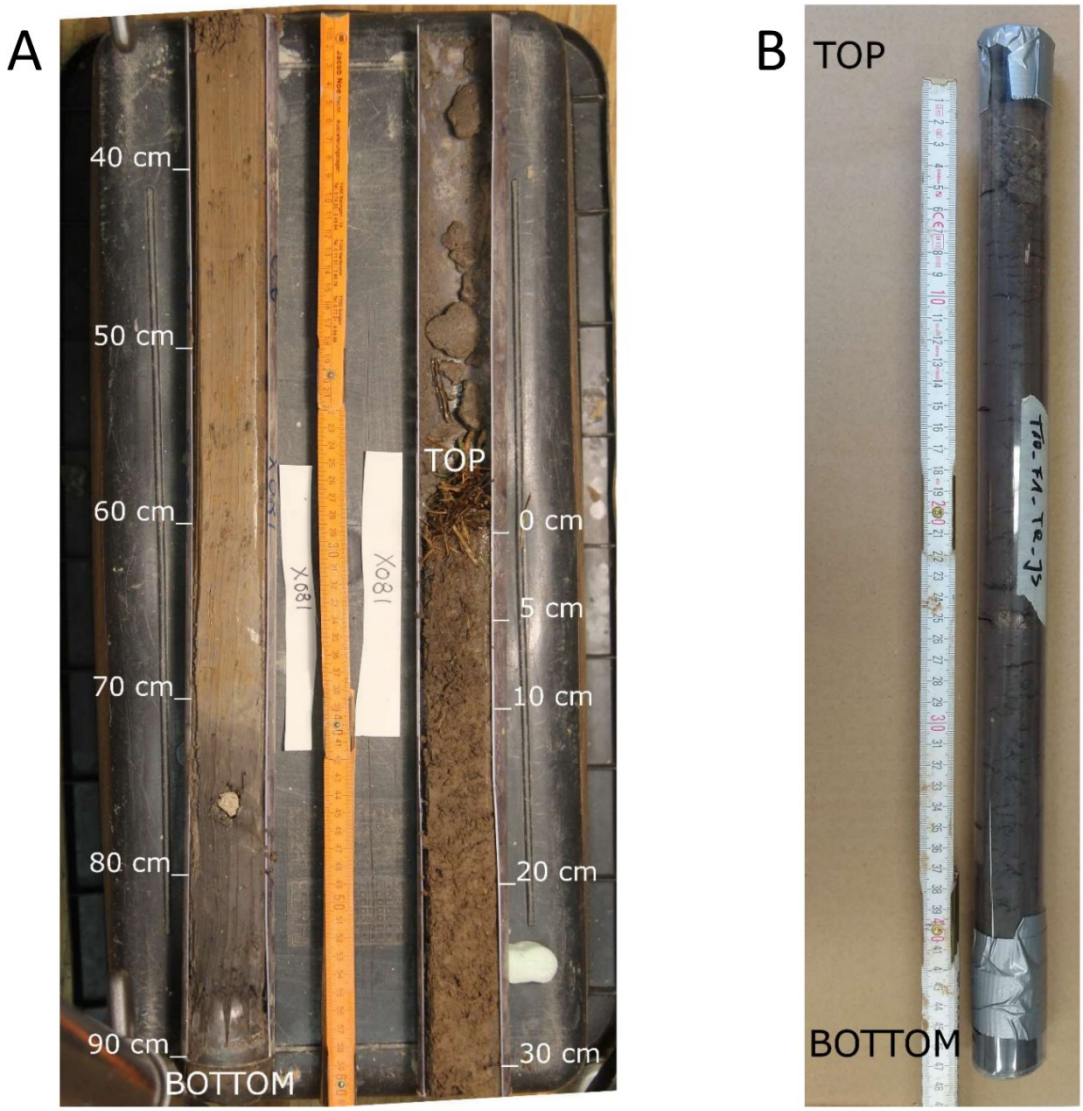

***Figure B25**: **A**. Photo of the upper 90 cm soil profile from a location 100 m NW' of the study site. A 1.20 m deep core was retrieved with a direct push probe (6610 DT, Geoprobe, Salina, Kansas, US), the core was cut in two parts lengthwise for better visibility of the sediments and crosswise at 0.6 m for taking the photo. The missing 30 cm are due to core loss at the bottom of the core. Depth in cm below ground level is depicted besides the core. The upper 70 cm of the core are of uniform red-brown color until at 71 cm the color abruptly changes to grey marking the transition from the Go to the Gr horizon in this Gleysol. Maximum sampling depth of the presented study was 50 cm, which was well within the Go horizon. (The photo is courtesy of S. Klingler and S. Martin.) **B**. Photo of a 50 cm soil core from the presented study (plot D1). The uniform red-brown color is visible through the plastic liner.*

B2 Soil organic matter

Determination of total organic carbon (TOC)

For the analysis of soil organic matter as total organic carbon (TOC), cores from plots D1-3 and from W1-3 were cut into the following segments: 0-5 cm depth, 5-15 cm, 15-25 cm, 25-35 cm, 35-45 cm, 45-50 cm. The corresponding depth segments from all D plots and from all W plots, respectively, were combined and aliquots of 10 g of soil were freeze-dried (CHRIST ALPHA 1-4, CHRIST, Germany) and were ground to a grain size of < 63 µm with a planetary mill. One 1 g aliquot of each sample was decalcified with 16% aqueous HCl and subsequently washed with ultrapure water until reaching at minimum a pH of 5. The sample was again dried and then weighed to determine the amount of inorganic carbon. Inorganic carbon was independently determined by acid titration of a second subsample to control the decalcification. The dried and decalcified subsample was analyzed for TOC in an elemental analyzer (Elementar vario EL, Elementar, Hanau, Germany) with four replicate measurements per sample. TOC was then normalized to the initial dry weight of the sample and expressed as weight-%.

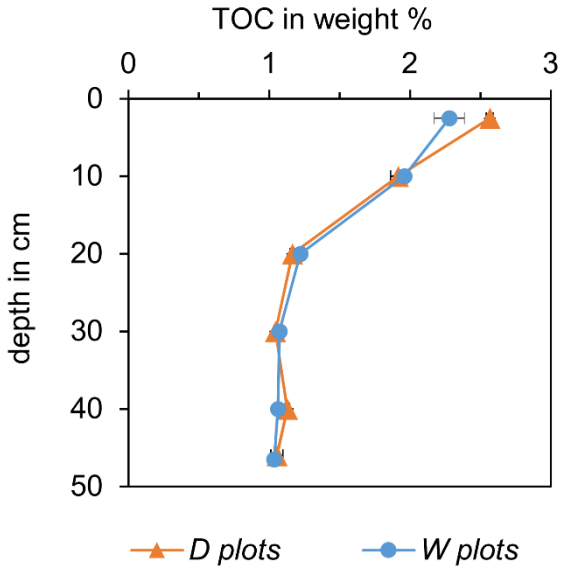

***Figure B26**: Distribution of soil organic carbon (as TOC) in weight-% in a 50-cm depth profile of the studied Gleysol on irrigated plots after 14 days of irrigation (W plots, blue dots) and dry control plots (D plots, orange triangles).*

B3 Soil texture

Determination of soil texture

For the analysis of grain size distribution, cores from plots D1-3 and from W1-3 were cut into the following segments: 0-5 cm depth, 5-15 cm, 15-25 cm, 25-35 cm, 35-45 cm, 45- 50 cm. The corresponding depth segments from all D plots and from all W plots, respectively, were combined. For each depth segment, grain size analysis was conducted following the German Standard (DIN Deutsches Institut für Normung e. V., 2017). Aliquots of 50 g per sample were sieved wet through sieves of 2 mm, 1 mm and 125 µm mesh size to separate the fraction smaller than 125 µm. The fraction bigger than 125 µm was dried and sieved dry through sieves of 500 µm, 250 µm, and 125 µm. The fraction smaller than 125 µm was further analyzed by sedimentation analysis using the integral suspension pressure method (ISP) (Durner et al., 2017) using a PARIO device (Meter Group, Munich, Germany).

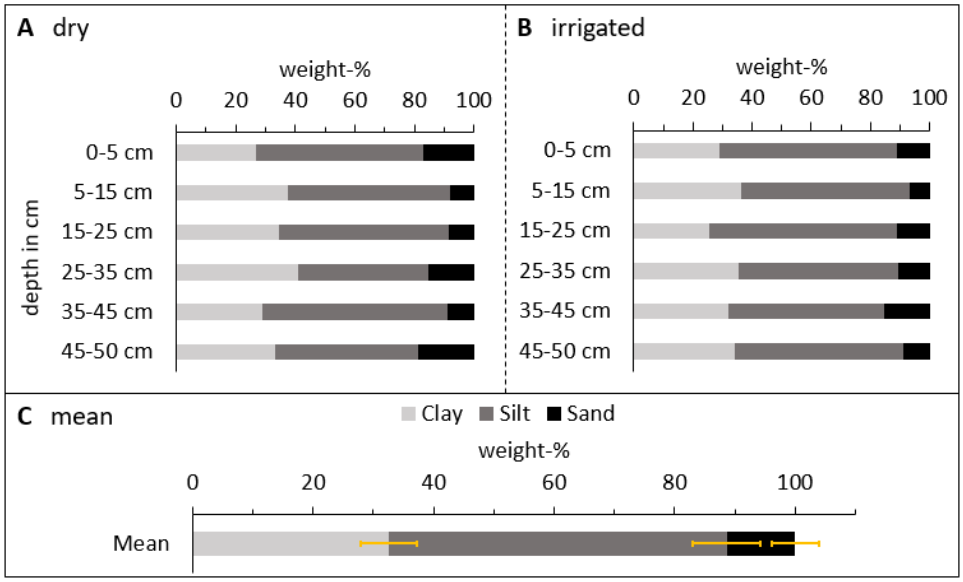

***Figure B27**: Grain size distribution in weight-% of clay (light grey), silt (dark grey), and sand (black). **A** and **B**. Grain size distribution in 50-cm soil profiles of the studied Gleysol on dry control plots (A) and irrigated plots (B). **C**. Mean values and standard deviations (yellow bars) of the grain size distribution calculated from all samples and depths from dry and irrigated plots (n = 12). The soil is a silty clay loam.*

B4 Weather data

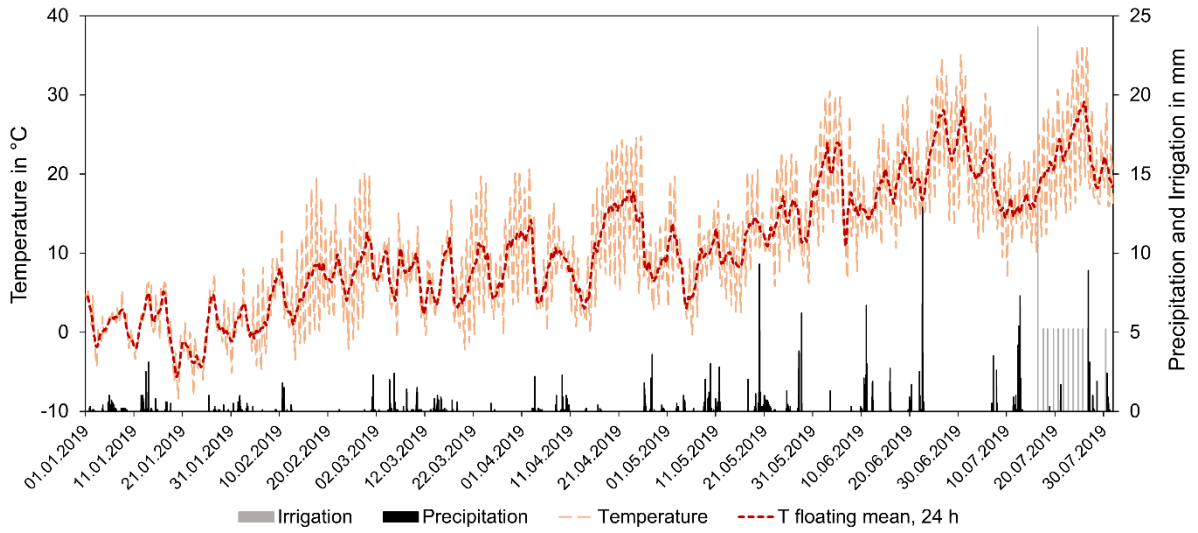

***Figure B28**: Hourly data of temperature (T) in °C (light red line), natural precipitation (black bars) and irrigation (grey bars) in mm and a 24-h floating mean of the temperature in °C for the period from 01.01.2019 until 31.07.2019 from the weather station in Tübingen-Unterjesingen. The experiment took place from 16.07.2019 until 30.07.2019.*

B5 Calculation of reference evapotranspiration ETo

The reference evaporation ETo was calculated according to FAO Irrigation and Drainage Paper No. 56 (Allen et al., 1998).

***Table B6**: Data on temperature (T), relative humidity (RH) and global radiation (Rs) from the weather station in TÜ-Unterjesingen used for the calculation of the reference evapotranspiration ETo for the period 1st to 31st July 2019*

Parameter	Measured value
T_{max} in °C	36.3
T_{mean} in °C	20.4
T_{min} in °C	6.9
RH_{max} in %	100.0
RH_{mean} in %	68.7
RH_{min} in %	26.0
Rs in W m^{-2}	236.0
ETo in mm day^{-1}	4.2

B6 Microbial community analysis

Relative sequence abundance

The methodology is described in the main text.

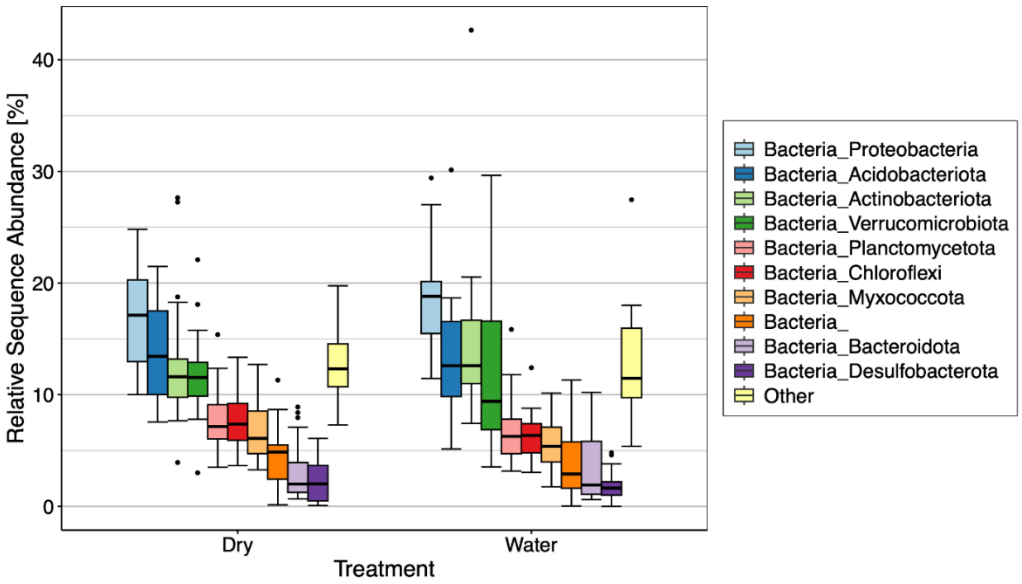

***Figure B29**: Relative sequence abundance of bacteria phyla in the studied soil sorted by dry and watered plots.*

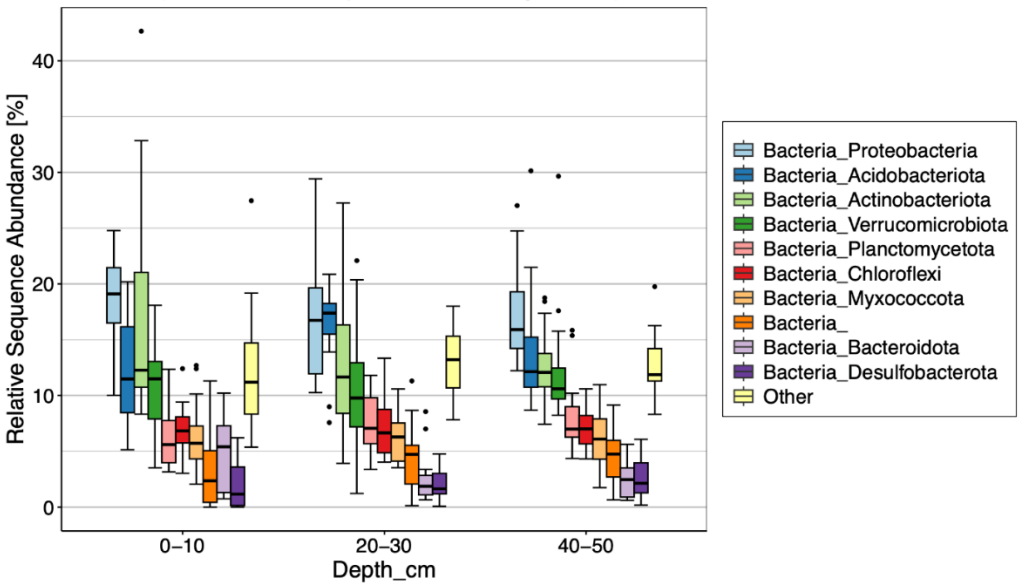

***Figure B30**: Relative sequence abundance of bacteria phyla in the studied soil sorted by depth (0-10 cm, 20-30 cm, 40-50 cm).*

B7 Coefficients of variation of nitrate and ammonium contents on W plots

Coefficients of variation were calculated from mean values and standard deviations (n = 3) of nitrate and ammonium contents along the soil profile.

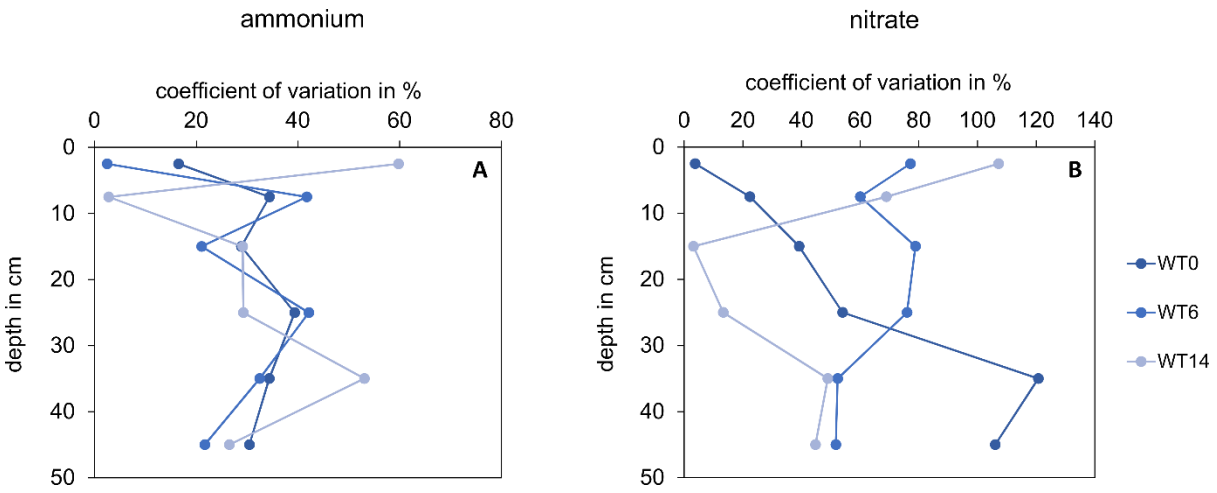

Figure B31: *Coefficients of variation of ammonium and nitrate contents on W plots at Days T0, T6 and T14.*

B8 Calculation atmospheric ammonium-N deposition

The atmospheric ammonium-N deposition on the cross-sectional area of an experimental soil core was calculated to evaluate potential sources of ammonium increase observed in the topsoil. Weekly atmospheric ammonium fluxes averaged over one year were taken from Beyn et al. (2014).

***Table B7**: Calculation of the atmospheric ammonium-N deposition on the cross-sectional area of a soil core with a diameter of 3.5 cm within one week.*

Atmospheric ammonium-flux average over one year in μM ammonium m^{-2} wk^{-1}	Source: Beyn et al. 2014
wet deposition	752
dry deposition	66.7
total	818.7

Molar mass M	
M(ammonium) in g mol^{-1}	18.0386
M(N) in g mol^{-1}	14.007

cross sectional area sample core in m^2	0.000 962

total ammonium-flux average over one year	
in μg ammonium m^{-2} wk^{-1}	14 768.20
in mg ammonium m^{-2} wk^{-1}	14.77
in μg ammonium-N m^{-2} wk^{-1}	11 467.53
in mg ammonium-N m^{-2} wk^{-1}	11.47

on cross-sectional area of a sample core	
in mg ammonium-N wk^{-1}	0.01103

B9 Calculation atmospheric nitrate-N deposition

The atmospheric nitrate-N deposition on the cross-sectional area of an experimental soil core was calculated to evaluate potential sources of nitrate increase observed in the topsoil. Weekly atmospheric nitrate fluxes averaged over one year were taken from Beyn et al. (2014).

***Table B8**: Calculation of the atmospheric nitrate-N deposition on the cross-sectional area of a soil core with a diameter of 3.5 cm within one week.*

Atmospheric nitrate-flux average over one year in μM nitrate m^{-2} wk^{-1}	Source: Beyn et al. 2014
wet deposition	468.9
dry deposition	60.6
total	529.5

Molar mass M	
M(nitrate) in g mol^{-1}	61.977
M(N) in g mol^{-1}	14.007

cross sectional area sample core in m^2 (radius = 3.5 cm)	0.000 962

total nitrate-flux average over one year	
in μg nitrate m^{-2} wk^{-1}	32 816.82
in mg nitrate m^{-2} wk^{-1}	32.82
in μg nitrate-N m^{-2} wk^{-1}	7 416.71
in mg nitrate-N m^{-2} wk^{-1}	7.42

on the cross-sectional area of a sample core	
in mg nitrate-N wk^{-1}	0.0071

Bibliography

Aanderud, Z. T., Jones, S. E., Fierer, N., & Lennon, J. T. (2015). Resuscitation of the rare biosphere contributes to pulses of ecosystem activity [Original Research]. *Frontiers in Microbiology*, *6*. https://doi.org/10.3389/fmicb.2015.00024

Adhikari, K., & Hartemink, A. E. (2016). Linking soils to ecosystem services — A global review. *Geoderma*, *262*, 101-111. https://doi.org/https://doi.org/10.1016/j.geoderma.2015.08.009

Aeschbacher, M., Graf, C., Schwarzenbach, R. P., & Sander, M. (2012). Antioxidant Properties of Humic Substances. *Environmental Science & Technology*, *46*(9), 4916-4925. https://doi.org/10.1021/es300039h

Aeschbacher, M., Sander, M., & Schwarzenbach, R. P. (2010). Novel Electrochemical Approach to Assess the Redox Properties of Humic Substances. *Environmental Science & Technology*, *44*(1), 87-93. https://doi.org/10.1021/es902627p

Aeschbacher, M., Vergari, D., Schwarzenbach, R. P., & Sander, M. (2011). Electrochemical Analysis of Proton and Electron Transfer Equilibria of the Reducible Moieties in Humic Acids. *Environmental Science & Technology*, *45*(19), 8385-8394. https://doi.org/10.1021/es201981g

Agrarmeteorologie Baden-Württemberg. (2021). *Wetterdaten, Station Unterjesingen*. Landwirtschaftliches Technologiezentrum Augustenberg. Retrieved 14.10.2021 from https://www.wetter-bw.de/Internet/AM/NotesBwAM.nsf/bwweb/4262596897754529c1257ca8002f9d19?OpenDocument

Alexander, M. (1999). *Biodegradation and Bioremediation* (2 ed.). Academic Press.

Allen, R. G., Pereira, L. S., Raes, D., & Smith, M. (1998). *FAO Irrigation and drainage paper 56 - Crop evapotranspiration - Guidelines for computing crop water requirements*. FAO - Food and Agriculture Organization of the United Nations.

American Meteorological Society. (2012, 25.04.2012). *American Meteorological Society: "Rain". Glossary of Meteorology*. Retrieved 03.02.2024 from https://glossary.ametsoc.org/wiki/Rain

American Meteorological Society. (2021, 25.04.2012). *"Rain". Glossary of Meteorology*. Retrieved 14.10.2021 from https://glossary.ametsoc.org/wiki/Rain

Armstrong, A., Valverde, A., Ramond, J.-B., Makhalanyane, T. P., Jansson, J. K., Hopkins, D. W., Aspray, T. J., Seely, M., Trindade, M. I., & Cowan, D. A. (2016). Temporal dynamics of hot desert microbial communities reveal structural and functional responses to water input. *Scientific Reports*, *6*(1), 34434. https://doi.org/10.1038/srep34434

Baldwin, D. S., & Mitchell, A. M. (2000). The effects of drying and re-flooding on the sediment and soil nutrient dynamics of lowland river–floodplain systems: a synthesis [https://doi.org/10.1002/1099-1646(200009/10)16:5<457::AID-RRR597>3.0.CO;2-B]. *Regulated Rivers: Research & Management*, *16*(5), 457-467. https://doi.org/https://doi.org/10.1002/1099-1646(200009/10)16:5<457::AID-RRR597>3.0.CO;2-B

Barnard, R. L., Osborne, C. A., & Firestone, M. K. (2013). Responses of soil bacterial and fungal communities to extreme desiccation and rewetting. *The ISME Journal*, *7*(11), 2229-2241. https://doi.org/10.1038/ismej.2013.104

Bauwe, A., Tiemeyer, B., Kahle, P., & Lennartz, B. (2015). Classifying hydrological events to quantify their impact on nitrate leaching across three spatial scales. *Journal of Hydrology*, *531*, 589-601. https://doi.org/https://doi.org/10.1016/j.jhydrol.2015.10.069

Beven, K. (1981). Kinematic subsurface stormflow [https://doi.org/10.1029/WR017i005p01419]. *Water Resources Research*, *17*(5), 1419-1424. https://doi.org/https://doi.org/10.1029/WR017i005p01419

Beven, K., & Germann, P. (2013). Macropores and water flow in soils revisited [https://doi.org/10.1002/wrcr.20156]. *Water Resources Research*, *49*(6), 3071-3092. https://doi.org/https://doi.org/10.1002/wrcr.20156

Beven, K., Zhang, D., & Mermoud, A. (2006). On the Value of Local Measurements for Prediction of Pesticide Transport at the Field Scale [https://doi.org/10.2136/vzj2005.0016]. *Vadose Zone Journal*, *5*(1), 222-233. https://doi.org/https://doi.org/10.2136/vzj2005.0016

Beyn, F., Matthias, V., & Dähnke, K. (2014). Changes in atmospheric nitrate deposition in Germany – An isotopic perspective. *Environmental Pollution*, *194*, 1-10. https://doi.org/https://doi.org/10.1016/j.envpol.2014.06.043

Birch, H. F. (1958). The effect of soil drying on humus decomposition and nitrogen availability. *Plant and Soil*, *10*(1), 9-31. https://doi.org/10.1007/BF01343734

Birch, H. F. (1960). Nitrification in soils after different periods of dryness. *Plant and Soil*, *12*(1), 81-96. https://doi.org/10.1007/BF01377763

Blazewicz, S. J., Schwartz, E., & Firestone, M. K. (2014). Growth and death of bacteria and fungi underlie rainfall-induced carbon dioxide pulses from seasonally dried soil. *Ecology*, *95*(5), 1162-1172. https://doi.org/https://doi.org/10.1890/13-1031.1

Blume, H.-P., Brümmer, G. W., Fleige, H., Horn, R., Kandeler, E., Kögel-Knabner, I., Kretzschmar, R., Stahr, K., & Wilke, B.-M. (2016). *Scheffer/Schachtschabel Soil Science* (Vol. 1). Springer, Berlin, Heidelberg. https://doi.org/https://doi.org/10.1007/978-3-642-30942-7

Booth, M. S., Stark, J. M., & Rastetter, E. (2005). CONTROLS ON NITROGEN CYCLING IN TERRESTRIAL ECOSYSTEMS: A SYNTHETIC ANALYSIS OF LITERATURE DATA. *Ecological Monographs*, *75*(2), 139-157. https://doi.org/https://doi.org/10.1890/04-0988

Borch, T., Kretzschmar, R., Kappler, A., Cappellen, P. V., Ginder-Vogel, M., Voegelin, A., & Campbell, K. (2010). Biogeochemical Redox Processes and their Impact on Contaminant Dynamics. *Environmental Science & Technology*, *44*(1), 15-23. https://doi.org/10.1021/es9026248

Borggaard, O. K., & Gimsing, A. L. (2008). Fate of glyphosate in soil and the possibility of leaching to ground and surface waters: a review [https://doi.org/10.1002/ps.1512]. *Pest Management Science*, *64*(4), 441-456. https://doi.org/https://doi.org/10.1002/ps.1512

Bouma, J. (1981). Comment on "Micro-, Meso-, and Macroporosity of Soil" [https://doi.org/10.2136/sssaj1981.03615995004500060050x]. *Soil Science Society of America Journal*, *45*(6), 1244-1245. https://doi.org/https://doi.org/10.2136/sssaj1981.03615995004500060050x

Bouma, J., & Dekker, L. W. (1978). A case study on infiltration into dry clay soil I. Morphological observations. *Geoderma*, *20*(1), 27-40. https://doi.org/https://doi.org/10.1016/0016-7061(78)90047-2

Bronswijk, J. J. B., Hamminga, W., & Oostindie, K. (1995). Rapid nutrient leaching to groundwater and surface water in clay soil areas. *European Journal of Agronomy*, *4*(4), 431-439. https://doi.org/https://doi.org/10.1016/S1161-0301(14)80095-6

Buss, S., Herbert, A., Morgan, P., Thornton, S., & Smith, J. (2004). A Review of Ammonium Attenuation in Soil and Groundwater. *Quarterly Journal of Engineering Geology and Hydrogeology - Q J ENG GEOL HYDROGEOL*, *37*, 347-359. https://doi.org/10.1144/1470-9236/04-005

Byrne James, M., Klueglein, N., Pearce, C., Rosso Kevin, M., Appel, E., & Kappler, A. (2015). Redox cycling of Fe(II) and Fe(III) in magnetite by Fe-metabolizing bacteria. *Science*, *347*(6229), 1473-1476. https://doi.org/10.1126/science.aaa4834

Callahan, B. J., McMurdie, P. J., & Holmes, S. P. (2017). Exact sequence variants should replace operational taxonomic units in marker-gene data analysis. *The ISME Journal*, *11*(12), 2639-2643. https://doi.org/10.1038/ismej.2017.119

Canfield, D., & Thamdrup, B. (2009). Towards a consistent classification scheme for geochemical environments, or, why we wish the term 'suboxic' would go away: Editorial. *Geobiology*, *7*, 385-392. https://doi.org/10.1111/j.1472-4669.2009.00214.x

Carini, P., Marsden, P. J., Leff, J. W., Morgan, E. E., Strickland, M. S., & Fierer, N. (2016). Relic DNA is abundant in soil and obscures estimates of soil microbial diversity. *Nature Microbiology*, *2*(3), 16242. https://doi.org/10.1038/nmicrobiol.2016.242

Carter, M. R., & Gregorich, E. G. (2008). *Soil sampling and methods of analysis H1 - Universitätsbibliothek H2 - 53 B 348* (2. ed. ed.). CRC Press.

Cavalli, D., Consolati, G., Marino, P., & Bechini, L. (2015). Measurement and simulation of soluble, exchangeable, and non-exchangeable ammonium in three soils. *Geoderma*, *259-260*, 116-125. https://doi.org/https://doi.org/10.1016/j.geoderma.2015.05.011

Ciglasch, H., Amelung, W., Totrakool, S., & Kaupenjohann, M. (2005). Water flow patterns and pesticide fluxes in an upland soil in northern Thailand [https://doi.org/10.1111/j.1365-2389.2005.00712.x]. *European Journal of Soil Science*, *56*(6), 765-777. https://doi.org/https://doi.org/10.1111/j.1365-2389.2005.00712.x

Coby, A. J., Picardal, F., Shelobolina, E., Xu, H., & Roden, E. E. (2011). Repeated anaerobic microbial redox cycling of iron. *Applied and environmental microbiology*, *77*(17), 6036-6042. https://doi.org/10.1128/AEM.00276-11

Cornell, R. M., & Schwertmann, U. (2003). *The Iron Oxides: Structure, Properties, Reactions, Occurences and Uses, Second Edition* (2 ed.). Wiley-VCH Verlag GmbH & Co. KGaA https://doi.org/https://doi.org/10.1002/3527602097.ch9

Coumou, D., & Rahmstorf, S. (2012). A decade of weather extremes. *Nature Climate Change*, *2*(7), 491-496. https://doi.org/10.1038/nclimate1452

Cui, M., & Caldwell, M. M. (1997). A large ephemeral release of nitrogen upon wetting of dry soil and corresponding root responses in the field. *Plant and Soil*, *191*(2), 291-299. https://doi.org/10.1023/A:1004290705961

de Jonge, H., de Jonge, L. W., & Jacobsen, O. H. (2000). [14C]Glyphosate transport in undisturbed topsoil columns. *Pest Management Science*, *56*(10), 909-915. https://doi.org/https://doi.org/10.1002/1526-4998(200010)56:10<909::AID-PS227>3.0.CO;2-5

de Jonge, L. W., Moldrup, P., Rubæk, G. H., Schelde, K., & Djurhuus, J. (2004). Particle Leaching and Particle-Facilitated Transport of Phosphorus at Field Scale. *Vadose Zone Journal*, *3*(2), 462-470. https://doi.org/https://doi.org/10.2136/vzj2004.0462

DIN Deutsches Institut für Normung e. V. (2003). *DIN ISO 14869-2 Soil quality - Dissolution for the determination of total element content - Part 2: Dissolution by alkaline fusion*.

DIN Deutsches Institut für Normung e. V. (2017). *DIN EN ISO 17892-4 Geotechnical investigation and testing - Laboratory testing of soil - Part 4: Determination of particle size distribution*.

Dorau, K., Bohn, B., Weihermüller, L., & Mansfeldt, T. (2021). Temperature-induced diurnal redox potential in soil [10.1039/D1EM00254F]. *Environmental Science: Processes & Impacts*, *23*(11), 1782-1790. https://doi.org/10.1039/D1EM00254F

Dorau, K., Uteau, D., Maisch, M., Kappler, A., Peth, S., & Mansfeldt, T. (2023). Redoxtrons – An experimental system to study redox processes within the capillary fringe [https://doi.org/10.1111/ejss.13347]. *European Journal of Soil Science*, *74*(1), e13347. https://doi.org/https://doi.org/10.1111/ejss.13347

Durner, W., Iden, S. C., & von Unold, G. (2017). The integral suspension pressure method (ISP) for precise particle-size analysis by gravitational sedimentation [https://doi.org/10.1002/2016WR019830]. *Water Resources Research*, *53*(1), 33-48. https://doi.org/https://doi.org/10.1002/2016WR019830

Esala, M. J. (1994). Deep-freezing pretreatment and time of extraction of soil samples for inorganic nitrogen determination. *Communications in Soil Science and Plant Analysis*, *25*(5-6), 651-662. https://doi.org/10.1080/00103629409369070

Esala, M. J. (1995). Changes in the extractable ammonium- and nitrate-nitrogen contents of soil samples during freezing and thawing. *Communications in Soil Science and Plant Analysis*, *26*(1-2), 61-68. https://doi.org/10.1080/00103629509369280

Fierer, N., & Schimel, J. P. (2002). Effects of drying–rewetting frequency on soil carbon and nitrogen transformations. *Soil Biology and Biochemistry*, *34*(6), 777-787. https://doi.org/https://doi.org/10.1016/S0038-0717(02)00007-X

Fierer, N., Schimel, J. P., & Holden, P. A. (2003). Influence of Drying–Rewetting Frequency on Soil Bacterial Community Structure. *Microbial Ecology*, *45*(1), 63-71. https://doi.org/10.1007/s00248-002-1007-2

Flury, M. (1996). Experimental Evidence of Transport of Pesticides through Field Soils—A Review [https://doi.org/10.2134/jeq1996.00472425002500010005x]. *Journal of Environmental Quality*, *25*(1), 25-45. https://doi.org/https://doi.org/10.2134/jeq1996.00472425002500010005x

Flury, M., Flühler, H., Jury, W. A., & Leuenberger, J. (1994). Susceptibility of soils to preferential flow of water: A field study [https://doi.org/10.1029/94WR00871]. *Water Resources Research*, *30*(7), 1945-1954. https://doi.org/https://doi.org/10.1029/94WR00871

Fowler, D., Coyle, M., Skiba, U., Sutton, M. A., Cape, J. N., Reis, S., Sheppard, L. J., Jenkins, A., Grizzetti, B., Galloway, J. N., Vitousek, P., Leach, A., Bouwman, A. F., Butterbach-Bahl, K., Dentener, F., Stevenson, D., Amann, M., & Voss, M. (2013). The global nitrogen cycle in the twenty-first century. *Philosophical Transactions of the Royal Society B: Biological Sciences*, *368*(1621), 20130164. https://doi.org/10.1098/rstb.2013.0164

Franklin, S. M., Kravchenko, A. N., Vargas, R., Vasilas, B., Fuhrmann, J. J., & Jin, Y. (2021). The unexplored role of preferential flow in soil carbon dynamics. *Soil Biology and Biochemistry*, *161*, 108398. https://doi.org/https://doi.org/10.1016/j.soilbio.2021.108398

German Meteorological Service (DWD). (2024). *German Meteorological Service (DWD): Monatliche Mittel/Summen, Niederschlag, Station Stuttgart-Echterdingen*. German Meteorological Sevice (DWD). Retrieved 02.02.2024 from https://www.dwd.de/DE/leistungen/kvo/baden_wuerttemberg.html?nn=480164

German Meteorological Sevice (DWD). (2021). *Klimatabelle Temperatur/Niederschlag, Station Stuttgart-Echterdingen*. German Meteorological Sevice (DWD). Retrieved 02.12.2021 from https://www.dwd.de/DE/leistungen/kvo/baden_wuerttemberg.html?nn=480164

Geyer, O. F., Gwinner, M. P., Geyer, M., & Ellwanger, D. (2011). *Geologie von Baden-Württemberg* (5., völlig neu bearb. Aufl. / hrsg. von Matthias Geyer ... unter Mitarb. von Dietrich Ellwanger ... ed.). Schweizerbart.

Gimsing, A. L., & Borggaard, O. K. (2002). Competitive adsorption and desorption of glyphosate and phosphate on clay silicates and oxides. *Clay Minerals*, *37*(3), 509-515. https://doi.org/10.1180/0009855023730049

Göransson, H., Godbold, D. L., Jones, D. L., & Rousk, J. (2013). Bacterial growth and respiration responses upon rewetting dry forest soils: Impact of drought-legacy. *Soil Biology and Biochemistry*, *57*, 477-486. https://doi.org/https://doi.org/10.1016/j.soilbio.2012.08.031

Gorski, C. A., Klüpfel, L., Voegelin, A., Sander, M., & Hofstetter, T. B. (2012). Redox Properties of Structural Fe in Clay Minerals. 2. Electrochemical and Spectroscopic Characterization of Electron Transfer Irreversibility in Ferruginous Smectite, SWa-1. *Environmental Science & Technology*, *46*(17), 9369-9377. https://doi.org/10.1021/es302014u

Grathwohl, P., Rügner, H., Wöhling, T., Osenbrück, K., Schwientek, M., Gayler, S., Wollschläger, U., Selle, B., Pause, M., Delfs, J.-O., Grzeschik, M., Weller, U., Ivanov, M., Cirpka, O. A., Maier, U., Kuch, B., Nowak, W., Wulfmeyer, V., Warrach-Sagi, K., . . . Teutsch, G. (2013). Catchments as reactors: a comprehensive approach for water fluxes and solute turnover. *Environmental Earth Sciences*, *69*(2), 317-333. https://doi.org/10.1007/s12665-013-2281-7

Gulu Zada, L. (2021). *Sorption of Selected Pesticides on Mineral Surfaces: Factors and Mechanisms* Dissertation, Eberhard Karls Universität Tübingen, 2019]. Tübingen. http://nbn-resolving.de/urn:nbn:de:bsz:21-dspace-867161

Haberer, C. M., Rolle, M., Cirpka, O. A., & Grathwohl, P. (2012). Oxygen Transfer in a Fluctuating Capillary Fringe [https://doi.org/10.2136/vzj2011.0056]. *Vadose Zone Journal*, *11*(3), vzj2011.0056. https://doi.org/https://doi.org/10.2136/vzj2011.0056

Hansen, J. I., Henriksen, K., & Blackburn, T. H. (1981). Seasonal Distribution of Nitrifying Bacteria and Rates of Nitrification in Coastal Marine Sediments. *Microbial Ecology*, *7*(4), 297-304. http://www.jstor.org/stable/4250672

Hardie, M. A., Cotching, W. E., Doyle, R. B., Holz, G., Lisson, S., & Mattern, K. (2011). Effect of antecedent soil moisture on preferential flow in a texture-contrast soil. *Journal of Hydrology*, *398*(3), 191-201. https://doi.org/https://doi.org/10.1016/j.jhydrol.2010.12.008

Hedlund, J., Longo, S. B., & York, R. (2020). Agriculture, Pesticide Use, and Economic Development: A Global Examination (1990–2014). *Rural Sociology*, *85*(2), 519-544. https://doi.org/https://doi.org/10.1111/ruso.12303

Hefting, M., Clément, J. C., Dowrick, D., Cosandey, A. C., Bernal, S., Cimpian, C., Tatur, A., Burt, T. P., & Pinay, G. (2004). Water table elevation controls on soil nitrogen cycling in riparian wetlands along a European climatic gradient. *Biogeochemistry*, *67*(1), 113-134. https://doi.org/10.1023/B:BIOG.0000015320.69868.33

Hergert, G. W., Ferguson, R. B., Shapiro, C. A., Penas, E. J., & Anderson, F. B. (1995). Classical Statistical and Geostatistical Analysis of Soil Nitrate-N Spatial Variability. In *Site-Specific Management for Agricultural Systems* (pp. 175-186). https://doi.org/https://doi.org/10.2134/1995.site-specificmanagement.c13

Horton, R. M., Mankin, J. S., Lesk, C., Coffel, E., & Raymond, C. (2016). A Review of Recent Advances in Research on Extreme Heat Events. *Current Climate Change Reports*, *2*(4), 242-259. https://doi.org/10.1007/s40641-016-0042-x

Houba, V. J. G., & Novozamsky, I. (1998). Influence of storage time and temperature of air-dried soils on pH and extractable nutrients using 0.01 mol/L CaCl2. *Fresenius' Journal of Analytical Chemistry*, *360*(3), 362-365. https://doi.org/10.1007/s002160050712

Houba, V. J. G., Novozamsky, I., Huybregts, A. W. M., & van der Lee, J. J. (1986). Comparison of soil extractions by 0.01M CaCl2, by EUF and by some conventional extraction procedures. *Plant and Soil*, *96*(3), 433-437. https://doi.org/10.1007/BF02375149

IUSS Working Group WRB. (2015). *World Reference Base for Soil Resources 2014, update 2015 International soil classification system for naming soils and creating legends for soil maps* (Vol. 106). FAO.

Jarvis, N., Koestel, J., & Larsbo, M. (2016). Understanding Preferential Flow in the Vadose Zone: Recent Advances and Future Prospects [https://doi.org/10.2136/vzj2016.09.0075]. *Vadose Zone Journal*, *15*(12), vzj2016.2009.0075. https://doi.org/https://doi.org/10.2136/vzj2016.09.0075

Jarvis, P., Rey, A., Petsikos, C., Wingate, L., Rayment, M., Pereira, J., Banza, J., David, J., Miglietta, F., Borghetti, M., Manca, G., & Valentini, R. (2007). Drying and wetting of Mediterranean soils stimulates decomposition and carbon dioxide emission: the "Birch effect"†. *Tree Physiology*, *27*(7), 929-940. https://doi.org/10.1093/treephys/27.7.929

Kanissery, R. G., Welsh, A., & Sims, G. K. (2015). Effect of Soil Aeration and Phosphate Addition on the Microbial Bioavailability of Carbon-14-Glyphosate. *Journal of Environmental Quality*, *44*(1), 137-144. https://doi.org/https://doi.org/10.2134/jeq2014.08.0331

Kasteel, R., Pütz, T., Vanderborght, J., & Vereecken, H. (2010). Fate of Two Herbicides in Zero-Tension Lysimeters and in Field Soil [https://doi.org/10.2134/jeq2009.0236]. *Journal of Environmental Quality*, *39*(4), 1451-1466. https://doi.org/https://doi.org/10.2134/jeq2009.0236

Kasteel, R., Schnitzler, F., Berns, A. E., Vanderborght, J., & Vereecken, H. (2013). Visualization of transport pathways for organic compounds in undisturbed soil monoliths. *Geoderma*, *195-196*, 70-78. https://doi.org/https://doi.org/10.1016/j.geoderma.2012.11.014

Kelly, B. P., & Pomes, M. L. (1998). Preferential Flow and Transport of Nitrate and Bromide in Clay pan Soil. *Groundwater*, *36*(3), 484-494. https://doi.org/https://doi.org/10.1111/j.1745-6584.1998.tb02820.x

Kendall, C. (1998). Chapter 16 - Tracing Nitrogen Sources and Cycling in Catchments. In C. Kendall & J. J. McDonnell (Eds.), *Isotope Tracers in Catchment Hydrology* (pp. 519-576). Elsevier. https://doi.org/https://doi.org/10.1016/B978-0-444-81546-0.50023-9

Kennedy, C. D., Bataille, C., Liu, Z., Ale, S., VanDeVelde, J., Roswell, C. R., Bowling, L. C., & Bowen, G. J. (2012). Dynamics of nitrate and chloride during storm events in agricultural catchments with different subsurface drainage intensity (Indiana, USA). *Journal of Hydrology*, *466-467*, 1-10. https://doi.org/https://doi.org/10.1016/j.jhydrol.2012.05.002

Keuper, F., van Bodegom, P. M., Dorrepaal, E., Weedon, J. T., van Hal, J., van Logtestijn, R. S. P., & Aerts, R. (2012). A frozen feast: thawing permafrost increases plant-available

nitrogen in subarctic peatlands [https://doi.org/10.1111/j.1365-2486.2012.02663.x]. *Global Change Biology*, *18*(6), 1998-2007. https://doi.org/https://doi.org/10.1111/j.1365-2486.2012.02663.x

Khan, S. U., Hooda, P. S., Blackwell, M. S. A., & Busquets, R. (2019). Microbial Biomass Responses to Soil Drying-Rewetting and Phosphorus Leaching [Original Research]. *Frontiers in Environmental Science*, *7*. https://doi.org/10.3389/fenvs.2019.00133

Kjær, J., Ernstsen, V., Jacobsen, O. H., Hansen, N., de Jonge, L. W., & Olsen, P. (2011). Transport modes and pathways of the strongly sorbing pesticides glyphosate and pendimethalin through structured drained soils. *Chemosphere*, *84*(4), 471-479. https://doi.org/https://doi.org/10.1016/j.chemosphere.2011.03.029

Kjær, J., Olsen, P., Ullum, M., & Grant, R. (2005). Leaching of Glyphosate and Amino-Methylphosphonic Acid from Danish Agricultural Field Sites [https://doi.org/10.2134/jeq2005.0608]. *Journal of Environmental Quality*, *34*(2), 608-620. https://doi.org/https://doi.org/10.2134/jeq2005.0608

Klingler, S., Cirpka, O. A., Werban, U., Leven, C., & Dietrich, P. (2020). Direct-Push Color Logging Images Spatial Heterogeneity of Organic Carbon in Floodplain Sediments. *Journal of Geophysical Research: Biogeosciences*, *125*(12), e2020JG005887. https://doi.org/https://doi.org/10.1029/2020JG005887

Klüpfel, L., Piepenbrock, A., Kappler, A., & Sander, M. (2014). Humic substances as fully regenerable electron acceptors in recurrently anoxic environments. *Nature Geoscience*, *7*(3), 195-200. https://doi.org/10.1038/ngeo2084

Kuderna, M., Pötsch, E., & Blum, W. (1993). Zur Wahl des Extraktionsmittels bei der Nmin-Bestimmung. *Bodenkultur*, *44 (1)*, 7-14.

Kuzyakov, Y., & Blagodatskaya, E. (2015). Microbial hotspots and hot moments in soil: Concept & review. *Soil Biology and Biochemistry*, *83*, 184-199. https://doi.org/https://doi.org/10.1016/j.soilbio.2015.01.025

Lair, G. J., Zehetner, F., Fiebig, M., Gerzabek, M. H., van Gestel, C. A. M., Hein, T., Hohensinner, S., Hsu, P., Jones, K. C., Jordan, G., Koelmans, A. A., Poot, A., Slijkerman, D. M. E., Totsche, K. U., Bondar-Kunze, E., & Barth, J. A. C. (2009). How do long-term development and periodical changes of river–floodplain systems affect the fate of contaminants? Results from European rivers. *Environmental Pollution*, *157*(12), 3336-3346. https://doi.org/https://doi.org/10.1016/j.envpol.2009.06.004

Landesamt für Geologie Rohstoffe und Bergbau Baden-Württemberg. (2021a). *LGRB-Kartenviewer - Layer GeoLa BK50 (1:50 000), Bodenkundliche Einheiten*. Regierungspraesidium Freiburg, Landesamt für Geologie, Rohstoffe und Bergbau. Retrieved 14.10.2021 from https://maps.lgrb-bw.de

Landesamt für Geologie Rohstoffe und Bergbau Baden-Württemberg. (2021b). *LGRB-Kartenviewer - Layer GeoLa GK50 (1:50 000), Geologische Einheiten (Flaechen)* Regierungspraesidium Freiburg, Landesamt für Geologie, Rohstoffe und Bergbau. Retrieved 14.10.2021 from https://maps.lgrb-bw.de

LaRowe, D. E., & Van Cappellen, P. (2011). Degradation of natural organic matter: A thermodynamic analysis. *Geochimica et Cosmochimica Acta*, *75*(8), 2030-2042. https://doi.org/https://doi.org/10.1016/j.gca.2011.01.020

Larsson, M. H., & Jarvis, N. J. (2000). Quantifying interactions between compound properties and macropore flow effects on pesticide leaching. *Pest Management Science*, *56*(2), 133-141. https://doi.org/https://doi.org/10.1002/(SICI)1526-4998(200002)56:2<133::AID-PS103>3.0.CO;2-N

Lau, M. P., Sander, M., Gelbrecht, J., & Hupfer, M. (2015). Solid phases as important electron acceptors in freshwater organic sediments. *Biogeochemistry*, *123*(1), 49-61. https://doi.org/10.1007/s10533-014-0052-5

Lennon, J. T., Muscarella, M. E., Placella, S. A., & Lehmkuhl, B. K. (2018). How, When, and Where Relic DNA Affects Microbial Diversity. *mBio*, *9*(3), 10.1128/mbio.00637-00618. https://doi.org/10.1128/mbio.00637-18

Loeppmann, S., Blagodatskaya, E., Pausch, J., & Kuzyakov, Y. (2016). Enzyme properties down the soil profile - A matter of substrate quality in rhizosphere and detritusphere. *Soil Biology and Biochemistry*, *103*, 274-283. https://doi.org/https://doi.org/10.1016/j.soilbio.2016.08.023

Ma, B. L., Ying, J., & Balchin, D. (2005). Impact of Sample Preservation Methods on the Extraction of Inorganic Nitrogen by Potassium Chloride. *Journal of Plant Nutrition*, *28*(5), 785-796. https://doi.org/10.1081/PLN-200055536

Mansfeldt, T. (2003). In situ long-term redox potential measurements in a dyked marsh soil. *Journal of Plant Nutrition and Soil Science*, *166*(2), 210-219. https://doi.org/https://doi.org/10.1002/jpln.200390031

Manzoni, S., Schimel, J. P., & Porporato, A. (2012). Responses of soil microbial communities to water stress: results from a meta-analysis [https://doi.org/10.1890/11-0026.1]. *Ecology*, *93*(4), 930-938. https://doi.org/https://doi.org/10.1890/11-0026.1

Martin, S., Klingler, S., Dietrich, P., Leven, C., & Cirpka, O. A. (2020). Structural controls on the hydrogeological functioning of a floodplain. *Hydrogeology Journal*, *28*(8), 2675-2696. https://doi.org/10.1007/s10040-020-02225-8

McGrath, G. S., Hinz, C., Sivapalan, M., Dressel, J., Pütz, T., & Vereecken, H. (2010). Identifying a rainfall event threshold triggering herbicide leaching by preferential flow [https://doi.org/10.1029/2008WR007506]. *Water Resources Research*, *46*(2). https://doi.org/https://doi.org/10.1029/2008WR007506

Mengel, K. (1991). Available nitrogen in soils and its determination by the 'Nmin-method' and by electroultrafiltration (EUF). *Fertilizer research*, *28*(3), 251-262. https://doi.org/10.1007/BF01054326

Nelson, D. W., & Bremner, J. M. (1972). Preservation of Soil Samples for Inorganic Nitrogen Analyses1 [https://doi.org/10.2134/agronj1972.00021962006400020021x]. *Agronomy Journal*, *64*(2), 196-199. https://doi.org/https://doi.org/10.2134/agronj1972.00021962006400020021x

Niemi, R. M., Vepsäläinen, M., Wallenius, K., Simpanen, S., Alakukku, L., & Pietola, L. (2005). Temporal and soil depth-related variation in soil enzyme activities and in root growth of red clover (Trifolium pratense) and timothy (Phleum pratense) in the field. *Applied Soil Ecology*, *30*(2), 113-125. https://doi.org/https://doi.org/10.1016/j.apsoil.2005.02.003

Nimmo, J. R. (2012). Preferential flow occurs in unsaturated conditions [https://doi.org/10.1002/hyp.8380]. *Hydrological Processes*, *26*(5), 786-789. https://doi.org/https://doi.org/10.1002/hyp.8380

Nimmo, J. R. (2021). The processes of preferential flow in the unsaturated zone [https://doi.org/10.1002/saj2.20143]. *Soil Science Society of America Journal*, *85*(1), 1-27. https://doi.org/https://doi.org/10.1002/saj2.20143

Nina, D. O., & Sigunga, D. O. (2012). Effects of drying method, storage period and carbon: nitrogen ratio on inorganic nitrogen contents of Vertisols. *African Journal of Environmental Science and Technology*, *6*(12), 7. https://doi.org/10.5897/AJEST12.151

Norgaard, T., Moldrup, P., Ferré, T., Olsen, P., Rosenbom, A., & de Jonge, L. (2014). Leaching of Glyphosate and Aminomethylphosphonic Acid from an Agricultural Field over a Twelve-Year Period. *Vadose Zone Journal*, *13*. https://doi.org/10.2136/vzj2014.05.0054

Oren, A. (2001). The bioenergetic basis for the decrease in metabolic diversity at increasing salt concentrations: implications for the functioning of salt lake ecosystems. In Melack J.M., Jellison R., & H. D.B. (Eds.), *Saline Lakes* (Vol. 162). Springer. https://doi.org/https://doi.org/10.1007/978-94-017-2934-5_6

Parker, S. S., & Schimel, J. P. (2011). Soil nitrogen availability and transformations differ between the summer and the growing season in a California grassland. *Applied Soil Ecology*, *48*(2), 185-192. https://doi.org/https://doi.org/10.1016/j.apsoil.2011.03.007

Patrick, W. H., Gambrell, R. P., & Faulkner, S. P. (1996). Redox Measurements of Soils. In D. L. Sparks (Ed.), *Methods of Soil Analysis* (pp. 1255-1273). https://doi.org/https://doi.org/10.2136/sssabookser5.3.c42

Peiffer, S., Kappler, A., Haderlein, S. B., Schmidt, C., Byrne, J. M., Kleindienst, S., Vogt, C., Richnow, H. H., Obst, M., Angenent, L. T., Bryce, C., McCammon, C., & Planer-Friedrich, B. (2021). A biogeochemical–hydrological framework for the role of redox-active compounds in aquatic systems. *Nature Geoscience*, *14*(5), 264-272. https://doi.org/10.1038/s41561-021-00742-z

Peiffer, S., Klemm, O., Pecher, K., & Hollerung, R. (1992). Redox measurements in aqueous solutions — A theoretical approach to data interpretation, based on electrode kinetics. *Journal of Contaminant Hydrology*, *10*(1), 1-18. https://doi.org/https://doi.org/10.1016/0169-7722(92)90041-C

Pelster, D. E., Chantigny, M. H., Angers, D. A., Bertrand, N., MacDonald, J. D., & Rochette, P. (2018). Can soil clay content predict ammonia volatilization losses from subsurface-banded urea in eastern Canadian soils? *Canadian Journal of Soil Science*, *98*(3), 556-565. https://doi.org/10.1139/cjss-2018-0036

Perkins, S. E., Alexander, L. V., & Nairn, J. R. (2012). Increasing frequency, intensity and duration of observed global heatwaves and warm spells. *Geophysical Research Letters*, *39*(20). https://doi.org/https://doi.org/10.1029/2012GL053361

Perret, J., Prasher, S. O., Kantzas, A., & Langford, C. (2000). A Two-Domain Approach Using CAT Scanning to Model Solute Transport in Soil. *Journal of Environmental Quality*, *29*(3), 995-1010. https://doi.org/https://doi.org/10.2134/jeq2000.00472425002900030039x

Pjevac, P., Schauberger, C., Poghosyan, L., Herbold, C. W., van Kessel, M. A. H. J., Daebeler, A., Steinberger, M., Jetten, M. S. M., Lücker, S., Wagner, M., & Daims, H. (2017). AmoA-Targeted Polymerase Chain Reaction Primers for the Specific Detection and Quantification of Comammox Nitrospira in the Environment [Methods]. *Frontiers in Microbiology*, *8*. https://doi.org/10.3389/fmicb.2017.01508

Placella, S., A., & Firestone, M., K. (2013). Transcriptional Response of Nitrifying Communities to Wetting of Dry Soil. *Applied and environmental microbiology*, *79*(10), 3294-3302. https://doi.org/10.1128/AEM.00404-13

Placella, S. A., Brodie, E. L., & Firestone, M. K. (2012). Rainfall-induced carbon dioxide pulses result from sequential resuscitation of phylogenetically clustered microbial groups. *Proceedings of the National Academy of Sciences*, *109*(27), 10931. https://doi.org/10.1073/pnas.1204306109

Preusser, S., Liebmann, P., Stucke, A., Wirsching, J., Müller, K., Mikutta, R., Guggenberger, G., Don, A., Kalbitz, K., Bachmann, J., Marhan, S., Poll, C., & Kandeler, E. (2021). Microbial Utilisation of Aboveground Litter-Derived Organic Carbon Within a Sandy

Dystric Cambisol Profile [Original Research]. *Frontiers in Soil Science*, *1*. https://www.frontiersin.org/articles/10.3389/fsoil.2021.666950

Rosenbom, A. E., Olsen, P., Plauborg, F., Grant, R., Juhler, R. K., Brüsch, W., & Kjær, J. (2015). Pesticide leaching through sandy and loamy fields – Long-term lessons learnt from the Danish Pesticide Leaching Assessment Programme. *Environmental Pollution*, *201*, 75-90. https://doi.org/https://doi.org/10.1016/j.envpol.2015.03.002

Rütting, T., Boeckx, P., Müller, C., & Klemedtsson, L. (2011). Assessment of the importance of dissimilatory nitrate reduction to ammonium for the terrestrial nitrogen cycle. *Biogeosciences*, *8*(7), 1779-1791. https://doi.org/10.5194/bg-8-1779-2011

Saetre, P., & Stark, J. M. (2005). Microbial dynamics and carbon and nitrogen cycling following re-wetting of soils beneath two semi-arid plant species. *Oecologia*, *142*(2), 247-260. https://doi.org/10.1007/s00442-004-1718-9

Salmon, V. G., Schädel, C., Bracho, R., Pegoraro, E., Celis, G., Mauritz, M., Mack, M. C., & Schuur, E. A. G. (2018). Adding Depth to Our Understanding of Nitrogen Dynamics in Permafrost Soils [https://doi.org/10.1029/2018JG004518]. *Journal of Geophysical Research: Biogeosciences*, *123*(8), 2497-2512. https://doi.org/https://doi.org/10.1029/2018JG004518

Sánchez Pérez, J. M., Antiguedad, I., Arrate, I., Garcı, x, a-Linares, C., & Morell, I. (2003). The influence of nitrate leaching through unsaturated soil on groundwater pollution in an agricultural area of the Basque country: a case study. *Science of The Total Environment*, *317*(1), 173-187. https://doi.org/https://doi.org/10.1016/S0048-9697(03)00262-6

Sander, M., Hofstetter, T. B., & Gorski, C. A. (2015). Electrochemical Analyses of Redox-Active Iron Minerals: A Review of Nonmediated and Mediated Approaches. *Environmental Science & Technology*, *49*(10), 5862-5878. https://doi.org/10.1021/acs.est.5b00006

Schimel, J., Balser, T. C., & Wallenstein, M. (2007). MICROBIAL STRESS-RESPONSE PHYSIOLOGY AND ITS IMPLICATIONS FOR ECOSYSTEM FUNCTION [https://doi.org/10.1890/06-0219]. *Ecology*, *88*(6), 1386-1394. https://doi.org/https://doi.org/10.1890/06-0219

Schimel, J. P. (2018). Life in Dry Soils: Effects of Drought on Soil Microbial Communities and Processes. *Annual Review of Ecology, Evolution, and Systematics*, *49*(1), 409-432. https://doi.org/10.1146/annurev-ecolsys-110617-062614

Schimel, J. P., & Bennett, J. (2004). NITROGEN MINERALIZATION: CHALLENGES OF A CHANGING PARADIGM. *Ecology*, *85*(3), 591-602. https://doi.org/https://doi.org/10.1890/03-8002

Schlögl, J., Wimmer, B., Cramaro, L., Wirsching, J., Poll, C., Pagel, H., Kandeler, E., Huhn, C., Griebler, C., Stumpp, C., & Haderlein, S. B. (2022). Heavy rainfall following a summer drought stimulates soil redox dynamics and facilitates rapid and deep translocation of glyphosate in floodplain soils [10.1039/D1EM00527H]. *Environmental Science: Processes & Impacts*, *24*(5), 825-838. https://doi.org/10.1039/D1EM00527H

Schwarzenbach, R. P., Gschwend, P. M., & Imboden, D. M. (2017). *Environmental organic chemistry* (Third edition ed.). Wiley.

Schwientek, M., Osenbrück, K., & Fleischer, M. (2013). Investigating hydrological drivers of nitrate export dynamics in two agricultural catchments in Germany using high-frequency data series. *Environmental Earth Sciences*, *69*(2), 381-393. https://doi.org/10.1007/s12665-013-2322-2

Skopp, J. (1981). Comment on "Micro-, Meso-, and Macroporosity of Soil" [https://doi.org/10.2136/sssaj1981.03615995004500060052x]. *Soil Science Society of America Journal*, *45*(6), 1246-1246. https://doi.org/https://doi.org/10.2136/sssaj1981.03615995004500060052x

Sørensen, S. R., Schultz, A., Jacobsen, O. S., & Aamand, J. (2006). Sorption, desorption and mineralisation of the herbicides glyphosate and MCPA in samples from two Danish soil and subsurface profiles. *Environmental Pollution*, *141*(1), 184-194. https://doi.org/https://doi.org/10.1016/j.envpol.2005.07.023

Sprankle, P., Meggitt, W. F., & Penner, D. (1975). Adsorption, Mobility, and Microbial Degradation of Glyphosate in the Soil. *Weed Science*, *23*(3), 229-234. https://doi.org/10.1017/S0043174500052929

Stock, S. C., Köster, M., Dippold, M. A., Nájera, F., Matus, F., Merino, C., Boy, J., Spielvogel, S., Gorbushina, A., & Kuzyakov, Y. (2019). Environmental drivers and stoichiometric constraints on enzyme activities in soils from rhizosphere to continental scale. *Geoderma*, *337*, 973-982. https://doi.org/https://doi.org/10.1016/j.geoderma.2018.10.030

Stone, W. W., & Wilson, J. T. (2006). Preferential Flow Estimates to an Agricultural Tile Drain with Implications for Glyphosate Transport [https://doi.org/10.2134/jeq2006.0068]. *Journal of Environmental Quality*, *35*(5), 1825-1835. https://doi.org/https://doi.org/10.2134/jeq2006.0068

Sviridov, A. V., Shushkova, T. V., Ermakova, I. T., Ivanova, E. V., Epiktetov, D. O., & Leontievsky, A. A. (2015). Microbial degradation of glyphosate herbicides (Review). *Applied Biochemistry and Microbiology*, *51*(2), 188-195. https://doi.org/10.1134/S0003683815020209

Thamdrup, B. (2012). New Pathways and Processes in the Global Nitrogen Cycle. *Annual Review of Ecology, Evolution, and Systematics*, *43*(1), 407-428. https://doi.org/10.1146/annurev-ecolsys-102710-145048

Tian, Y., Schindlbacher, A., Malo, C. U., Shi, C., Heinzle, J., Kwatcho Kengdo, S., Inselsbacher, E., Borken, W., & Wanek, W. (2023). Long-term warming of a forest soil reduces microbial biomass and its carbon and nitrogen use efficiencies. *Soil Biology and Biochemistry*, *184*, 109109. https://doi.org/https://doi.org/10.1016/j.soilbio.2023.109109

Tournier, E., Amenc, L., Pablo, A. L., Legname, E., Blanchart, E., Plassard, C., Robin, A., & Bernard, L. (2015). Modification of a commercial DNA extraction kit for safe and rapid recovery of DNA and RNA simultaneously from soil, without the use of harmful solvents. *MethodsX*, *2*, 182-191. https://doi.org/https://doi.org/10.1016/j.mex.2015.03.007

Tratnyek, P. G., Grundl, T. J., & Haderlein, S. B. (2011). *Aquatic redox chemistry* (Vol. 1). American Chemical Society. https://doi.org/10.1021/bk-2011-1071

Umweltforschungszentrum. (2023, 01.02.2023). *UFZ Drought Monitor Germany*. Retrieved 08.04.2024 from https://www.ufz.de/index.php?de=40990

Unger, S., Máguas, C., Pereira, J. S., David, T. S., & Werner, C. (2010). The influence of precipitation pulses on soil respiration – Assessing the "Birch effect" by stable carbon isotopes. *Soil Biology and Biochemistry*, *42*(10), 1800-1810. https://doi.org/https://doi.org/10.1016/j.soilbio.2010.06.019

Usman, M., Byrne, J. M., Chaudhary, A., Orsetti, S., Hanna, K., Ruby, C., Kappler, A., & Haderlein, S. B. (2018). Magnetite and Green Rust: Synthesis, Properties, and

Environmental Applications of Mixed-Valent Iron Minerals. *Chemical Reviews*, *118*(7), 3251-3304. https://doi.org/10.1021/acs.chemrev.7b00224

van Erp, P. J., Houba, V. J. G., & van Beusichem, M. L. (2001). EFFECT OF DRYING TEMPERATURE ON AMOUNT OF NUTRIENT ELEMENTS EXTRACTED WITH 0.01 M CaCl2 SOIL EXTRACTION PROCEDURE. *Communications in Soil Science and Plant Analysis*, *32*(1-2), 33-48. https://doi.org/10.1081/CSS-100102991

van Grinsven, H. J. M., ten Berge, H. F. M., Dalgaard, T., Fraters, B., Durand, P., Hart, A., Hofman, G., Jacobsen, B. H., Lalor, S. T. J., Lesschen, J. P., Osterburg, B., Richards, K. G., Techen, A. K., Vertès, F., Webb, J., & Willems, W. J. (2012). Management, regulation and environmental impacts of nitrogen fertilization in northwestern Europe under the Nitrates Directive; a benchmark study. *Biogeosciences*, *9*(12), 5143-5160. https://doi.org/10.5194/bg-9-5143-2012

VDLUFA. (2011). 2.1.2 Extraktion von Böden, Sekundärrohstoffen und Bodenhilfsstoffen mit Königswasser. In *Methodenbuch Band VII Umweltanalytik* (Vol. 4, pp. 690). VDLUFA Verband Deutscher Landwirtschaftlicher Untersuchungs- und Forschungsanstalten e.V.

Veach, A. M., & Zeglin, L. H. (2020). Historical Drought Affects Microbial Population Dynamics and Activity During Soil Drying and Re-Wet. *Microbial Ecology*, *79*(3), 662-674. https://doi.org/10.1007/s00248-019-01432-5

Venterink, H. O., Wiegman, F., Van der Lee, G. E. M., & Vermaat, J. E. (2003). Role of Active Floodplains for Nutrient Retention in the River Rhine. *Journal of Environmental Quality*, *32*(4), 1430-1435. https://doi.org/https://doi.org/10.2134/jeq2003.1430

Voigt, C., Marushchak, M. E., Lamprecht, R. E., Jackowicz-Korczyński, M., Lindgren, A., Mastepanov, M., Granlund, L., Christensen, T. R., Tahvanainen, T., Martikainen, P. J., & Biasi, C. (2017). Increased nitrous oxide emissions from Arctic peatlands after permafrost thaw. *Proceedings of the National Academy of Sciences*, *114*(24), 6238. https://doi.org/10.1073/pnas.1702902114

Vos, M., Wolf, A. B., Jennings, S. J., & Kowalchuk, G. A. (2013). Micro-scale determinants of bacterial diversity in soil. *FEMS Microbiology Reviews*, *37*(6), 936-954. https://doi.org/10.1111/1574-6976.12023

Wassenaar, L. I., Hendry, M. J., Chostner, V. L., & Lis, G. P. (2008). High Resolution Pore Water δ2H and δ18O Measurements by H2O(liquid)−H2O(vapor) Equilibration Laser Spectroscopy. *Environmental Science & Technology*, *42*(24), 9262-9267. https://doi.org/10.1021/es802065s

Wheatley, R. E., Macdonald, R. A., & Smith, A. M. (1989). Extraction of nitrogen from soils. *Biology and Fertility of Soils*, *8*, 189-190.

Wimmer, B., Langarica-Fuentes, A., Schwarz, E., Kleindienst, S., Huhn, C., & Pagel, H. (2023). Mechanistic modeling indicates rapid glyphosate dissipation and sorption-driven persistence of its metabolite AMPA in soil. *Journal of Environmental Quality*, *52*(2), 393-405. https://doi.org/https://doi.org/10.1002/jeq2.20437

Wimmer, B., Neidhardt, H., Schwientek, M., Haderlein, S. B., & Huhn, C. (2022). Phosphate addition enhances alkaline extraction of glyphosate from highly sorptive soils and aquatic sediments [https://doi.org/10.1002/ps.6883]. *Pest Management Science*, *n/a*(n/a). https://doi.org/https://doi.org/10.1002/ps.6883

Wimmer, B., Pattky, M., Zada, L. G., Meixner, M., Haderlein, S. B., Zimmermann, H.-P., & Huhn, C. (2020). Capillary electrophoresis-mass spectrometry for the direct analysis of glyphosate: method development and application to beer beverages and

environmental studies. *Analytical and Bioanalytical Chemistry*, *412*(20), 4967-4983. https://doi.org/10.1007/s00216-020-02751-0

Wirsching, J., Wimmer, B., Ditterich, F., Schlögl, J., Martin-Laurent, F., Huhn, C., Haderlein, S., Kandeler, E., & Poll, C. (2022). 13C assimilation as well as functional gene abundance and expression elucidate the biodegradation of glyphosate in a field experiment. *Environmental Pollution*, *306*, 119382. https://doi.org/https://doi.org/10.1016/j.envpol.2022.119382

Zehe, E., & Flühler, H. (2001). Preferential transport of isoproturon at a plot scale and a field scale tile-drained site. *Journal of Hydrology*, *247*(1), 100-115. https://doi.org/https://doi.org/10.1016/S0022-1694(01)00370-5

Zhan, H., Feng, Y., Fan, X., & Chen, S. (2018). Recent advances in glyphosate biodegradation. *Applied Microbiology and Biotechnology*, *102*(12), 5033-5043. https://doi.org/10.1007/s00253-018-9035-0

Zhang, Z., & Furman, A. (2021). Soil redox dynamics under dynamic hydrologic regimes - A review. *Science of The Total Environment*, *763*, 143026. https://doi.org/https://doi.org/10.1016/j.scitotenv.2020.143026

Publication List

Peer-reviewed articles

1) **J. Schlögl**, B. Wimmer, L. Cramaro, J. Wirsching, C. Poll, H. Pagel, E. Kandeler, C. Huhn, C. Griebler, C. Stumpp and S. B. Haderlein, Heavy rainfall following a summer drought stimulates soil redox dynamics and facilitates rapid and deep translocation of glyphosate in floodplain soils, Environmental Science: Processes & Impacts, 2022, 24, 825-838 DOI: 10.1039/D1EM00527H.
2) J. Wirsching, B. Wimmer, F. Ditterich, **J. Schlögl**, F. Martin-Laurent, C. Huhn, S. Haderlein, E. Kandeler and C. Poll, 13C assimilation as well as functional gene abundance and expression elucidate the biodegradation of glyphosate in a field experiment, Environmental Pollution, 2022, 306, 119382 DOI: https://doi.org/10.1016/j.envpol.2022.119382.
3) M. Finkel, A. Baur, T. K. D. Weber, K. Osenbrück, H. Rügner, C. Leven, M. Schwientek, **J. Schlögl**, U. Hahn, T. Streck, O. A. Cirpka, T. Walter and P. Grathwohl, Managing collaborative research data for integrated, interdisciplinary environmental research, Earth Science Informatics, 2020, 13, 641-654 DOI: 10.1007/s12145-020-00441-0.
4) M. Silver, K. Knöller, **J. Schlögl**, C. Kübeck and C. Schüth, Nitrogen cycling and origin of ammonium during infiltration of treated wastewater for managed aquifer recharge, Applied Geochemistry, 2018, 97, 71-80 DOI: https://doi.org/10.1016/j.apgeochem.2018.08.003.

Articles in preparation

1) **J. Schlögl**, C. Karwautz, L. Cramaro, W. Wanek, J. Prommer, T. Böckle, A. Kappler, S. B. Haderlein and C. Griebler, Dynamics of nitrogen cycling, redox conditions, and microbial community composition in a floodplain soil induced by a heavy rainfall after summer drought, in prep.
2) **J. Schlögl**, A. Kappler and S. B. Haderlein, Inorganic nitrogen extraction revisited: stability of nitrate and ammonium during sample storage and extraction, in prep.

Selected conference contributions

(= presenting author)*

Posters

1) **Schlögl, J.***, Cramaro, L., Griebler, C., Haderlein, S.B., Dynamics of redox potential and nutrient turnover in dry floodplain soils during a simulated rainfall event, EGU

General Assembly 2020, Online, 4–8 May 2020, EGU2020-19106, https://doi.org/10.5194/egusphere-egu2020-19106, 2020

2) **Schlögl, J**.*, Subdiaga, E., Haderlein, S. B., Method refinement for the measurement of electrochemical properties of floodplain soils, EGU General Assembly 2019, Vienna, 7-12 April 2020, EGU2019-7489, 2019
3) **Schlögl, J**.*, Subdiaga, E., Haderlein, S. B., Method refinement for the measurement of electrochemical properties of floodplain soils, GDCh Umwelt 2018, Münster
4) Silver, M.*, **Schlögl, J.**, Knöller, K., and Schüth, C., Fate of nitrate and origin of ammonium during infiltration of treated wastewater investigated through stable isotopes, EGU General Assembly 2017, 23-28 April 2017, EGU2017-7437, 2017